STUDIES OF THE KINETICS OF POWDER INJECTION REFINING OF HOT – METAL/MOLTEN STEEL BY A MATHEMATICAL MODEL

by

KARNATI SRINIVASA RAO

DEPARTMENT OF METALLURGICAL ENGINEERING

INDIAN INSTITUTE OF TECHNOLOGY KANPUR

MAY, 1993

STUDIES OF THE KINETICS OF POWDER INJECTION REFINING OF HOT-METAL/MOLTEN STEEL BY A MATHEMATICAL MODEL

A Thesis Submitted
in Partial Fulfilment of the Requirements
for the Degree of
MASTER OF TECHNOLOGY

by

KARNATI SRINIVASA RAO

to the

DEPARTMENT OF METALLURGICAL ENGINEERING
INDIAN INSTITUTE OF TECHNOLOGY KANPUR
May, 1993

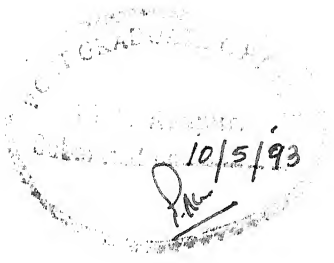

CERTIFICATE

This is to certify that the present work, entitled "Studies of the Kinetics of Powder Injection Refining of Hot-metal/Molten Steel by a Mathematical Model" by Karnati Srinivasa Rao has been carried out under my supervision and it has not been submitted elsewhere for a degree.

May, 1993

Dr. S. C. Koria
Professor
Department of Metallurgical Engineering
Indian Institute of Technology
Kanpur - 208016

ACKNOWLEDGEMENT

I wish to express my deep sense of indebtness and gratitude to Dr. S. C. Koria, Professor, Department of Metallurgical Engineering, IIT Kanpur, who guided and helped to complete this work.

I am thankful to Prof. A. Ghosh, Department of Metallurgical Engineering for his valuable suggestions and Mr. Dinesh Patel for his help in proof reading, Mr. Sarbjeet Singh for his continuous encouragement and all other my friends, Mr. V. P. Gupta for his excellent tracing.

Last but not the least my sincere thanks to Mr. Yash Pal who did a wonderful work in typing the material.

May 1993
Kanpur

Karnati Srinivasa Rao

CONTENT

SYNOPSIS

In the present investigation the influence of powder injection parameters, for example mass flow rate of the powdered flux, carrier gas flow rate etc., on the kinetics of impurity extraction via a mathematical model is studied.

Effect of impurities of interest i.e., sulphur, phosphorous and nitrogen, on steel properties is presented in chapter 1. A mathematical model is developed for two cases; that is with slag carry-over and without slag carry-over'. A general solution is obtained for the case 'with slag carry-over'. Whereas FDM is used for the case 'without slag carry-over' for the reasons given in chapter 2. Investigation on model parameters selection is done. These are also presented in Chapter 2.

Chapter 3 is reserved for the study of model parameters on concentration vs time curves under the two sections 'with slag carry over' and 'without slag carry-over', transitoric rate contribution in the overall refining process and its dependency on these model parameters and transitoric efficiency..

In chapter 4 applications of developed model are presented. It involves the evaluation of model parameters from the given concentration vs time curves, and from the experimentals results collected from the literature by using the selected equations in chapter 3.

Conclusions and suggestions are given in chapter 5 and chapter 6 respectively. Solutions procedures of developed model equations with the slag carry-over and without slag carry-over are presented in Appendix -1 and Appendix -2 respectively. Appendix - 3 gives detailed description of transitoric rate contribution. Programme code for model results is presented in Appendix - 5 and the procedure is documented in flow-charts 1 and 2.

LIST OF FIGURES

LIST OF SYMBOLS

Symbol	Meaning
A	Interfacial area
A_P	Interfacial area in permanent contact mode
A_T	Interfacial area in transitoric contact mode
A_{Pr}	Surface area of particle
A_T	Injected interfacial area per unit time
B_P	Permanent contact parameter $= \frac{\beta_P A_P}{V_m} t_{inj}$
B_T	Transitoric contact parameter $= \frac{\beta_T A_T}{V_m} t_{inj}$
C_D	Drag coefficient
$C_N{}^{3-}$	Nitride capacity
C_P	Phosphorus capacity
C_S	Sulphide capacity
D_x	Diffusivity of solute x in the melt
E	Transitoric efficiency parameter
H	Bath depth (Cm)
H_o	Lance immersion depth (Cm)
N_{Re}	Reynolds number
N_{Sh}	Sherwood number
N_{Sc}	Schmidt number
N_{Pe}	Peclet number
K	Equilibrium constant
K_P	Permanent rate constant (min^{-1})
K_T	Transitoric rate constant (min^{-1})
M_i	Atomic or molecular wt. of component i
P_{atm}	Atmospheric pressure

P_{Fe}	Ferrostatic pressure
Q_B	Cuvic per flow rate (Nm^3/min)
R	Total rate
R_P	Permanent contact rate
R_T	Transitoric contact rate
T	Operating temperature (deg. K)
V_{Pr}	Volume of particle
V_m	Volume of the melt
X_i	Mole fraction of component i
Y_C	Mass fraction of carry-over slag to melt
Y_S	Mass fraction of synthetic flux to melt
$a_{\underline{Al}}$	Activity of dissolved Al in the melt
$a_{\underline{N}}$	Activity of dissolved Nitrogen in the melt
$a_{\underline{S}}$	Activity of dissolved Sulphur in the melt
d_C	Dia of reactor (Cm)
d_P	Dia of particle
f	transitoric rate contribution parameter
$f_{\underline{N}}$	Activity coefficient of nitrogen in the melt
$f_{\underline{P}}$	Activity coefficient of Phosphorus in the melt
$f_{\underline{S}}$	Activity coefficient of Sulphur in the melt
g	Acceleration due to gravity
m_C	Mass of carry-over slag
m_L	Mass of the melt
m_S	Mass of synthetic flux
$\dot{m}_S$	Mass flow rate of synthetic flux
n_{slag}	Number of moles of slag phase
P_{N_2}	Partial pressure of Nitrogen

p_{O_2}	Partial pressure of Oxygen
p_{S_2}	Partial pressure of Sulphur
r	Radius of particle or droplet
t	Time
t_{inj}	Injection time
t_R	Residence time
u_T	Terminal velocity of the particle or droplet
u_Z	Plume velocity
$[x]$	Concentration of solute x in the melt (wt%)
(x)	Concentration of solute x in the slag (wt%)
$[x_o]$	Initial concentration of x in the melt (wt%)
(x_P)	Concentration of x in the accumulated slag (wt%)
(x_T)	Concentration of x in the rising flux (wt%)
α	Dimensionless melt concentration = $[x]/[x_o]$
β	Mass transfer coefficient
β_m	Metal side mass transfer coefficient
β_P	Mass transfer coefficient in permanent contact reaction
β_S	Slag side mass transfer coefficient
γ_i	Activity coefficient of compoent i
ε	Stirring energy (W/T)
η^*	Partition coefficient
η_S^*	Partition coefficient of injected flux
η_N^*	Partition coefficient of injected flux (Nitrogen)
η_P^*	Partition coefficient of injected flux (Phsophorus)
η_{Su}^*	Partition coefficient of injected flux (Sulphur)
(η_o^*)	Overall top slag partition coefficient
$(\eta_o^*)_{av}$	Average top slag partition coefficient

θ_S	$(B_P/\lambda_S) / (1+B_T/\lambda_S \cdot f)$
λ_S	$\eta_S^* \gamma_S$
μ_c	Viscocity of continuous phase
μ_d	Viscocity of discontinuous phase
ρ_C	Density of continuous phase
ρ_m	Density of melt
τ	Dimensionless time - t/t_{inj}
τ_{av}	Average dimensionless time
ϕ_S	$(B_P+B_T) / (1 + \frac{B_T}{\lambda_S} f)$
Λ	Optical basicity

CHAPTER 1

INTRODUCTION

A tremendous increase in the interest and development of refining processes by injection metallurgy, including powder and gas injection, has found growing acceptance since it calls for quicker processing at reasonable reaction efficiency for a wider span of heat size. This is to meet the demands for high quality products like pipe line steels. Applications of injection metallurgy are mostly found in steel processing units. Therefore, a brief review on physical metallurgy of impurities, with respect to sulphur, phosphorus and nitrogen in steel is required.

1.1 Physical Metallurgy of Impurities (S, P, N,) in Steels:

Increasing demand of steel materials for more stringent applications have called for much efforts to decrease impurity elements to extra-low concentrations. For example extra-deep drawing high tensile strength strip, super-ferritic stainless steel strip, hydrogen-induced-crack (HIC) and sulphide-stress-corrosion- crack (SSCC) resistant high tensile strength plate and pipe, Cr-Mo pressure vessel plate, 9% Ni plate for cryogenic temperature service etc.

Generally impurities present either as dissolved in the matrix, often not uniformly distributed but enrich to certain structural features like grain boundaries, or in the form of NMI.

1.1.1 Sulphur:

Except in free machining steels, sulphur is the highly undesirable element in steels. It has been so well known that sulphur causes hot-shortness when the steel is forged or rolled at elevated temperature by forming low melting point eutectic alloy i.e., FeS at the grain boundaries. It also deteriorates the ductility of steel materials via precipitation during solidification of and deformation during rolling of manganese sulphides and pitting corrosion in Austenitic stainless steels.

Among the properties relevant to represent the ductility, shelf energy at low temperature and reduction of area (RA) in through thickness direction are most markedly influenced by the sulphur. For example in heavy reactor pressure vessel plates used in nuclear power plant, the shelf energy in V-notch charpy test improves from 19 to 22 Kgf-m with the decrease of sulphur from 60 to 30 ppm [1]. The values of RA in through-thickness direction of lamellar tear resistant carbon steel plate linearly go up as sulphur reduces from 50 to 20 ppm when dissolved oxygen falls in between 10 to 20 ppm [2].

The most important problems with sulphur in hydrogen environment is the formation of HIC and SSCC. Formation of HIC and SSCC have been well known in HSLA steels used for pipe lines. Effective measures to prevent their formation is to control both the sulphur concentration in the melt and the shape of sulphide inclusions.

SSCC is also caused by the pitting corrosion often observed in Austenitic stainless steels. Origin of pitting corrosion is located to be NMI among which manganese sulphides are most harmful. It was confirmed that pitting potential of 18% Cr - 8% Ni steel increases when steel composition is changed from 1.0% Mn and 50 ppm S to 0.2% Mn and ≤ 10 ppm S [3].

Thus for high quality steel sulphur should be kept as low as possible.

1.1.2 Phosphorus:

Next to sulphur, phosphorus is the undesirable element in steels. It has the tendency to segregate to grain boundaries. It has been so well known to deteriorate ductility of steel material, thereby increasing the tendency of steel when cold worked, making it cold-short. It also known to cause temper embrittlement, HIC, Stress-Corrosion-Cracking (SCC) etc.

Steel materials most sensitive to phosphorus is 9% Ni steel plate used for cryogenic temperature service. Even very low concentrations of phosphorus make 9% Ni steel susceptible to temper embrittlement and deteriorate low temperature ductility. Even for air cooled specimen more than 5 Kgf-m absorbed energy at $-196^{\circ}C$ is gained by decreasing phosphorus from 130 to 80 ppm. Similarly crack opening displacement (COD) also improve from 0.06 to 0.2 as phosphorus decreases from 80 to 10 ppm, for the furnace cooled specimen [2]. Temper embrittlement of low carbon Ni-Cr-Mo steels will be appreciably deteriorated by phosphorus. Forged

plates of these steels show improvement in ductile to brittle transition temperature is improved from 100°C to 0°C at 0.3% Si and 50 to -75°C at 0.02% Si by decreasing phosphorus from 150 to 20 ppm [4]. Similarly by decreasing phosphorus from 170 to 60 ppm notch toughness of reactor pressure vessel plate in nuclear power plant can be improved from -150 to -175°C. In all these grades of steels decrease of phosphorus decreases intergranular segregation and hence improves their granular embrittlement, contributing to increased ductility of steels.

Similar to sulphur phosphorus also causes HIC of HSLA steels used for line pipes to transport sour gas and air. In case of sulphur the culprit was shape of sulphides, whereas in case of phosphorus local enrichment of phosphorus. If the steels are to be free from HIC, phosphorus must be less than 0.1% for Mn of 2.2%. The same threshold values are applicable to prevent the formation of SCC in this grade of steel [2].

Transgranular SCC susceptibility of the austenitic stainless steels is extremely improved by decreasing phosphorus from 100 to 20 ppm.

Besides low temperature properties of steels, it also deteriorates hot ductility of steels especially when the concentration is above 100 ppm. The embrittlement at P > 100 ppm is due to the formation of liquid film or brittle eutectic phosphide at austenitic grain boundaries. The remedy is to decrease phosphorus below 100 ppm and/or cooling the strand cast

slabs in the secondary cooling zone at slower rate to avoid segregation of phosphorus.

Therefore decrease of phosphorus to very low levels (tenth order ppm) is essential to produce high quality steels.

1.1.3 Nitrogen:

For steel products like deep drawn steels and line pipes very low concentration of nitrogen in steel is required, since affects yield point elongation, ductility, and corrosion of steels.

Decrease in nitrogen is effective to prevent yield point phenomenon, a drop of elongation to fracture, When nitrogen is decreased from 80 to 20 ppm the sharp increase in the ductility of weld bonds of Al- killed steel plate was observed [2].

Presence of nitrogen (and carbon) causes intergranular corrosion of super ferritic stainless steel strips. Their limiting value decrease as the concentration of Cr increases. For example 130 ppm of Ni+C for 26% Cr and 80 ppm for 30% Cr steel. Such mal-influence of nitrogen (and carbon) is due to the formation of Cr-depleted zone around the intergranularly precipitated chromium carbonitrides.

The decrease of nitrogen to extra-low concentrations helps considerably improving yield point elongation, elongation to fracture and pitting corrosion of steels.

The demand for the production of high quality steel materials changed the philosophy of steelmaking. Powder injection is being increasingly employed by the steel industry since it involves less

investment, is easy to operate and facilitates quicker processing at reasonable reaction efficiency for a wide span of heat sizes. Despite its growing acceptance, the kinetics of refining processes are poorly understood. The kinetics have a direct impact on the quality of the product and the cost of production, because the particles reside in the melt for very less time say of the order of 1 sec or so. Thus the identification of process variables is necessary to study the kinetics of powder injection refining.

1.2 Literature Survey

Usually sulphur and phosphorus are removed from steels via slag/metal reactions, whereas Nitrogen removal is done by degassing. But there have been several reports of Nitrogen removal from steel by the addition of flux and to regard nitrogen removal as one of the slag/metal reactions. Slag/metal reactions of interest are desulphurisation (hereafter termed as DeS), dephosphorisation (hereafter, termed as DeP) and denitronization (hereafter termed as DeN).

The efficiency of slag/metal reactions depends on how good the metal and slag are in contact with each other. The following are the types of contact modes of slag with metal.

(i) Permanent contact

(ii) Transitoric contact

(iii) Counter current contact

Schenck [5] defined the removal without relative movement of the phases as permanent phase contact and with relative movement

of the phases as transitoric phase contact or counter current flow process. In transitoric phase contact only one phase is mobile, whereas in counter current flow process both phases move in opposite direction to each other.

These three contact modes are schematically shown in Fig. 1.1, Fig. 1.2 and Fig. 1.3. The contact modes of interest are (i) and (ii) only.

As the production of high quality steels require decrease of impurity to low concentrations, powder injection refining is being widely employed in steel industry. In the plant as well as laboratory scale sufficient experimental work was done in the powder injection, refining. In the literature powder injection refining was purely correlated to the transitoric contact mode. But practically the top slag formed from the injected flux is not removed. Hence its influence on the powder injection refining is to be considered. Only Robertson et al. [6] take into account the top slag contribution in the powder injection refining process via permanent contact reaction. Although these are two more reference ([7],[8]) on powder injection taking into account the top slag influence on the kinetics of refining, they are based on Robertson et al, work.

In spite of the development of powder injection refining process, it is still unexplained whether permanent contact mode or transitoric contact mode dominates the process. Although Robertson et al., tried to describe the powder injection refining

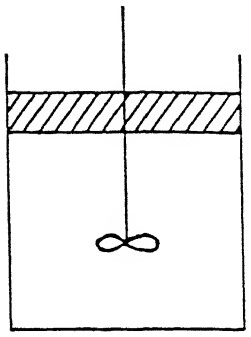

Fig. 1.1 Permanent contact mode

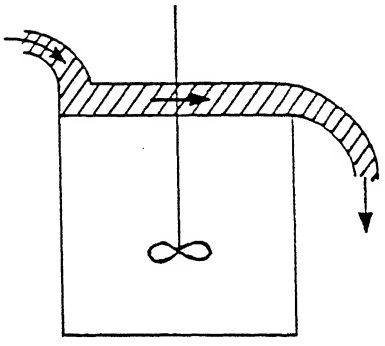

Fig. 1.2 Transitoric contact mode

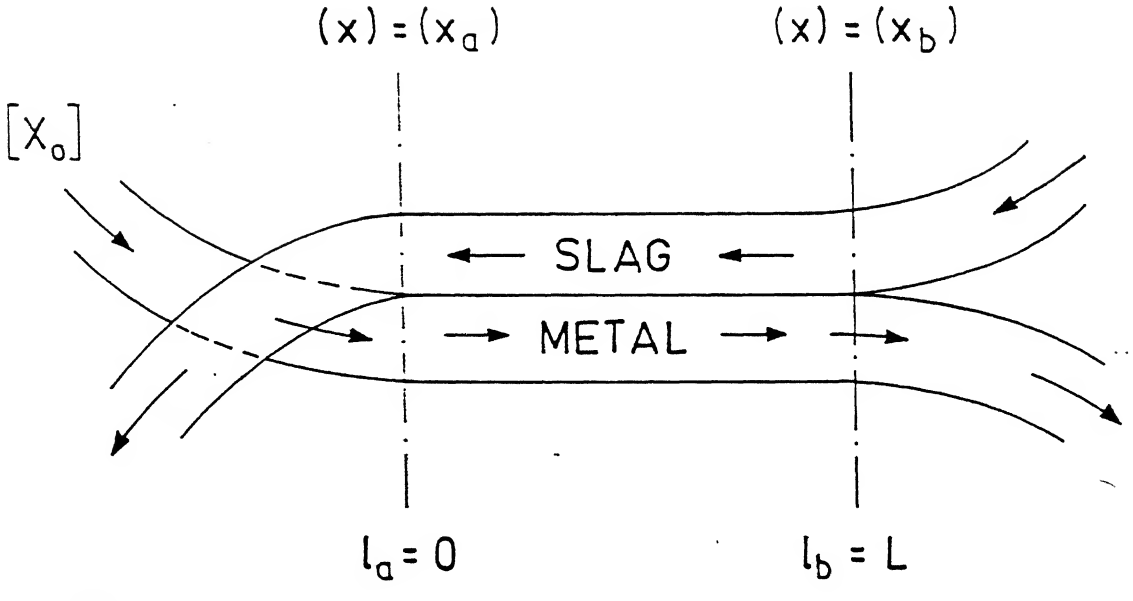

Fig. 1.3 Counter-current contact mode

via a mathematical model, the effect of injection variables were not described explicitly. The solution method they specified is FDM. This model requires the prefixing of permanent rate constant i.e., Kp value, Robertson et al., assumed a Kp value to fit their experimental data in the model. In the Ref. [7] and [8] Kp was prefixed by the permanent contact mode experiments.

In Robertson et al., model the experimental points can be fitted by many number of combinations of Kp and E. (Kp and E are the two variable in their model). Thus when Kp is assumed to be certain value, some value of E will be obtained by fitting the experimental data points in the model. There are also some works where Kp value is fixed by assuming weak agitation and strong agitation [9]. Despite the uncertainty in the determination of critical agitation (or stirring energy) assumption of weak agitation and strong agitation and there by fixing the Kp value involve more uncertainty in the validity of the results.

In the process of metal holding in a ladle resulphurisation and rephosphorisation, i.e, reversion of sulphur and phosphorus from slag to steel are reported [9],[10].

The sources of resuphurisation and rephosphorisation are

(a) carry-over slag from the previous refining unit

(b) erosion of ladle lining

The effect of carry-over slag on slag/metal refining is more prominant then the erosion of ladle lining because of the improvement in the quality of ladle lining refractories. Although

use of devices such as refractory sphere, slide gate etc, and EBT (Eccentric Bottom tapping) in EAF control slag carry-over in the ladle, but can not eliminate it completely. E.T. Turkdogan discussed the reactions that occur between liquid steel and slag in the ladle [10]. But the discussion is confined to theoretical considerations only. He presented the effect of furnace slag carry-over on the recovery of Al added and rephosphorisation in the tap ladle. In the ref [9] resulphurisation due to FeO contact of the overall slag is presented.

The experimental conditions of powder injection as well as dumping (or permanent contact mode) are compiled from literature and are presented in Table 1.1 and Table 1.2 for hot-metal and steel respectively. The data from their tables is used in the following chapter to obtain the range of variation of powder injection parameters like loading ratio, stirring energy etc.

1.3 Aim of the Present work:

The present work is aimed at

(i) The development of a mathematical model to obtain melt concentration as a function of time.

(ii) The study of various parameters on transitoric mode of contact contribution and the conditions under which permanent or transitoric contact mode dominate the refining process.

CHAPTER 2

MODEL DESCRIPTION

In this chapter the basis for model formulation and the numerical solution procedure for the governing differential equations with slag carry-over from BOF and without slag carry-over, the significance of model parameters and the selection of equations are presented.

2.1 Basis for Model Formulation:

In slag/metal refining processes required amount of slag forming materials are either added to the top surface of the molten metal or injected directly into the bath at some injection rate. Out of these two types of additions, powder injection is being increasingly employed by the steel industry since it facilitates quicker procesing of wide span of heat sizes and high recovery of vaporizing fluxes Like CaC_2, CaSi etc. Usual slag forming materials are mixtures of either CaO, $CaSi_2$, Al_2O_3, CaF_2 or calcium based compounds such as CaC_2, CaSi, CaAl or magnesium and or sodium carbonate and lime or calcium carbonate and lime. Inspite of its increasing applications, the kinetics of powder injection refining processes are poorly understood. The kinetics have a direct impact on the quality of the product and the cost of production because the injected particles reside in the melt for very less time say 1 sec or so. Thus to maximize the extent of refining, refining rate and the reagent utilization, the effect of operating variables such as solid flow rate, gas flow rate, type

of flux etc., must be clearly understood.

Thus the present model is developed to study the kinetics of slag/metal reactions caused by the injection of slag forming materials with carrier gas via a lance submerged into the molten bath. The gas-particle mixture penetrates into the melt until their momentum is dissipated. The powder particles detach from the gas and disperse into the bath, and the particles start to rise to the top surface of the bath because they are buoyant. The carrier gas due to byoyancy effect accelerates rapidly. The drag force between gas and liquid causes the stirring in the bath. The accumulated injected flux on the top surface of the melt is not removed in powder injection processes. All these events are shown in Fig. 2.1. The physico-chemical characteristics of the resultant top slag would depend on whether there is slag present on the top of molten metal prior to start of the powder injection or not. Such slag may be carried over from the previous steelmaking unit eg. BOF. In the absence of slag carry-over the characteristics of the resulting top slag and injected flux are same. The accumulated top slag also takes part in the refining process.

The removal of an impurity from metal can occur during the rise of slag particles and by the slag which is accumulating on the bath surface. The former mode of impurity removal is transitoric whereas the later is permanent mode. Thus the total rate of impurity removal in case of powder injection can be

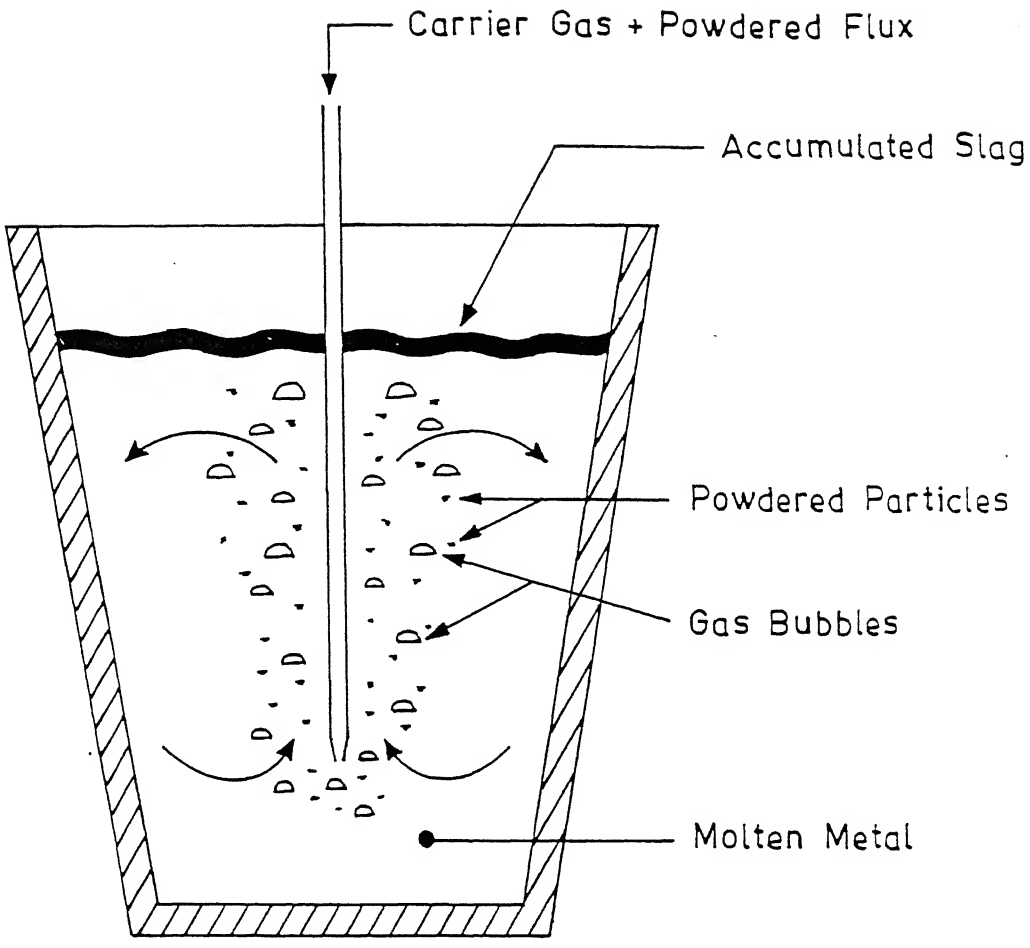

Fig. 2.1 Schematic model of powder injection refining

expressed by

$$R = R_T + R_P \qquad (2.1)$$

Where R_T is rate of removal of impurity during the rise of powder particles and R_P is the rate due to accumulated slag.

Usually the slag-metal reaction rate is expressed by the mass transport controlled first order rate equation

$$-\frac{d[x]}{dt} = \frac{1}{\left[\frac{1}{\beta_m} + \frac{1}{\eta_S^* \beta_S}\right]} \frac{A}{V} \left\{[x] - \frac{(x)}{\eta_S^*}\right\} \qquad (2.2)$$

Equation (2.2) contain two mass transport steps in series, one from the metal to slag interface, and the other into the bulk of the slag from the interface.

Although the ratio of β_m to β_S is 5-10, use of high partition coefficient slags (η_S^* = 100-2000) in refining processes makes $1/\eta_S^*\beta_S$ much smaller than $1/\beta_m$. Thus we can make the assumption that metal side mass transfer resistance is the rate controlling step. Therefore the equation (2.2) can be rewritten by using $\beta_m = \beta$

$$-\frac{d[x]}{dt} = \beta \frac{A}{V} \left\{[x] - \frac{(x)}{\eta_S^*}\right\} \qquad (2.3)$$

This is the general form of mass transfer equation applicable to the rate of removal of impurity whenever slag is contacted with the metal. Using equations (2.1) and (2.3) the following mass transfer equation in case of powder injection can be derived.

$$-\frac{d[x]}{dt} = \frac{\beta_T A_T}{V_m}\left\{[x] - \frac{(x_T)}{\eta_S^*}\right\} + \frac{\beta_P A_P}{V_m}\left\{[x'] - \frac{(x_P)}{\eta_S^*}\right\} \qquad (2.4)$$

where $[x'] = [x] - \frac{(x_T)}{\eta_S^*}$ (2.5)

A_T is the interfacial area for transitoric reaction and can be determined by powder size and powder injection rate because the components of the powder are assumed to be non-volatile and do not dissolve in the melt during its entire refining period.

A_P is the interfacial area for the permanent reaction which depends on bath stirring intensity produced by the carrier gas when it leave the melt. When emulsification of top slag into the melt occurs, A_P depends on the mass of slag emulsified and the drop size. In the absence of emulsification the interfacial area available for the reaction is simply the cross-sectional area of the melt container or the ladle.

Concentration of impurity in the top slag at any instant of time is given by

$$(x) = (x_T) + (x_P) \qquad (2.6)$$

Combining equations (2.4), (2.5) and (2.6), we get

$$-\frac{d[x]}{dt} = \frac{\beta_T A_T}{V_m}\left\{[x] - \frac{(x_T)}{\eta_S^*}\right\} + \frac{\beta_P A_P}{V_m}\left\{[x] - \frac{(x)}{\eta_S^*}\right\} \qquad (2.7)$$

The mass balance equation are

$$\dot{m}_S(x_T) = -\,m_L \frac{d[x]}{dt}\bigg|_T \qquad (2.8)$$

$$\dot{m}_S t(x) = m_L \Delta x = m_L \left[[x_o] - [x] \right] \qquad (2.9)$$

Equation (2.8) is the mass balance equation for the rising flux. Equation (2.9) is the mass balance equation for the resulting top slag and implies that the decrease in total impurity concentration in the melt is equal to increase in impurity concentration in the accumulated slag.

By putting equations (2.8) and (2.9) into (2.7), we get

$$-\frac{d[x]}{dt} = \frac{\beta_T A_T}{V_m} \left\{ [x] + \frac{1}{\eta_S^* \frac{m_S}{m_L}} \frac{d[x]}{dt}\bigg|_T \right\} + \frac{\beta_P A_P}{V_m} \left\{ [x] - \frac{[x_o]-[x]}{\eta_S^* \frac{m_S}{m_L} \frac{t}{t_{inj}}} \right\} \qquad (2.10)$$

Defining the variables

$$\left.\begin{aligned} \lambda_S &= \eta_S^* \frac{m_S}{m_L} = \eta_S^* Y_S \\ K_P &= \frac{\beta_P A_P}{V_m}, \qquad K_T = \frac{\beta_T A_T}{V_m} \\ B_P &= \frac{\beta_P A_P}{Vm} t_{inj}, \quad B_T = \frac{\beta_T A_T}{V_m} t_{inj} \\ \tau &= \frac{t}{t_{inj}}, \quad \alpha = \frac{[x]}{[x_o]} \end{aligned}\right] \qquad (2.11)$$

and substituting them into equation (2.10), we get

$$-\frac{d\alpha}{d\tau} = \alpha \left\{ \frac{B_T + B_P \left[1 + \frac{1}{\lambda_S \tau}\right]}{1 + \frac{B_T}{\lambda_S} f} \right\} - \frac{B_P/\lambda_S}{\left[1 + \frac{B_T}{\lambda_S} f\right]} \qquad (2.12)$$

where

$$f = \left\{ \left[-\frac{d\alpha}{d\tau} \right] \Big|_{\tau} \right\} \Big/ \left\{ -\frac{d\alpha}{d\tau} \right\} \qquad (2.13)$$

is the transitoric rate contribution in the overall powder injection refining process.

Defining $\phi_s = \dfrac{B_t + B_p}{\left[1 + \dfrac{B_T}{\lambda_S} f\right]}$ and $\theta_S = \dfrac{B_P / \lambda_S}{\left[1 + \dfrac{B_T}{\lambda_S} f\right]}$ (2.14)

and substituting them into equation (2.12), we get

$$\frac{d(\alpha-1)}{d\tau} + (\alpha - 1)\left\{\phi_S + \frac{\theta_S}{\tau}\right\} = -\phi_S \qquad (2.15)$$

Equation (2.15) is the governing differential equation describing the decrease of impurity with time in powder injection refining without slag carry-over from BOF.

3.1.2 With Carry-over Slag:

In most cases there occurs some carry-over of slag while transferring molten steel from the steelmaking unit into the ladle in which further powder injection refining is planned to be performed. The carry-over slag is normally oxidizing in nature and is a mixture of CaO, SiO_2, Al_2O_3, P_2O_5, MnO, FeO, MgO etc. When powdered flux is injected into the molten bath, on its rise to the top surface of the melt it will be mixed into the already existing top slag. As both top slag and powdered flux are of different composition the overall top slag composition changes through-out the injection period. Thus the partition coefficient of the resultant top slag is different from that of the injected flux. Indicating top slag partition coefficient as η_o^*, equation (2.7) can be modified as

$$-\frac{d[x]}{dt} = \frac{\beta_T A_T}{V_m}\left\{[x] - \frac{(x_T)}{\eta_S^*}\right\} + \frac{\beta_P A_P}{V_m}\left\{[x] - \frac{(x)}{\eta_o^*}\right\} \qquad (2.16)$$

The masws balance equations are

$$\dot{m}_S(x_T) = -\, m_L \frac{d[x]}{dt}\bigg|_T \qquad (2.8)$$

$$(\dot{m}_S t + m_C)(x) = m_L \Delta x = m_L\left[[x_o] - [x]\right] \qquad (2.17)$$

Defining $Y_C = \dfrac{m_C}{m_L}$ (2.18)

Putting equation (2.8), (2.11), (2.17) and (2.18) in (2.16), we get

$$-\frac{d\alpha}{d\tau} = \alpha\,\frac{\left\{B_T + B_P\left[1 + \dfrac{1}{\eta_o^*\,(Y_S\tau + Y_C)}\right]\right\}}{\left[1 + \dfrac{B_T}{\lambda_S} f\right]} - \frac{\dfrac{B_P}{\eta_S^*\,(Y_S\tau + Y_C)}}{\left[1 + \dfrac{B_T}{\lambda_S} f\right]} \qquad (2.19)$$

Substituting (2.14) into (2.19), we get

$$\frac{d(\alpha-1)}{d\tau} + \left\{\phi_S + \frac{\theta_S}{\tau}\left[\frac{1}{\dfrac{\eta_o^*}{\eta_S^*}\left[1 + \dfrac{Y_C}{Y_S\tau}\right]}\right]\right\}(\alpha-1) = -\phi_S \qquad (2.20)$$

Equation (2.20) is the governing differential equation for concentration change of the impurity in the melt with time during the powder injection when slag is carried-over from BOF prior to start of the injection. In the absence of slag carry-over $Y_C = 0$ and $\eta_o^* = \eta_S^*$; thus the equation (2.20) will be reduced to equation (2.15).

To solve differential equations (2.15) and (2.20) the following assumption is must i.e., the melt concentration is

uniform in the bulk metal.

2.2 Solution Procedures:

In equation (2.15) time dependent variable is only α, where as in equation (2.20) there are two time dependent variables i.e, α and η_o^*. Analytical solution for equation (2.15) can be obtained. But the presence of two time dependent variables in equation (2.20) forced to adapt numerical solution method.

2.2.1 Without Slag Carry-over:

The form of differential equation (2.15) is very much similar to that of Leibnitz's linear equation

$$\frac{dy}{dx} + Yf(x) = C \qquad (2.21)$$

Standard solution for equation (2.21) is available and can be obtained from any standard mathematics book. Due to their similarity in the form of differential equation, solution of equation (2.21) can be used to get the general solution for equation (2.15). The detailed solution is given in Appendix 1, and the final solution is

$$\alpha = 1 - (\phi_S \tau) \exp(-\phi_S \tau) \sum_{m=0}^{\infty} \frac{(\phi_S \tau)^m}{m!(1 + \theta_S + m)} \qquad (2.22)$$

The summation series in equation (2.22) is convergent type and the maximum number of terms required would depend on the magnitude of B_T as per the following equation

$$N \ln \left[\frac{B_T}{1 + \frac{B_T}{\lambda_S}} \right] - \ln (N + 1)! = -7.601 \qquad (2.23)$$

[N = maximum number of terms]

upto the third decimal accuracy.

For example when $\left[\frac{B_T}{1 + \frac{B_T}{\lambda_S}}\right] = 2$, the maximum number of terms to be considered in the summation series of equation (2.21) are 9.

2.2.2 With Slag Carry-over:

To integrate the equation (2.20), equation of η_o^* as a function of time must be available. But it is impossible to get single correlation of η_o^* as a function of time for all types of slags. But it is possible to evaluate η_o^* in time steps with the knowledge of mass flow rate of flux, composition of injected flux and top flux composition at the beginning of injection process. The suitable solution procedure is FDM. The available methods to solve equation (2.20) are

(a) Implicit FDM

(b) Explicit FDM

(c) Crank-Nicholson's FDM

Out of these three solution procedures, Crank-Nicholson's FDM is chosen to solve equation (2.20). Detailed solution is given in Appendix 2.

The final solution is

$$\alpha_{j+1} = 1 - (1-\alpha_j)\left[\frac{1-T}{1+T}\right] - \frac{\phi_S \Delta\tau}{1+T} \qquad (2.24)$$

Where

$$T = \frac{\Delta\tau}{2}\left\{\phi_S + \theta_S \frac{\eta_S^*}{[(\eta_o^*)_{av}]_{j+1}\left[(\tau_{av})_{j+1} + \frac{Y_C}{Y_S}\right]}\right\}$$

$$(\tau_{av})_{j+1} = \frac{\tau_{j+1} + \tau_j}{2} \qquad (2.25)$$

$$\left[(\eta_o^*)_{av}\right]_{j+1} = \frac{(\eta_o^*)_{j+1} + (\eta_o^*)_j}{2} \; ; \; \Delta\tau = \text{Time Step}$$

2.3 Approximations From General Solution:

Approximations, under the given conditions, are necessary to avoid unnecessary calculations. Once general solution is obtained it is easy to make approximations from it.

2.3.1 $B_T \rightarrow \infty$

i.e. $\frac{\beta_T A_T}{V_m} t_{inj} \rightarrow \infty$

As β_T, V_m and t_{inj} are finite, the extreme condition $B_T \rightarrow \infty$, is equivalent i.e. injection of fine powders at higher mass flow rate. By putting this condition in equation (2.14) one can get $\phi_S = \lambda_S$ and $\theta_S = 0$ and the equation (2.22) will be reduced to

$$\alpha = \exp(-\lambda_S \tau) \qquad (2.26)$$

2.3.2 $\lambda_S \rightarrow \infty$

i.e., either $\eta_S^* \rightarrow \infty$ or $Y \rightarrow \infty$

Thus the condition can be understood in terms of use of either higher partition coefficient flux or large amount of flux. By adding this condition to equation (2.14), $\phi_S = B_T + B_P$, $\theta_S = 0$. Hence equation (2.22) will be approximated to

$$\alpha = \exp\left[-(B_P + B_T)\,\tau\right] \qquad (2.27)$$

2.3.3 Equilibrium Concentration at each τ:

(i) At equilibrium, Rate = 0 i.e., $-\frac{d\alpha}{d\tau} = 0$

(ii) Equilibrium can be achieved through the resulting top slag only i.e., at each τ equilibrium concentration can be calculated by putting $B_T = 0$

From equation (2.12) by substituting equilibrium condition

$$\alpha_{eq} = \frac{1}{1+\lambda_S\tau} \qquad (\tau \leq 1) \qquad (2.28)$$

If $\tau \geq 1$, $\tau = 1$

$$\alpha_{eq} = \frac{1}{1+\lambda_S} \qquad (2.29)$$

2.4 Selection and Significance of Parameters:

From equation (2.24)

$$\alpha = \alpha\,(\phi_S,\ \theta_S,\ \tau,\ \eta_o^*,\ Y_C) \qquad (2.30)$$

From equation (2.14) and (2.11)

$$\phi_S = \phi_S(\beta_T,\ A_T,\ \beta_P,\ A_P,\ V_m,\ \eta_S^*,\ Y_S,\ t_{inj},\ f) \qquad (2.31)$$

$$\theta_S = \theta_S(\beta_T,\ A_T,\ \beta_P,\ A_P,\ V_m,\ \eta_S^*,\ Y_S,\ t_{inj},\ f) \qquad (2.32)$$

$$\tau = \beta(t_{inj}) \qquad (2.33)$$

In Appendix - 3 detailed description of f is given. Dependency of transitoric rate contribution in the overall process of refining is given by

$$f = f(\beta_T,\ A_T,\ \beta_P,\ A_P,\ V_m,\ \eta_S^*,\ Y_S) \qquad (2.31)$$

Usually t_{inj}, Y_C, Y_S, V_m are specific to a system. Thus the parameters to be evaluated are η_S^*, β_T, A_T, β_P, A_P. In the following sections selection of equation for each parameter as a

function of process variables is done.

2.4.1 Partition Coefficient of the Slag/Metal System:

Partition coefficient characterizes the state of the dynamic equilibrium with respect to the transferring entity. At equilibrium partition coefficient attains a maximum value and would depend upon the composition of slag and melt, and the operating temperature of the system. The transferring entities under consideration in the present study are sulphur, phosphorus and nitrogen. Hence the partition coefficient for the above entities are given below.

Partition coefficient of the impurity is defined as the ratio of solute (or transferring entity) concentration in the slag to that in the melt.

$$\eta^{*} = \frac{(x)}{[x]} \qquad (2.35)$$

2.4.1.1 Sulphur:

Sulphur distribution between molten metal and slag can be represented by an electrochemical reaction

$$\underline{S} + (O^{2-}) \Leftrightarrow (S^{2-}) + \underline{O} \qquad (2.36)$$

Equation (2.36) can be written as the combination of

$$\frac{1}{2}\{S_2\} + (O^{2-}) \Leftrightarrow (S^{2-}) + \frac{1}{2}\{O_2\} \qquad (2.37)$$

$$\frac{1}{2}\{S_2\} = \underline{S} \qquad (2.38)$$

$$\underline{O} = \frac{1}{2}\{O_2\} \qquad (2.39)$$

For equation (2.37) sulphide capacity is defined as

$$C_S = (\text{wt\% S}) \sqrt{\frac{P_{O_2}}{P_{S_2}}} \qquad (2.40)$$

$$K_{(2.34)} = a_{\underline{S}} / \gamma P_{S_2} \quad (2.41)$$

$$K_{(2.35)} = \gamma P_{O_2} / a_{\underline{O}} \quad (2.42)$$

Putting equations (2.41) and (2.42) in (2.40)

$$C_S = (wt\%S) \frac{a_{\underline{O}}}{a_{\underline{S}}} \cdot K_{(2.34)} K_{(2.35)} \quad (2.43)$$

From the definition of partition coefficient $\eta^*_{Su} = \frac{(\%S)}{[\%S]}$ (2.44)

Combining equations (2.43) and (2.44)

$$C_S = \eta^*_{Su} \frac{a_{\underline{O}}}{f_{\underline{S}}} K_{(2.34)} K_{(2.35)} \quad (2.45)$$

$$\log \eta^*_{Su} = \log C_S - \log \left[\frac{a_{\underline{O}}}{f_{\underline{S}}}\right] - \left[\log K_{(2.34)} + \log K_{(2.35)}\right] \quad (2.46)$$

$\log K_{(2.34)} + \log K_{(2.35)}$ is given by $\frac{936}{T} - 1.375$ and thus equation (2.46) becomes

$$\log \eta^*_{Su} = \log C_S - \log \left[\frac{a_{\underline{O}}}{f_{\underline{S}}}\right] - \frac{936}{T} + 1.375 \quad (2.47)$$

C_S is strong function of composition of slag system. Basic slags have high C_S. Thus from equation (2.47) the favourable conditions for deS are drawn to be

→ high slag basicity

→ low $a_{\underline{O}}$ or reducing atmosphere

Due to low concentration of solute elements or dissolved elements in the mild steel grade $f_{\underline{S}}$ can be taken as 1, where as in hot metal it is evaluated to be nearly 3.

In the literature several correlations are given for sulphide capacity evaluation as a function of slag composition and temperature. All of them are listed in Table 2.1.

Equation (2) in Table 2.1 employs optical basicity concept.

Optical basicity of slag system can be evaluated by the following equation:

$$\Lambda = \frac{\left[aX_{A_xO_a}\Lambda_{A_xO_a} + bX_{B_yO_b}\Lambda_{B_yO_b} + .. \right] + \left[CX_{CF_C}\Lambda_{CF_C} + dX_{DF_d}\Lambda_{DF_d} \right]}{\left[aX_{A_xO_a} + bX_{B_yO_b} + \ldots \right] + \left[CX_{CF_d} + dx_{DF_d} + \ldots\ldots \right]} \quad (2.48)$$

where X = Mole fraction of oxide or fluoride

a,b,..c,d...., ..= Oxidation numbers

Λ_i = Optical basicity of oxide or fluoride given in Table 2.2.

Activity of oxygen is controlled by the type and amount of deoxidizer. To reduce soluble oxygen to very low level and to have low deoxidizer conccontration in the melt a strong deoxidizer must be added. Normally Al is used to reduce the level of oxygen. Thus in equation (2.47) $a_{\underline{O}}$ can be correlated to the Al in the melt by the reaction

$$2\underline{Al} + 3\underline{O} \Leftrightarrow \langle Al_2O_3 \rangle \quad (2.49)$$

$$\log K_{(2.45)} = \frac{64900}{T} - 20.63 \quad (2.50)$$

In equation (2.49) it is assumed that the melt is in equilibrium with the suspended Al_2O_3 particles, i.e. $a_{Al_2O_3}=1$. By putting the $a_{\underline{O}}$ evaluated from equation (2.50) in the equation (2.47) the following equation

$$\log \eta^*_{Su} = \log C_S + \frac{2}{3}\log\left[\frac{a_{\underline{Al}}}{f_{\underline{S}}}\right] + \frac{20697.3}{T} - 5.5 \quad (2.51)$$

can be obtained.

In case of carbon saturated iron $a_{\underline{O}}$ is approximately equal to 6×10^{-5}.

The optical basicity correlation (Equation (2) in Table 2.1) is used in this work to evaluate sulphide capacity and thus sulphur partition coefficient by equation (2.51).

2.4.1.2 Phosphorus:

Phosphorus distribution between molten metal and slag can be represented by an electrochemical reaction

$$\underline{P} + \frac{5}{2}\underline{O} + \frac{3}{2}(O^{2-}) = (PO_4^{3-}) \qquad (2.52)$$

Phosphorus capacity for the above reaction (2.52) is usually given by

$$C_P = \frac{(\%P)}{a_{\underline{P}} \cdot a_{\underline{O}}^{5/2}} \qquad (2.53)$$

From the definition of partition coefficient

$$\eta_P^* = (\%P)/[\%P] \qquad (2.54)$$

Combining equation (2.53) and (2.54)

$$\log \eta_P^* = \log C_P + \frac{5}{2} \log a_{\underline{O}} + \log f_{\underline{P}} \qquad (2.55)$$

$\log f_{\underline{P}}$ = 0 for mild steels

= 0.6043 for hot metal

Same as sulphide capacity, phosphorus capacity is also strong function of slag system and is high for highly basic slags. Thus from equation (2.55) the favourable conditions for deP are drawn to be

: high slag basicity

: high $a_{\underline{O}}$ or oxidizing atmosphere

Similar to sulphide capacity, phosphorus capacity

correlations are also available in the literature, as a function of slag composition and temperature, and are listed in table 2.3. In correlation (2) of Table 2.3 optical basicity can be evaluated as explained in section (2.4.1.1). Correlation 1 of Table 2.3 gives activity coefficient of $PO_{2.5}$ formed from the reaction

$$\underline{P} + 2.5\underline{O} = (PO_{2.5}) \qquad (2.56)$$

$$\log K_{(2.56)} = \frac{17060}{T} - 8.51 \qquad (2.57)$$

Phosphorus capacity (C_p) can be obtained by the following procedure:

$$K_{(2.56)} = \frac{a_{(PO_{2.5})}}{a_{\underline{P}} \cdot a_{\underline{O}}^{2.5}} = \frac{\nu_{PO_{2.5}} X_{PO_{2.5}}}{a_{\underline{P}} \cdot a_{\underline{O}}^{2.5}}$$

$$= \frac{(\%P)}{a_{\underline{P}} a_{\underline{O}}^{2.5}} \frac{\nu_{PO_{2.5}}}{M_P n_{Slag}}$$

$$= C_P \cdot \frac{\nu_{PO_{2.5}}}{M_P n_{Slag}}$$

$$= \log C_P = \log K_{(3.56)} - \log \left[\frac{\nu_{PO_{2.5}}}{M_P n_{Slag}} \right] \qquad (2.58)$$

where M_P = atomic wt. of Phosphorus

n_{slag} = number of moles of slag

Optical basicity correlation (Equation (2), Table 2.3) is used in this work to evaluate C_P. But for slag systems containing special components, for example $CaCl_2$, the regular solution model with the interaction energies of the components collected from literature is used in C_P calculation.

2.4.1.3 Nitrogen:

Nitrogen distributes between slag and metal according to the electrochemical reaction

$$\underline{N} + \frac{3}{2}(O^{2-}) = (N^{3-}) + \frac{3}{2}\underline{O} \qquad (2.59)$$

Equation (2.59) can be written as the combination of

$$\frac{1}{2}\{N_2\} + \frac{3}{2}(O^{2-}) = (N^{3-}) + \frac{3}{4}\{O_2\} \qquad (2.60)$$

$$\frac{1}{2}\{N_2\} = \underline{N} \qquad (2.61)$$

$$\Delta G^{o}_{2.61} = 3590 + 23.89T \text{ (J/mole)}$$

$$\frac{1}{2}\{O_2\} = \underline{O} \qquad (2.62)$$

$$\Delta G^{o}_{2.62} = -117150 - 2.887T \text{)J/mole)}$$

For equation (2.60) nitride capacity is defined by

$$C_N{}^{3-} = (\%N^{3-})\frac{P_{O_2}^{3/4}}{P_{N_2}^{1/2}} \qquad (2.63)$$

$$K_{(2.61)} = \frac{a_{\underline{N}}}{\sqrt{P_{N_2}}} \qquad (2.64)$$

$$K_{(2.62)} = \frac{a_{\underline{O}}}{\sqrt{P_{O_2}}} \qquad (2.65)$$

Putting (2.64) and (2.65) in (2.63) we get

$$C_N{}^{3-} = (\%N^{3-})\frac{K_{(2.61)}}{a_{\underline{N}}}\left[\frac{a_{\underline{O}}}{K_{(2.62)}}\right]^{3/2} \qquad (2.66)$$

From the definition of partition coefficient

$$\eta_N^{*} = \frac{(\%N)}{[\%N]} \qquad (2.67)$$

Combining (2.67) and (2.66), we get

$$\log \eta_N^{*} = \log C_N{}^{3-} - \frac{3}{2}\log a_{\underline{O}} + \log f_{\underline{N}} + \left[\frac{3}{2}\log K_{(2.62)} - \log K_{(2.61)}\right]$$

$$= \log C_N^{3-} - \frac{3}{2} \log a_{\underline{O}} + \log f_{\underline{N}} + \frac{9366.8}{T} + 1.4742 \qquad (2.68)$$

According to equation (2.66), it is evident that in order to obtain a high value of nitrogen distribution ratio, it is required that the slags have high nitride capacity and the metal low oxygen activity. In contrast to sulphide capacity, nitride capacity decreases with increasing basicity of slag. Nitride capacity for two slags systems is shown (Fig. 2.2 and 2.3).

As explained in the section (2.4.1.1) $a_{\underline{O}}$ can be correlated to the $a_{\underline{Al}}$. Thus the following equation relating partition coefficient with nitride capacity and dissolved aluminium activity

$$\log \eta_N^* = \log C_N^{3-} - \frac{3}{2} \log a_{\underline{Al}} + \log f_{\underline{N}} + \frac{1}{2} \log a_{Al_2O_3} + \frac{41816.8}{T} + 8.8408 \qquad (2.69)$$

can be obtained.

For some slag systems nitrogen partition coefficient as a function of dissolved Al content in the melt is shown in Fig. 2.4. In the nitrogen partition coefficient calculation, because of unavailability of correlations, nitride capacity values from Fig. 2.2 and 2.3 are used.

2.4.2 Transitoric rate constant (K_T):

To differentiate the rate constant terms appearing in equations 2.22 and 2.24, the one designated by K_T i.e., rate constant for the rising flux, is termed as transitoric rate constant and the other designed by K_P i.e, rate constant for the accumulated top slag, is termed as permanent rate constant.

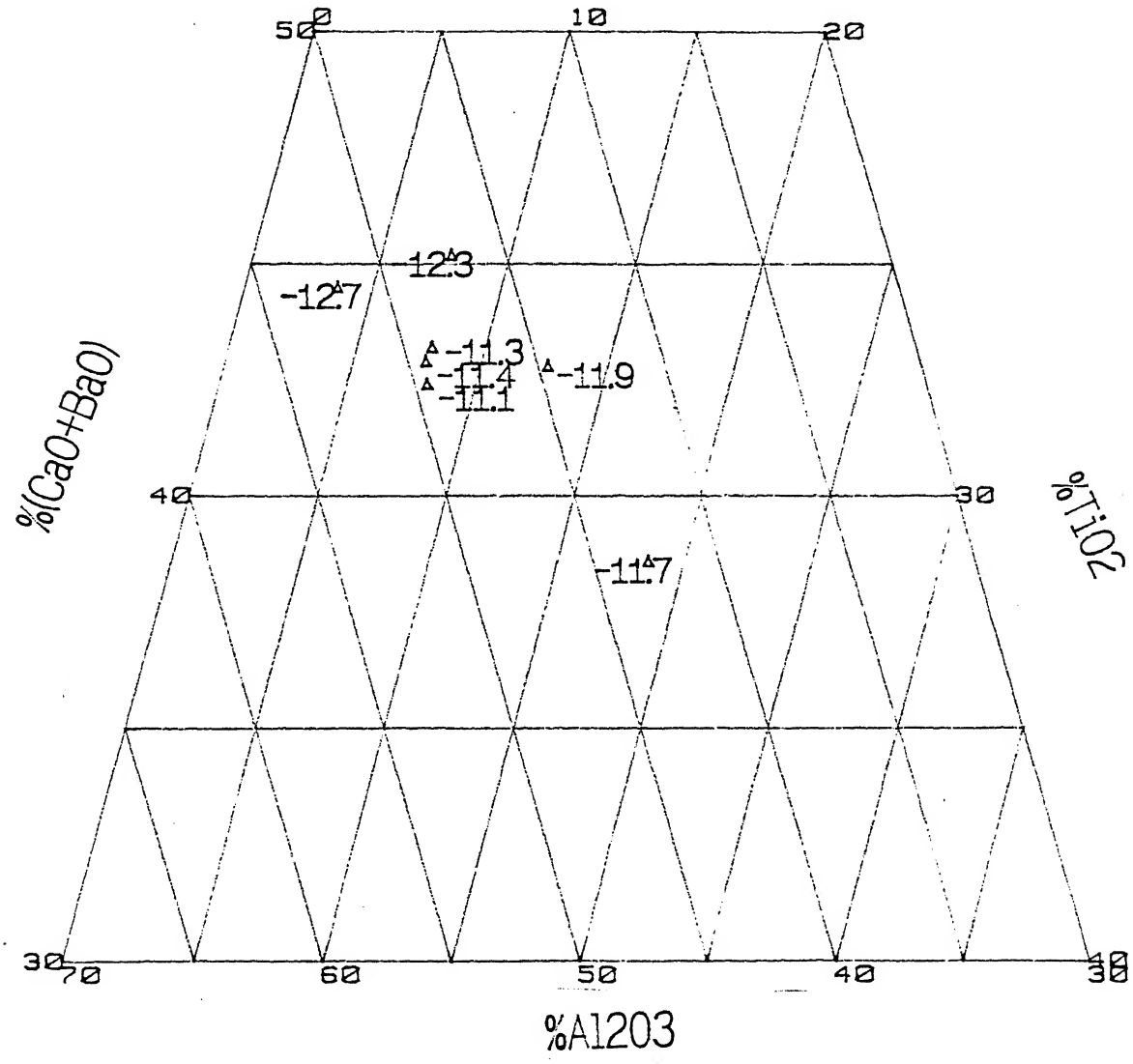

Fig. 2.3 Nitride Capacity of $CaO-BaO-Al_2O_3-TiO_2$ at 1873K

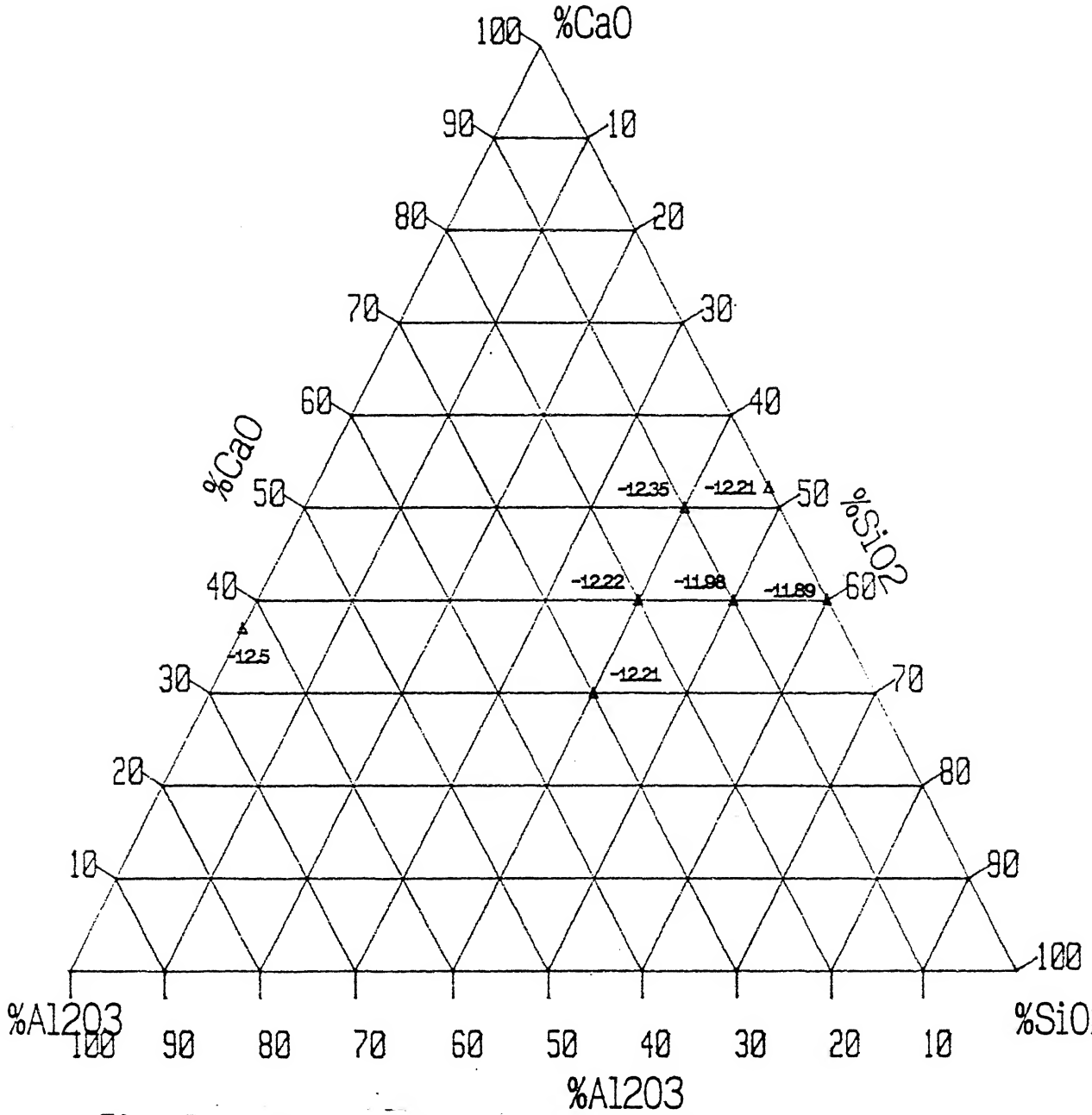

Fig. 2.2 Nitride Capacity of $CaO-SiO_2-Al_2O_3$ system at 1873 K

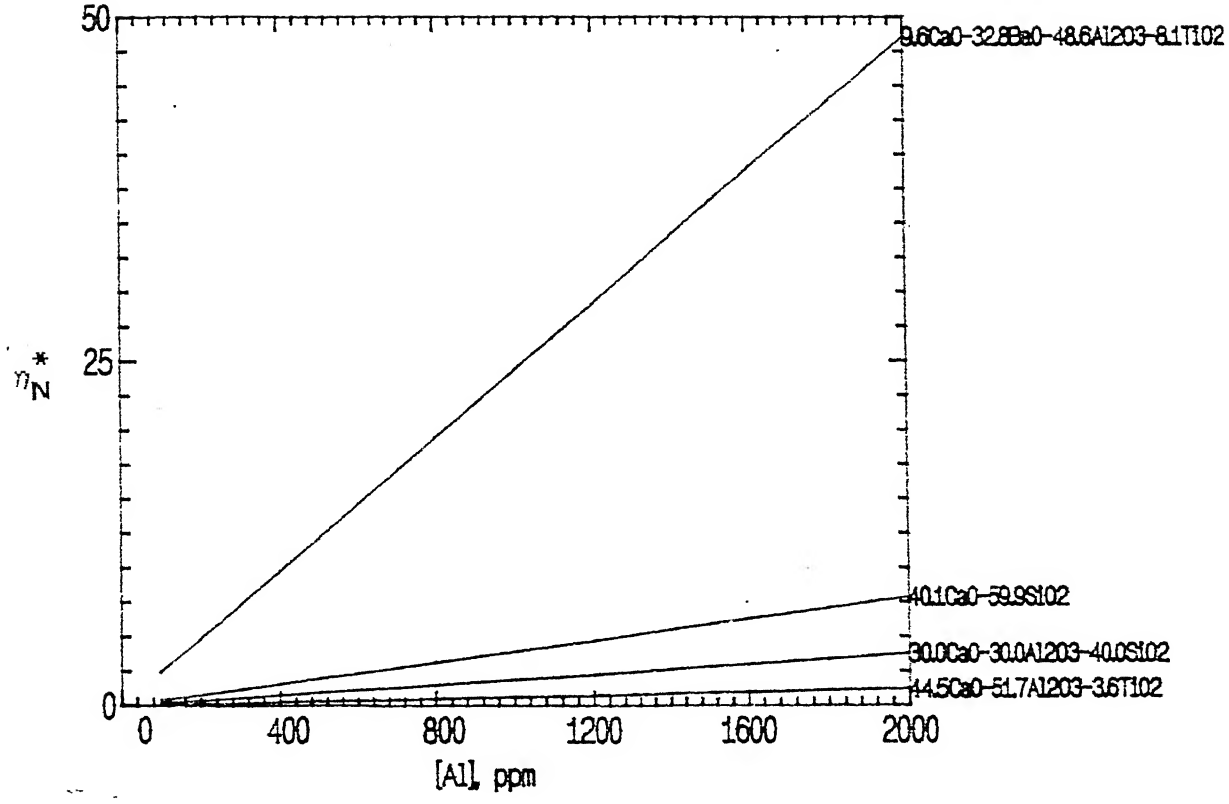

Fig. 2.4 Nitrogen partition coefficient as a function of sol.Al

Transitoric rate constant depends on transitoric mass transfer conefficient (β_T) (similar to K_T, β_T means the mass transfer coefficient for the rising flux), transitoric area (A_T) i.e., slag/melt interfacial area of the rising flux and the volume of the melt. As the volume of the melt is specific to a system, the main parameters are β_T and A_T. Rate of impurity extraction by the rising flux depends on the magnitude of this rate constant besides the driving force term i.e., concentration gradient term in equation (2.4). Hence, the parameters on which K_T depends, are discussed in this section.

2.4.2.1 Transitoric mass transfer coefficient (β_T):

Mass transfer coefficient is the furnction of diffusivity of the solute, fluid properties, injected powder-properties etc. Due to its complex dependency on these variables it is usually expressed by empirical correlations. The magnitude of transitoric mass transfer coefficient (β_T) is strongly influence by the state of injected flux i.e., whether it is in solid or liquid form during its rise in the molten metal. Depending upon the melting point of the flux it might remain in the solid or liquid form during its rise. When melting point of the flux is more than the refining temperature i.e, 1623K in case of hot-metal and 1873K in steel, injection of premelted flux is useful, since it melts at faster rate, upon its contact with the molten melt.

When injected flux melts in the molten bath, it forms liquid droplets. There are large number of correlation available in the

literature to describe mass transfer in a wide variety of liquid-liquid system involving drops. These correlations are listed in Table 2.4 and compared in Fig. 2.5. A band is observed in this Figure with the equation 1 (table 2.4) for solid spheres as lower boundary and equation 5 (Table 2.4) for circulating and oscillating drops combined with penetration theory as upper boundary. Drops rising through the melt have high degree of internal circulation caused by stirring, and also as per penetration theory, there will be surface renewal at liquid-liquid interface caused by bubbles. That is why equation 5 from Table 2.4 is used in this work for the rising drops in the molten metal.

When injected flux is in the solid form on its contact with the melt, the solid reaction product formed at the flux/metal interface slows down the overall mass transfer coefficient. For the mass transfer between solid and liquid phase Asai et al, [54] proposed that

$$N_{Sh} \propto N_{Re}^{a_1} N_{Sc}^{a_2} \qquad (2.70)$$

where a_1 and a_2 are arbitrary constants

When this type of situation is encountered the equation for solid spheres i.e., equation 1 from Table (2.3) is the probable solution in the absence of other data.

Apart from fluid properties and diffusivity of the solute in the melt, the terminal velocity of the droplets in the melt must be known to evaluate β_T. It can be evaluated as per the following procedure.

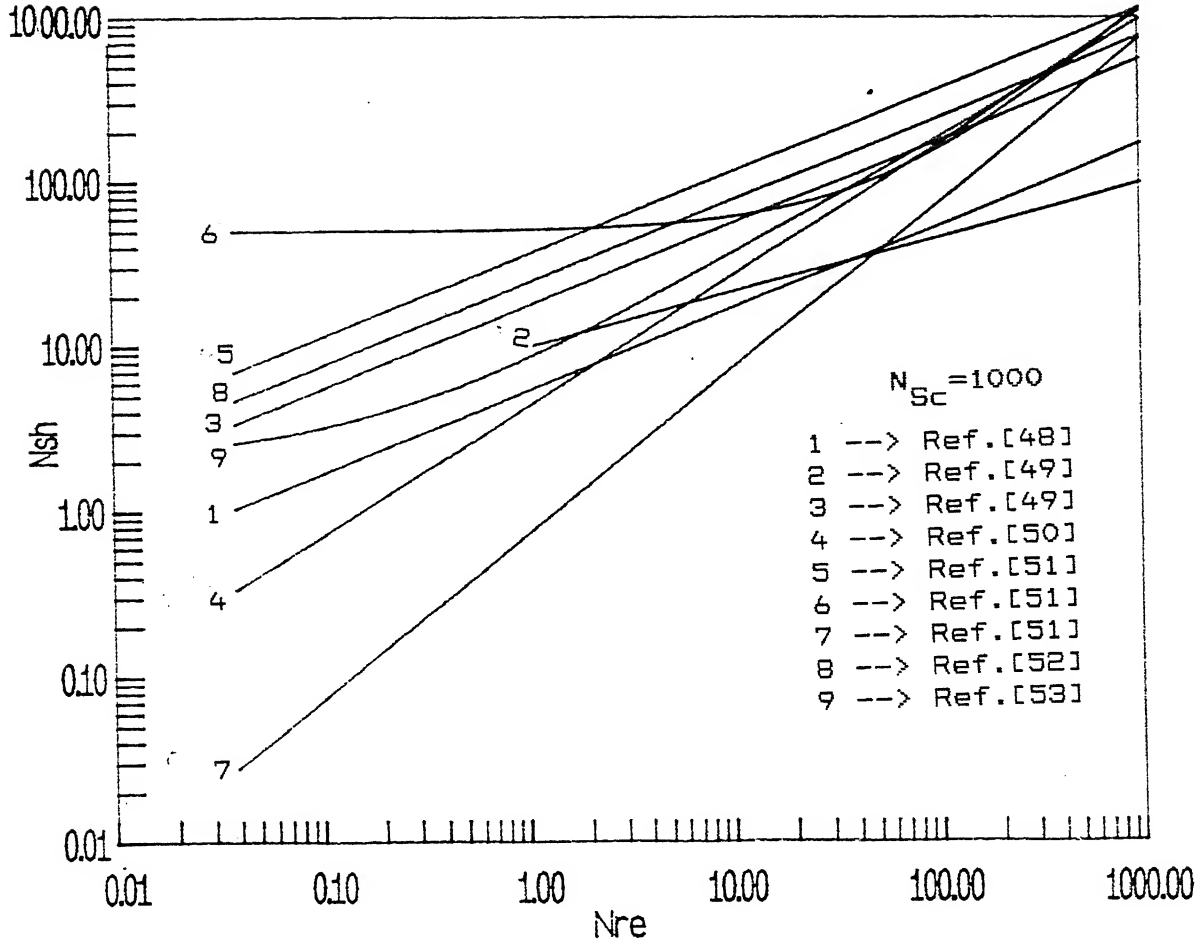

Fig. 2.5 Transitoric mass transfer coefficient correlations comparison

2.4.2.2 Terminal velocity of the droplets in the melt:

When the drops reach the state of terminal velocity, the sum of all the forces acting on the drops i.e., the summation of gravity force, buoyancy force and force due to fluid motion, must be zero.

Then,

$$\frac{4}{3}\pi R^3 \rho_m g - \frac{4}{3}\pi R^3 \rho_s g - \frac{C_D \pi R^2 u^2}{2}\rho_m = 0 \qquad (\rho_m > \rho_s) \tag{2.71}$$

$$u_T = \left[\frac{8}{3}\left[\frac{\rho_m - \rho_s}{\rho_m}\right]\frac{gR}{C_D}\right]^{1/2} \tag{2.72}$$

To solve equation (2.72) for terminal velocity, C_D must be known. The approximate equation given for C_D is [53].

$$C_D = \frac{24}{R_C} + \frac{4}{\sqrt{R_e}} + 0.4 \tag{2.73}$$

By solving equation (2.72) and (2.73) simultaneously for the given drop diameter and fluid properties, terminal velocity can be obtained.

2.4.2.3 Transitoric interfacial area (A_T):

Transitoric interfacial area is the effective interfacial area available in the residence time t_R when the powdered flux of diameter d_p is injected at the mass flow rate $\dot{m}_s$. The magnitude of interfacial area is affected by the amount of particles wetted by the molten metal. In the calculation of A_T, from the following correlation, it is assumed that the whole injected flux is available for the reaction. Therefore,

$$A_T = \dot{A}t_R = \left[\frac{6}{dp}\right]\left[\frac{\dot{m}_S}{\rho_s}\right]t_R \qquad (2.74)$$

Residence time of injected flux in the bath is the ratio of lance submergence depth to the velocity of the rising flux. Usually lance submergence depth, if not given, is 50% of the melt depth. Thus the only unknown is the velocity of the rising flux in the molten metal. The particles rise with terminal velocity with respect to liquid. As the carrier gas stirr the bath, the rising velocity of the particles can be obtained by adding its terminal velocity and the molten metal velocity. As the molten metal velocity is much greater than the terminal velocity ofthe particles, particle velocity can be taken as the molten metal velocity. To calculate the molten metal velocity, the equation (2.75) [55] derived for the mean rising velocity of the molten metal in the plume zone is used.

Mean rising velocity of the molten metal in the plume zone

$$U_Z = 19.9\left[\frac{\dot{Q}_B}{d_C^2}\right]\left[\frac{gd_C^S}{Q_B^2}\right]\left[\frac{H}{d_C}\right]^{0.2}\left[\frac{H_O}{H}\right]^{0.52} \qquad (2.75)$$

$$t_R = \frac{H_O}{U_Z} \qquad (2.76)$$

2.4.3 Permanent Rate Constant (K_P):

Similar to transitoric rate constant permanent rate constant also depends on mass transfer of solute from bulk metal to the top slag, total interfacial area (i.e., ladle cross-sectional area and emulsified area) and the volume of the melt. As the equilibrium conditions put a constraint on the driving force term

effectiveness of top slag in the refining processes will be decided by the magnitude of the rate constant. That is higher the magnitude of the rate constant, faster will be the refining reactions. In a slag/metal system the main contribution to the permanent rate constant will be from mass transfer coefficient and total interfacial area. The entrainment of top slag into the molten metal enhances both β_p and A_p. But unfortunately quantitative data on entrainment volume, number, size of droplets etc., is not available. In the literature empirical correlations, on mass transfer coefficient, for systems related to the (undisturbed) area of liquid/liquid interface and for systems involving drops (see Table 2.4) are available. But due to the uncertainity in the determination of drop diameter and entrained mass of top slag, rate constant is usually corelated to the stirring energy supplied via carrier gas to the molten metal. For this purpose the rate curves presented in the literature for various slag systems (see table 2.5) for permanent contact mode (alternatively termed as dumping) experiments were evaluated for K_p. The evaluated data show that K_p vary in between 0.0093 to 0.55 depending upon the type of slag system, state of the system i.e, whether it is in liquid or solid state, and the stirring intensity. Thus the evaluation of K_p as a function of stirring energy, from this table alone, will be erroneous. Therefore K_p is evaluated, in gas stirring, from the following two correlations.

(a) for Phosphorus [56]

$$K_p = 7.0 \times 10^{-3} (\dot{\varepsilon})^{0.4} \quad (2.77)$$

(b) for Sulphur [57]

$$K_p = 7.6 \times 10^{-6} (\dot{\varepsilon})^{2.1} \quad (2.78)$$

Equation (2.77) was derived by using oxidizing basic slags with $\dot{\varepsilon}$ values in the range 10 to 500 W/T in 250T ladle, whereas equation (2.78) was derived at $\dot{\varepsilon}$ values in the range 60 to 100 W/T with 2.5T liquid steel. Depending upon the requirement extrapolation or interpolation of equations (2.77) and (2.78) is done.

In inductively stirred melts, where no breakage of top slag/metal interfacial area occurs, β_p varies from

0.002 - 0.003 Cm/sec. [38].

Thus the correlations selected in this section for the calculation of model parameters are used in later chapter for the applications of model to study deS, deP and deN.

CHAPTER 3

RESULTS AND DISCUSSION

In chapter 2 the equations for powder injection refining process with and without slag carry-over were derived (Equation 2.22 without slag carry-over and Equation 2.24 with slag carry-over). With slag carry-over and without slag carry-over are discussed explicitly to give their distinguishing features. This chapter is devoted to the parameters influencing change in melt concentration with time and also their effect on rate of impurity extraction by the top slag and the rising flux.

3.1 No Slag Carry-Over:

From equation 2.22 it can be seen that the melt concentration with time depends on variables ϕ and θ. Furhter ϕ_S and θ_S depend on B_P, B_T, λ_S and f. As ϕ_S and θ_S depend on the same parameters, they can not be varied independently. Thus B_P, B_T, λ_S and f are the variables to be studied. As given in Appendix-3, f is function of B_P, B_T and λ_S; thus the parameters influencing melt concentration with time are reduced to B_P, B_T, λ_S. λ_S can be varied by varying composition of flux and/or mass fraction of flux to melt. B_P can be varied by varying time of injection and/or stirring energy i.e., carrier gas flow rate. B_T can be changed by changing time of injection and/or mass flow rate of flux and/or lance immersion depth and/or powder particle size.

In refining processes metal sampling is done in time intervals to know whether the end point is reached or not. Hence

the concentration vs time curve arises from this process. To give salient features of concentration vs time curves, it is necessary to plot them as a function of independent variables on which they depend. And also it is necessary to know rate of change of melt concentration with time. Thus the effect of λ_S, B_P and B_T on concentration change with time are discussed independently. Evaluation of concentration as a function of time for the given B_P, B_T and λ_S is shown in Flow-chart 1.

3.1.1 Influence of Flux Type and/or its amount:

The influence of type of flux is characterized quantitatively by the partition coefficient. Both η_S^* and Y_S are grouped in λ_S. The effect of λ_S on dimensionless concentration change with time is shown in lower part of the Fig. (3.1a). The upper part shows the variation of rate as a function of time for two selected values of λ_S. The plot is divided into two periods, t^* from 0 to 1 is the injection period and 1 onwards it is the stirring period. The selected B_P and B_T values to study λ_S effect on α vs τ curve are 0.4 and 0.9 respectively. λ_S is varied between 1 to 18. Analysis of λ_S effect above 18 is unnecessary because of negligible difference between concentration curves between λ_S=15 and λ_S=18. This is the indication of ineffectiveness of λ_S above 15. The equilibrium curves, evaluated from equation (2.28) and equation (2.29), are also superimposed in this plot.

The increasing difference between equilibrium and kinetic curves with increasing λ_S value can be observed from Fig. 3.1(a).

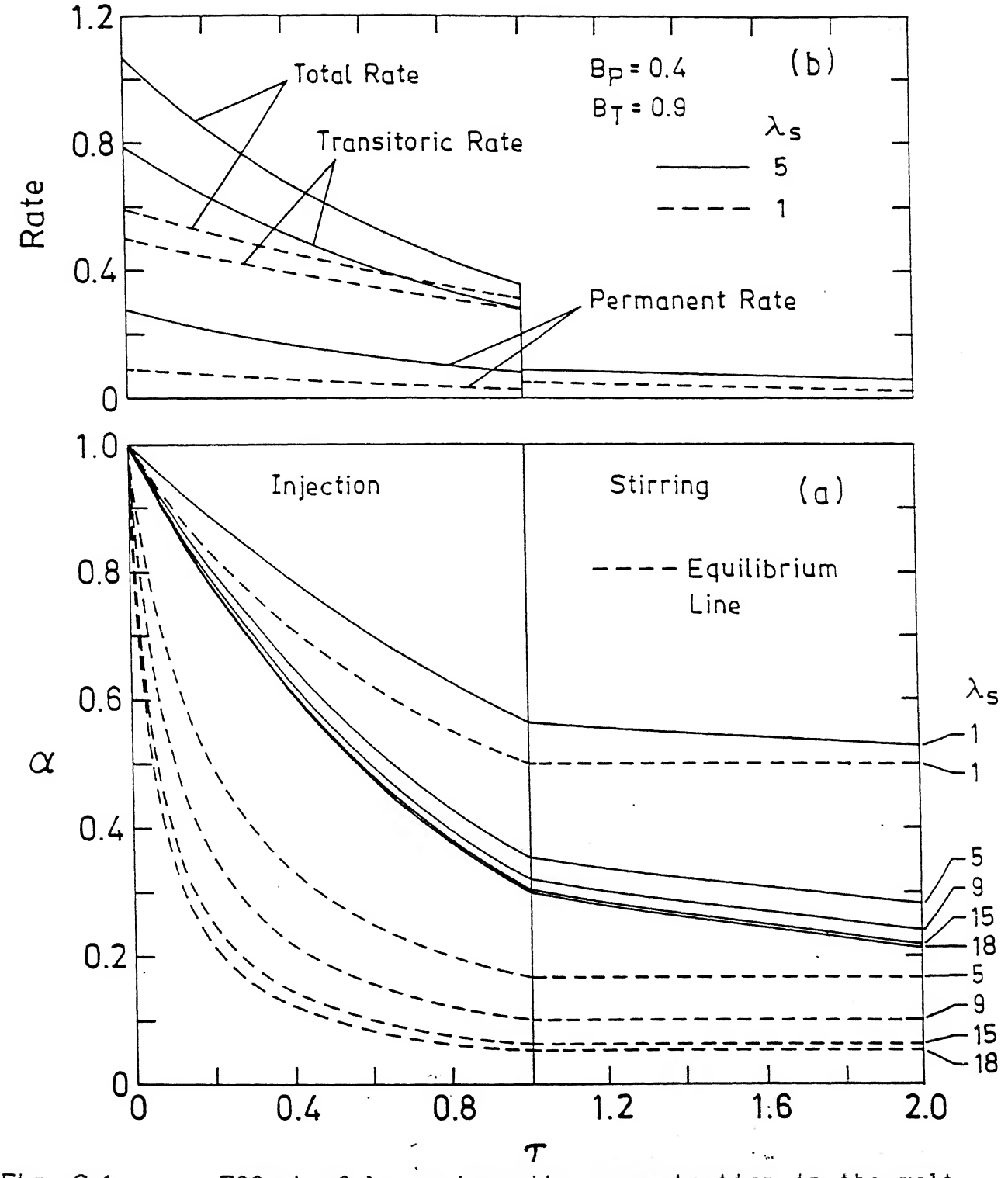

Fig. 3.1 Effect of λ_S on impurity concentration in the melt and its rate of removal as a function of time (B_P=0.4, B_T=0.9)

This indicates that λ_S affects the contribution from the rising flux in the injection period, otherwise the difference between equilibrium and kinetic curve would have been the same. And also the increase in difference in stirring period indicates that the top slag must be effective at higher λ_S value in the overall refining process. This observation will be confirmed in the later section where B_p effect on concentration curve is discussed. The rapid decrease in concentration when λ_S is increased from 1 to 5 is due to increase in driving force for impurity removal. Above 15 the increase in driving force is negligibly small. This is due to the negligible contribution from $(x)/\eta^*$ for the driving force term in the Eq. 2.4. The independent rate variation i.e., permanent rate, transitoric rate and total rate with time, is shown in Fig. 3.1(b) for two λ_S values i.e., λ_S=1 and λ_S=5. At τ=1 the difference between transitoric and permanent rates at λ_S=5 is less than that at λ_S=1. That is, the top slag is effective at higher λ_S values. The increase in magnitude of rate indicates that increase in stirring might be helpful. This will be analysed in the following section.

3.1.2 *Influence of Transitoric Parameter (B_T):*

B_T involves both t_{inj} and K_T. Prolonged time of refining is undesirable from kinetic point of view. Analysis of literataure experimental data suggests that t_{inj} is nearly 10 min in powder injection refining processes. Hence the variation of B_T must be understood as the variation of K_T. Although K_T involves volume of

the melt, mass transfer coefficient, mass-flow rate of the flux and residence time, its significant variation will be affected by mass flow rate of the flux and residence time only. Hence its variation can be thought of varying mass flow rate of the flux and/or residence time of powder particles in the molten bath. The effect of transitoric parameter on dimensionless concentration as a function of dimensionless time is shown in Fig. 3.2(a) and Fig. 3.3(a) for two λ values 1 and 5.

From Fig. 3.2(a) and Fig. 3.3(a) three types of B_T values can be identified, depending upon the melt concentration in relation to the equilibrium concentration at τ=1.

i. B_T giving the melt concentration above the equilibrium concentration at τ=1.

(e.g.: B_T=0.6, 0.9 in Fig. 3.2(a) and B_T=0.6, 0.9, 1.9 in Fig. 3.3(a)).

ii. B_T giving the melt concentration equal to the equilibrium concentration at τ=1

(e.g.: B_T = 0.19 in Fig. 3.2(a)).

iii. B_T giving the melt concentration below the equilibrium concentration at τ=1

(e.g.: B_T=4.16 in Fig. 3.2(a) and Fig. 3.3(a))

Corresponding rate curves are given in Fig. 3.2(b) and Fig. 3.3(b).

For B_T=4.16 in Fig. 3.2(b) and Fig. 3.2(b) negative rate can be observed i.e., impurity is transferring from slag to the melt.

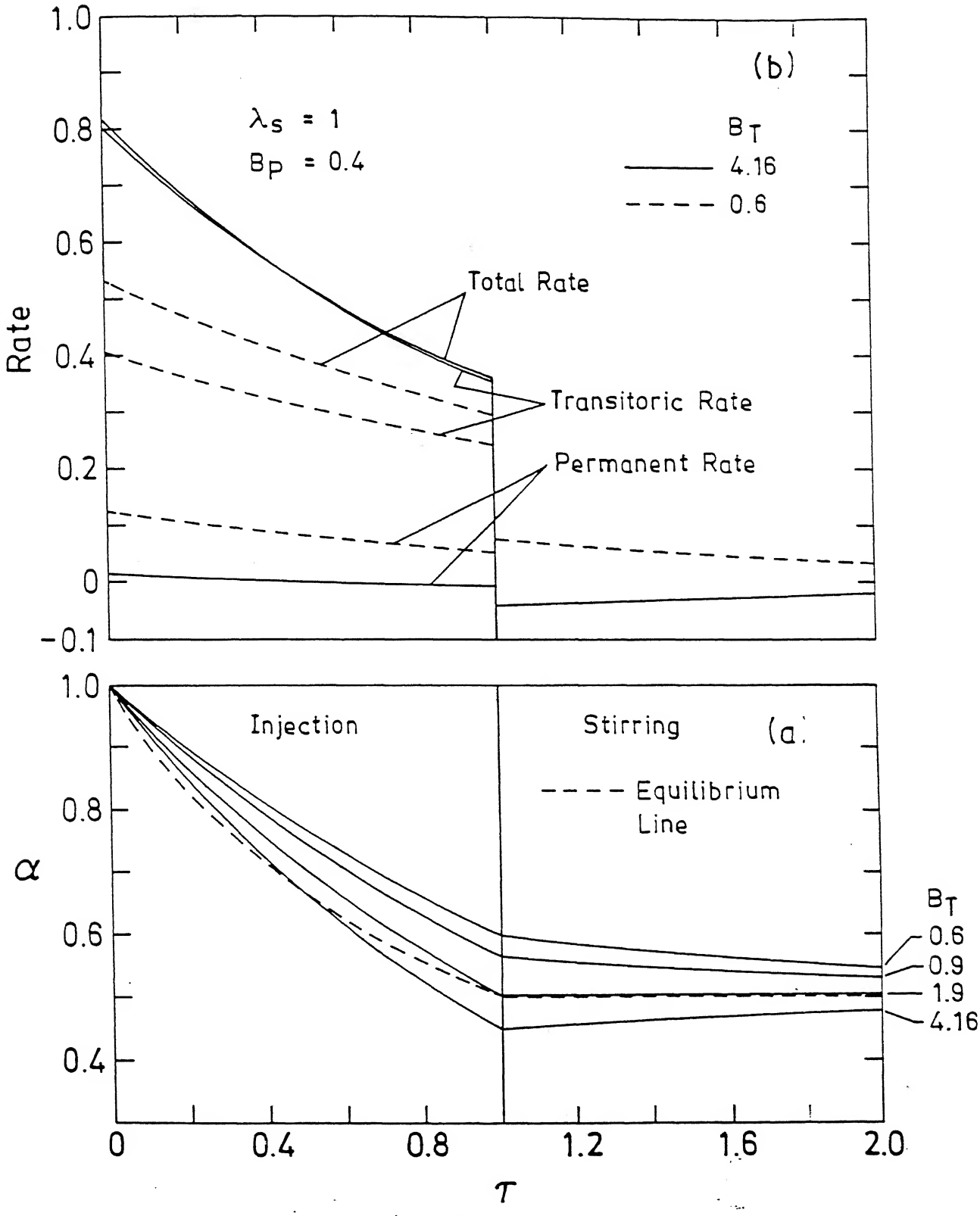

Fig. 3.2 Effect of B_T on impurity concentration in the melt and its rate of removal as a function of time (λ_S=1)

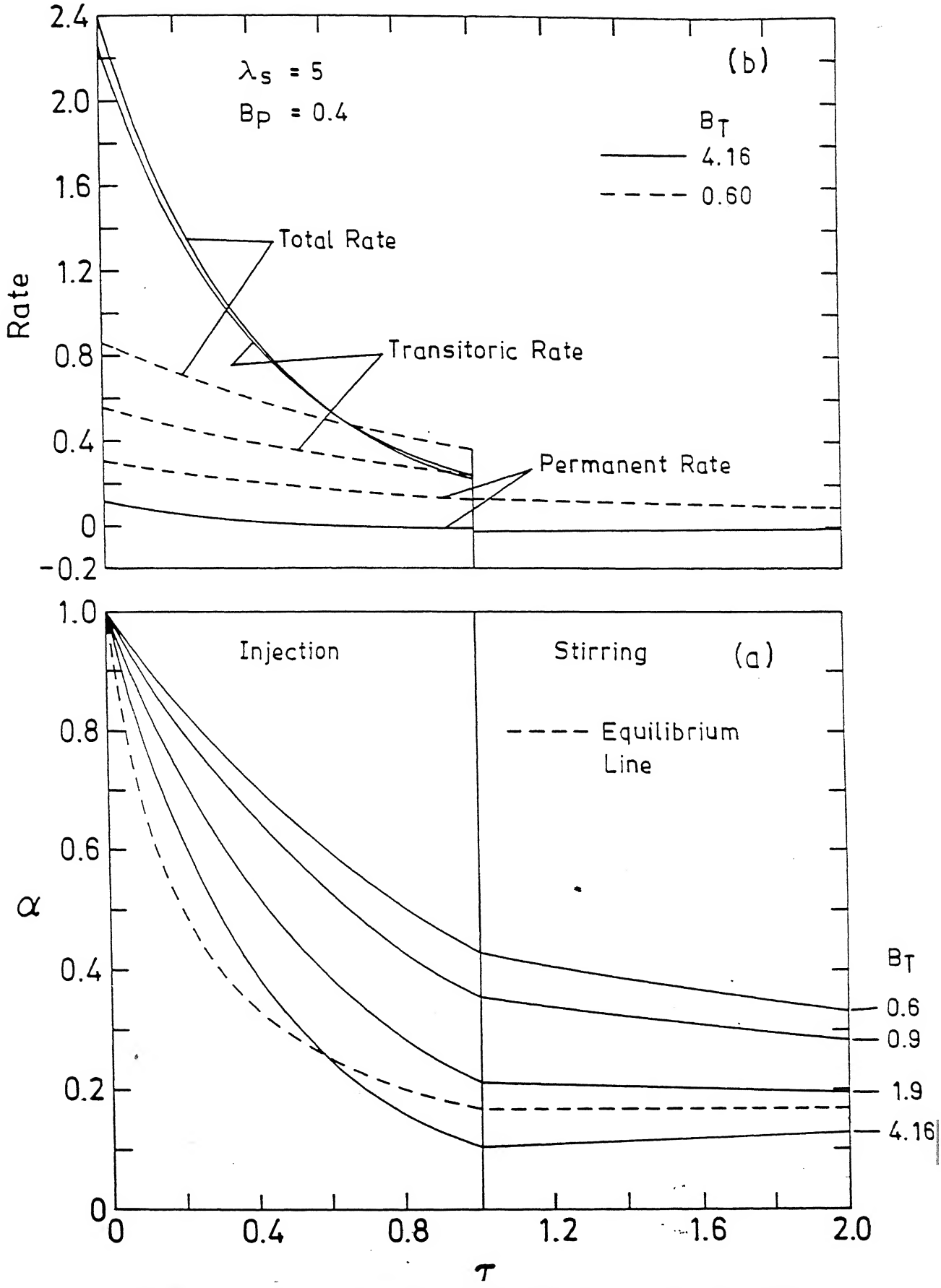

Fig. 3.3 Effect of B_T on impurity concetration in the melt and its rate of removal as a function of time (λ_s=5)

This is the phenomena of back transfer. Thus the first B_T type i.e, B_T=0.6, 0.9 in Fig. 3.2(a) and B_T=0.6, 0.9, 1.9 in Fig. 3.3(a) can be termed as 'B_T corresponds to no back-transfer condition', second B_T type i.e. B_T=1.9 in Fig. 3.2(a) is 'B_T corresponds to equilibrium conditions' and termed as optimum B_T, and the third B_T type i.e., B_T=4.16 in Fig. 3.2(a) and Fig.3.3(a) can be termed as 'B_T corresponds to back transfer condition'. In case of 'B_T corresponds to back transfer condition' any further stirring, after the injection period, is unnecessary because in this region top slag deteriorates the advantage of injection processes by way of back transfer. For 'B_T corresponds to equilibrium condition' also no further strirring is needed, because the top slag attains equilibrium value at τ=1 and can not extract the impurity. Stirring is advantageous only, for 'B_T corresponds to no back transfer condition'.

In Fig. 3.3(a), the departure of kinetic curve from equilibrium curve is observed to be larger than that in Fig. 3.2(a) and the delay in the intersection of kinetic and equilibrium curve can be observed. Although there is large decrease in concentration value when λ_S is increased from 1 to 5, but the increased difference between kinetic and equilibrium curve suggests that there might be decrease in transitoric effeciency. This also indicates that the top slag contribution can be increased at higher λ_S values by way of stirring.

Hence in injection process the effect of top slag must be

This is the phenomena of back transfer. Thus the first B_T type i.e, B_T=0.6, 0.9 in Fig. 3.2(a) and B_T=0.6, 0.9, 1.9 in Fig. 3.3(a) can be termed as 'B_T corresponds to no back-transfer condition', second B_T type i.e. B_T=1.9 in Fig. 3.2(a) is 'B_T corresponds to equilibrium conditions' and termed as optimum B_T, and the third B_T type i.e., B_T=4.16 in Fig. 3.2(a) and Fig.3.3(a) can be termed as 'B_T corresponds to back transfer condition'. In case of 'B_T corresponds to back transfer condition' any further stirring, after the injection period, is unnecessary because in this region top slag deteriorates the advantage of injection processes by way of back transfer. For 'B_T corresponds to equilibrium condition' also no further strirring is needed, because the top slag attains equilibrium value at τ=1 and can not extract the impurity. Stirring is advantageous only, for 'B_T corresponds to no back transfer condition'.

In Fig. 3.3(a), the departure of kinetic curve from equilibrium curve is observed to be larger than that in Fig. 3.2(a) and the delay in the intersection of kinetic and equilibrium curve can be observed. Although there is large decrease in concentration value when λ_S is increased from 1 to 5, but the increased difference between kinetic and equilibrium curve suggests that there might be decrease in transitoric effeciency. This also indicates that the top slag contribution can be increased at higher λ_S values by way of stirring.

Hence in injection process the effect of top slag must be

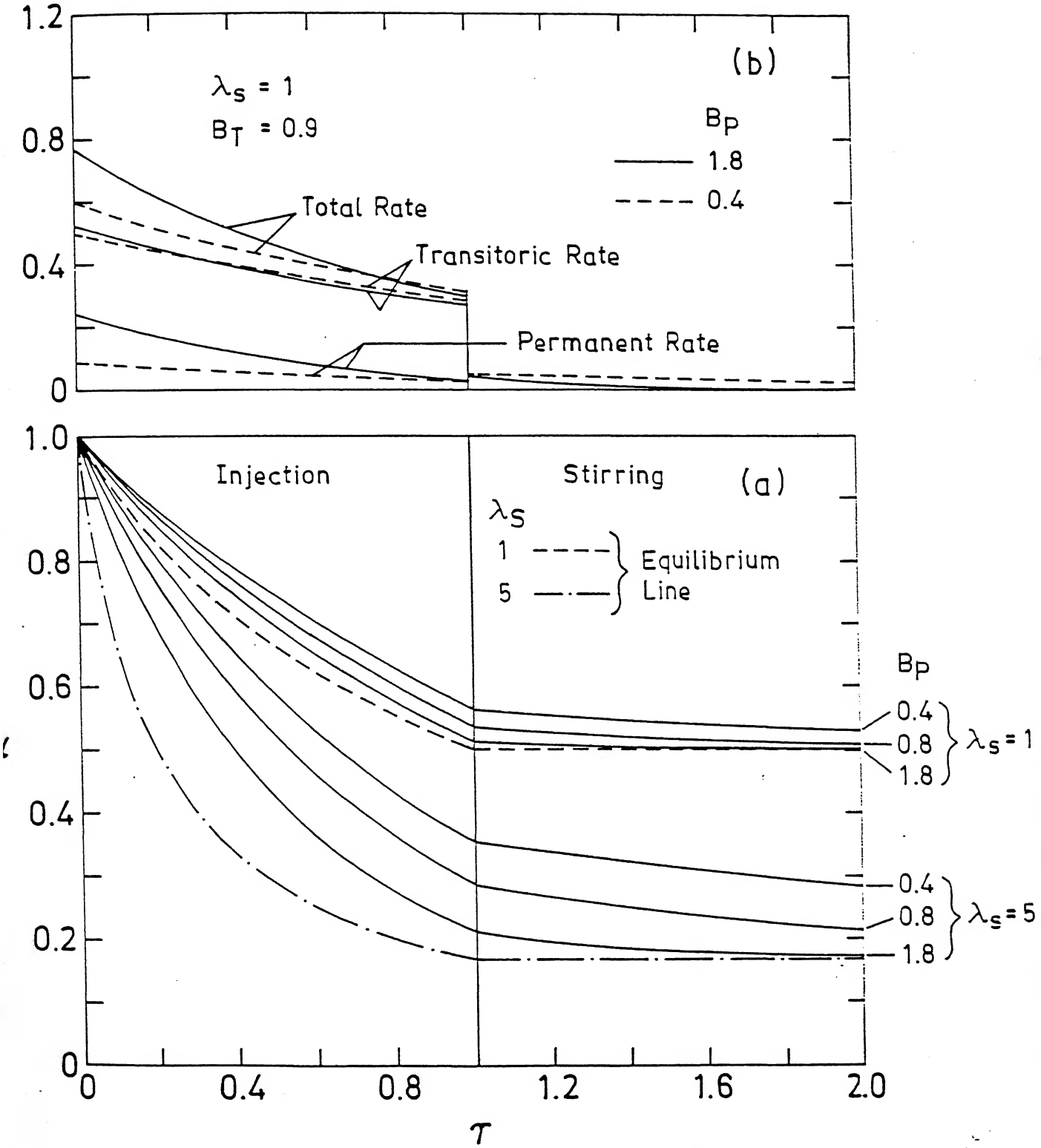

Fig. 3.4 Effect of B_p on impurity concetration in the melt and its rate of removal as a function of time (B_T =0.9)

3.5 Effect of B_P on rate of impurity extraction as a function time (B_T=0.9, B_P=1.8, λ_S=5)

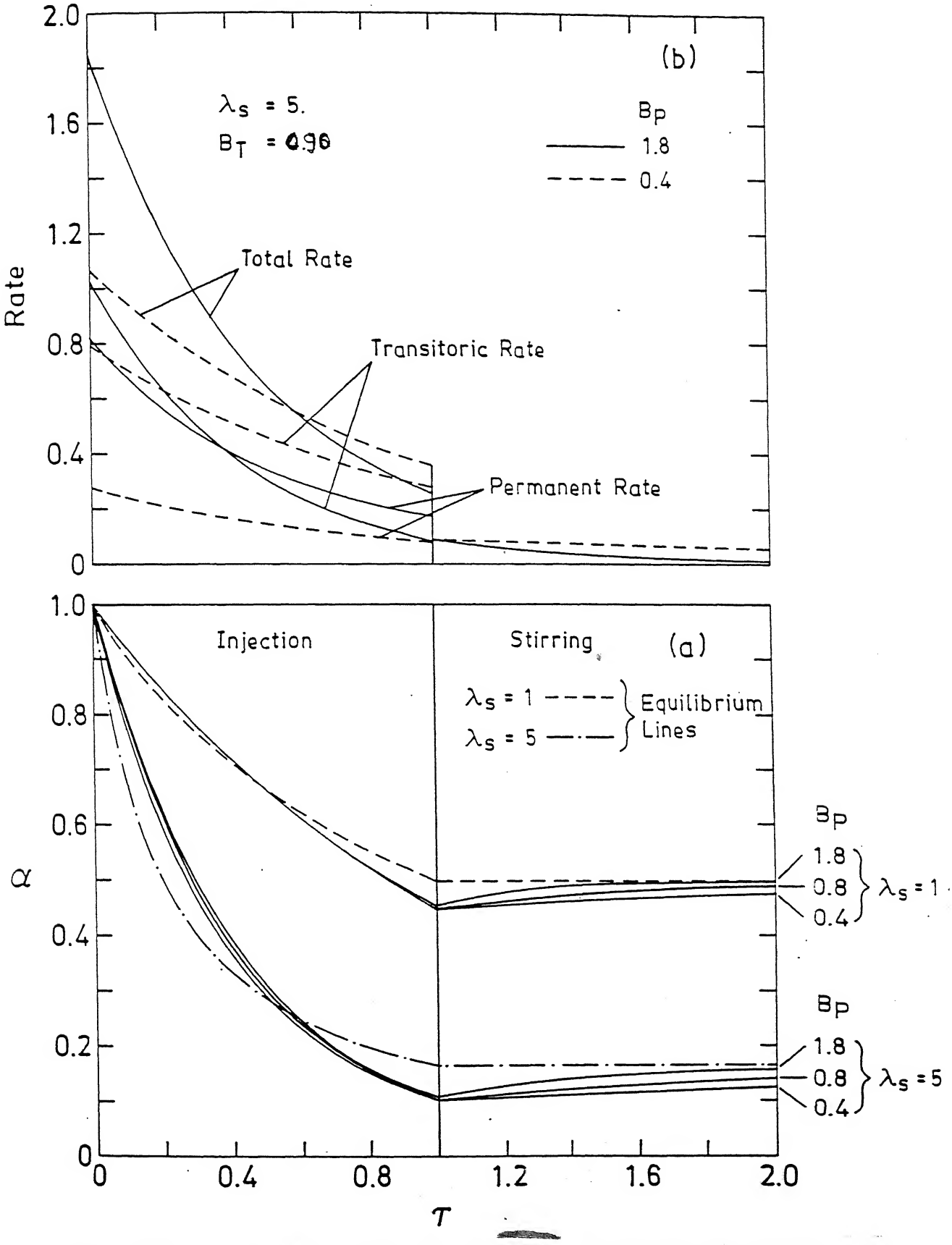

Fig. 3.6 Effect of B_P on impurity concetration in the melt with time (B_T=4.16)

than at λ_S=1. Thus the large shift in concentration curve at λ_S=5 when B_P is varied from 0.4 to 1.8 at B_T=0.9 indicates that stirring effect is more dominant at higher λ_S values. A glance at Fig. 3.6 gives the view that the top slag is not effective for B_T values giving excess impurity removal, in injection period, and after the injection period back transfer is proportional to the B_P value. Observation of Fig. 3.4(a) and Fig. 3.6 causes to make the conclusion that B_P is effective parameter to reach equilibrium melt concentration. That is why top slag is only effective when the kinetic curve is above the equilibrium curve. This fact is also shown in Fig. 3.4(b) and Fib. 3.5 , where rate is plotted as a function of dimensionless time. In Fig. 3.4(b) i.e. λ_S=1, B_T=0.9 rising flux is still dominant as its rate at all values of τ is above the rate of impurity extraction correspond to the top slag, whereas in Fig. 3.5 for B_P=1.8 top slag rate is higher than that of rising flux upto τ is 0.4. Hence the higher stirring intensity, when mass flow rate of flux is low, makes the top slag as effective as the rising flux.

3.1.4 Transitoric rate Contribution and Transitoric Efficiency:

In the literature there is no agreement on the domination of permanent contact reaction of transitory contact reaction in the powder injection refining process. Therefore rate contribution from either of them and the factors influencing the rate contribution, relation between transitoric efficiency parameters and the transitoric rate contribution have been included in this

chapter.

3.1.4.1 Transitoric rate contribution:

The method to obtian transitoric rate contribution is given in flow-chart 1 for the given B_p, B_T and λ_S values. It was already discussed that it depends on B_p, B_T and λ_S only. B_T value is selected from no back transfer region, because above this B_T value, B_p has no effect in the injection period as given in section 3.1.3 (see also Fig. 3.4(b)).

Fig. 3.7 shows the variation of transitoric rate contribution as a function of λ_S for various value of B_T. B_p is fixed to 0.4. For a set of B_p and B_T, variation in transitoric rate contribution can be neglected after λ_S is 10. This is due to the decreasing influence of $(x)/\eta^*$ in the rate equation (3.4). It can be seen from Fig. 3.7, the major change in transitoric rate contribution can be brought by changing B_T from 0.2 to 2.0. The reason for λ_S having negligible influence on transitoric rate contribution, after 10, is due to lethargic improvement in the driving force. Whereas increase in B_T increases the rate of impurity extraction and thus transitoric rate contribution increases.

Fig. 3.8 shows the same axes but the influence of B_p. Here B_T is 0.6. Effect of λ_S on transitoric rate contribution is same as that in Fig. 3.7. But increase in B_p decreases the transitoric rate contribution continuously. At high value of B_p, for example at B_p=1.8, permanent rate contribution is as high as 70%, when λ_S is 19.

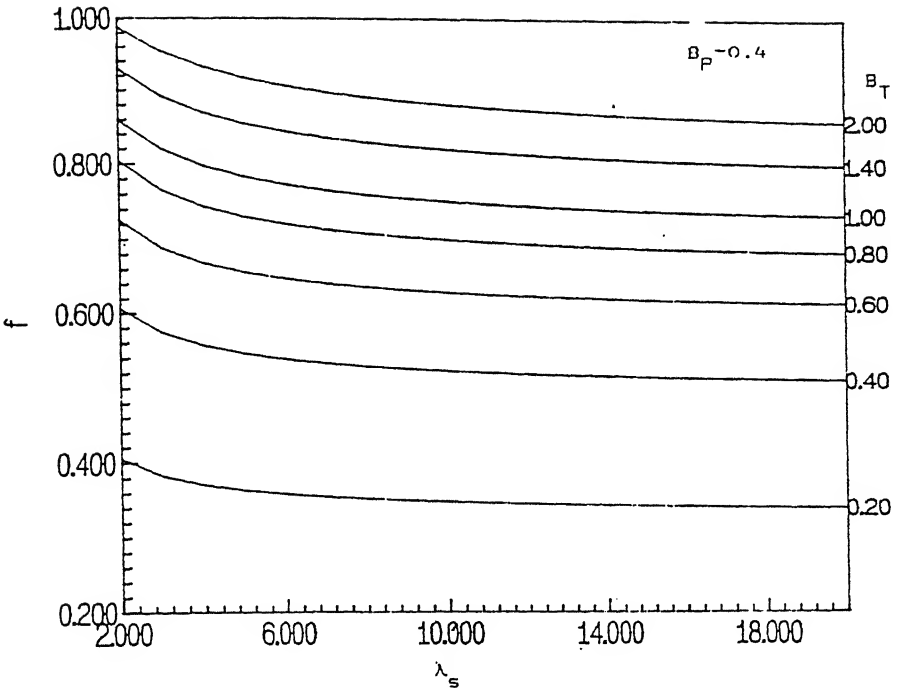

Fig. 3.7 Variation of transitoric rate contribution with λ_s for various values of B_T (B_P=0.4)

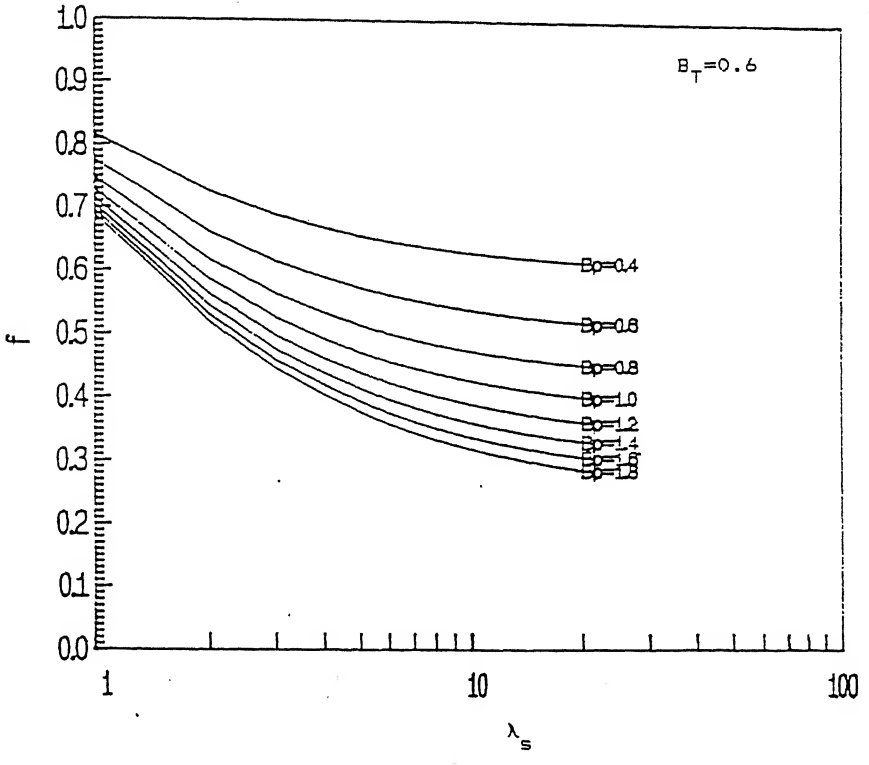

Fig. 3.8 Variation of transitoric rate contribution with λ_S for various values of B_P (B_T=0.6)

Thus with one set of B_p, B_T and λ_S, it will not be wise to elucidate if the permanent contact reaction or transitory contact reaction dominates the powder injection process. Relative contribution is entirely depends on the magnitude of B_p, B_T and λ_S.

3.1.4.2 *Transitoric efficiency:*

Transitoric efficiency is the ratio of impurity concentration removed by the rising flux when it reaches to the top surface of the melt to the concentration it can remove i.e., equilibrium impurity concentration in the injected flux.

Combining equation (2.8) and the transitoric rate contribution term in equation (2.12) we get

$$(x_T) = \frac{[x_o]}{Y_S} \propto \frac{B_T}{1+\frac{B_T}{\lambda_S}} \qquad (3.1)$$

with the definition of λ_S (see equation 2.11) equation (3.1) can be rewritten as

$$(x_T) = [x]\eta_S^* \frac{\frac{B_T}{\lambda_S}}{1+\frac{B_T}{\lambda_S} f} \qquad (3.2)$$

$\eta_S^*[x]$ in equation (3.2) is the equilibrium concentration of the injected flux.

$\frac{\frac{B_T}{\lambda_S}}{1+\frac{B_T}{\lambda_S} f}$ indicates how close the concentration of injected flux to the equilibrium concentration when it reaches to the top

surface of the melt. If transitoric efficiency is denoted by E, then

$$E = \frac{\frac{B_T}{\lambda_S}}{1+\frac{B_T}{\lambda_S} f} \qquad (3.3)$$

For the pure transitoric reaction the same equation (3.3) can be applied by putting f=1.

3.1.5 Optimum B_T:

B_T is significantly affected by the mass flux flox rate. In the section (3.1.2) three types of B_T values were defined. Optimum B_T is defined as the one just above which back transfer (from slag to melt) of impurity occurs. Optimum B_T is obtained by putting the equilibrium concentration at τ=1, calculated from equation (2.29), into equation 2.22, for the known B_P and λ_S values. Magnitude of B_T will also be affected by the B_P and λ_S values, since shifting of concentration vs. time curve can also be done by these two parameters.

Critical B_T as a function of λ_S for various values of B_P is represented in Fig. 3.9. AT higher values of λ_S critical B_T is high. In section (3.1.1) it was already discussed that the increase in λ_S increases the difference between kinetic and equilibrium curve. This is the reason for the increment of B_T with λ_S. Because of the same reason increase in B_P decreases optimum B_t value.

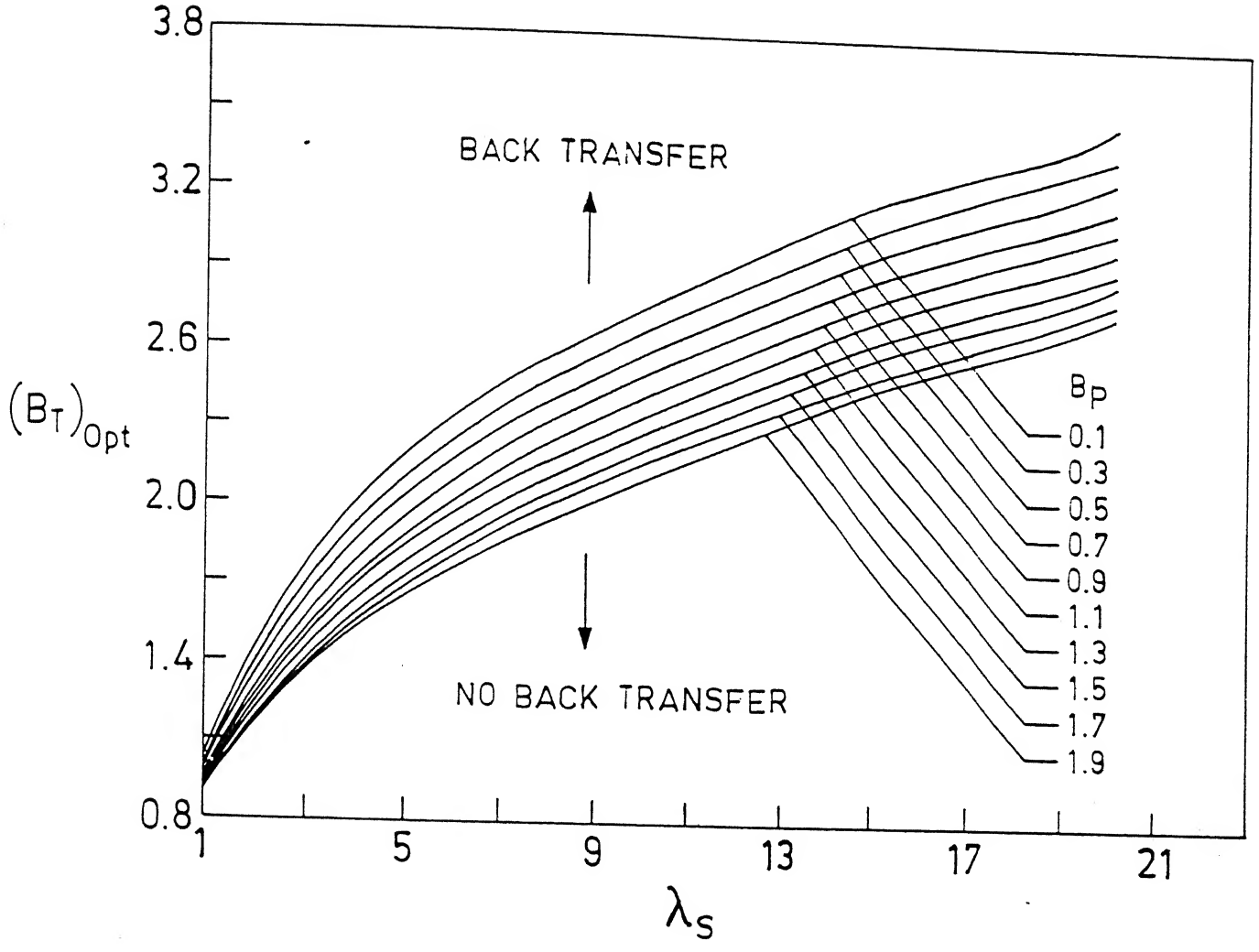

Fig. 3.9 Optimum B_T variation with λ_S for various values of B_P.

Thus the identification of optimum B_T value optimizes the powder injection refining process with respect to the variables like loading ratio, mass flux flow rate etc.

3.2 Slag Carry-over:

Usually in ladle metallurgical processes there will be carried-over slag from BOF on the top of the melt at the beginning of the injection process. The main component of BOF slag is FeO. For deS it is deleterious whereas for deP it is beneficial. Average BOF slag composition is 48%CaO, 18% SiO_2, 6%Mgo, 4%Mno, 7%Al_2O_3, 2%P_2O_5 and 20%Fe_tO. Prior to flux injection as there is some slag of different composition on the top of the molten metal, study of its effect, during powder injection, on refining processes is essential.

When powdered flux is injected into the molten bath, on its rise to the top surface of the melt it will be mixed into the already existing top slag. As both top slag and powdered flux are of different composition and as there is assimilation of injected flux with top slag continuously through out the injection period, the overall top slag composition also changes.

When equation (2.24) and equation (2.22) are compared, there are two additional terms i.e., η_o^* (top slag partition coefficient) and Y_C (Mass fraction of carried-over slag from BOF at $\tau=0$) in equation (2.24).

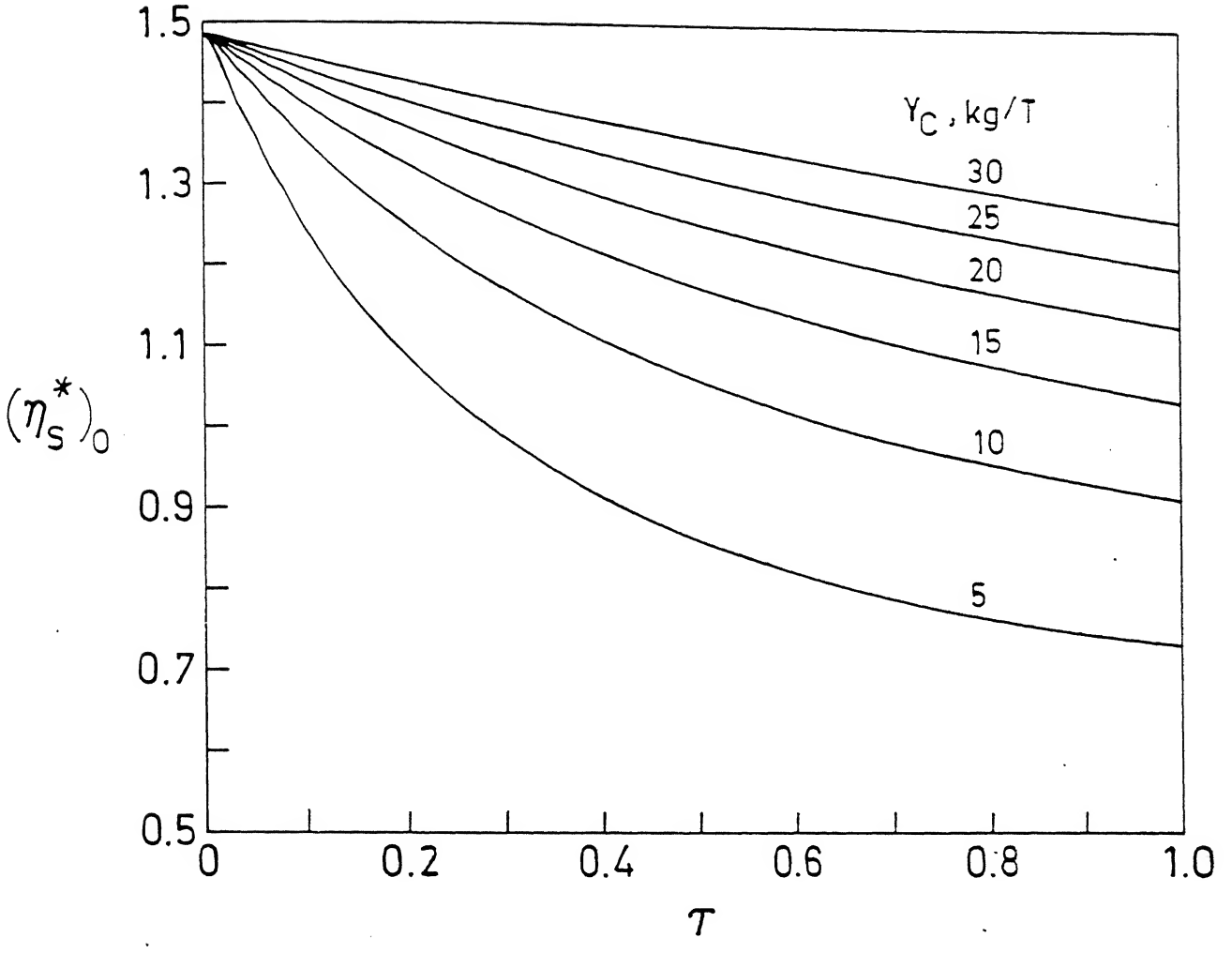

Fig. 3.10 Variation of $(\eta_s^*)_o$ as a function of time for various values of carry-over slag mass.

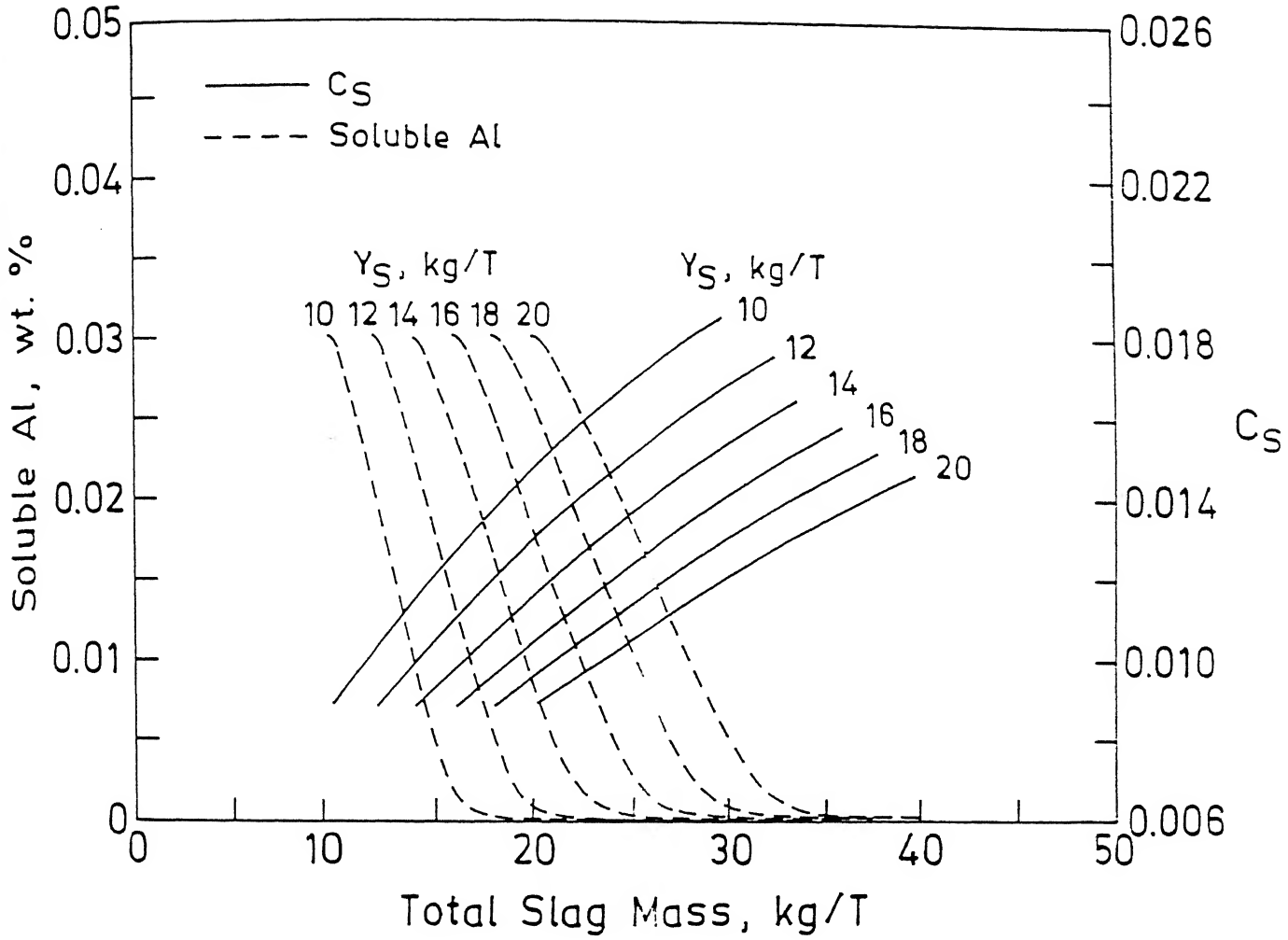

Fig. 3.11 Sol.Al and Cs variation with synthetic slag and carry-over slag mass.

3.2.1 Variation of η_o^* as a function of τ:

η_o^* is the overall partition coefficient of the slag which consists of caried-over slag and accumulated injected flux per unit of time. As top slag composition changes with time, η_o^* also changes. Thus the decrease or increase in η_o^* affects the powder injection refining process. To study its variation with time two examples are chosen. One for sulphur and the other for phosphorus.

3.2.1.1 Sulphur:

For sulphur removal synthetic flux of composition 60% CaO,-40%Al_2O_3 is chosen for injection. η_S^* for this flux is 276 for 0.03% soluble Al in liquid steel. Mass of synthetic flux is 10 Kg/(T of steel), and the mass of carried-over slag is varied from 10 - 50 Kg/(T of steel), the average carry-over slag composition is given in the section 3.2, injection rate is kept at 1 kg/T of Steel. For the above conditions overall slag composition is calculated at each τ (τ varies from 0 to 1) and C_S is computed by optical basicity equation and equilibrium Al concentration of the melt is computed from the reaction

$$(FeO) + \underline{Al} = [Fe] + (Al_2O_3) \qquad (3.4)$$

$$\Delta G^o_{(3.4)} = -878,552.12 + 233.89\ J/mole$$

The calculation procedure is given in Appendix-4. In Fig. 3.10, the variation of $(\eta_S^*)_o$ as a function of time (τ) is shown. In this figure it is clear that the carry-over slag's partition coefficient is much less than that of synthetic slag. This is due

to FeO present in the carry-over slag. Increase in $(\eta_S^*)_o$ with increase in slag carry-over mass is also observed in this figure. This increase in $(\eta_S^*)_o$ can be explained with fig. 3.11 in which soluble Al loss, C_S are plotted as a function of total slag mass i.e., mass of synthetic slag and carried-over slag.

Computation of C_S and soluble Al in the melt is same as explained above. C_S increases gently along each iso Y_S line, with carry-over slag mass, but drastic decrease in soluble Al content can be seen at Y_C in the range 0 - 10Kg/(T of Steel). When Y_C is greater than 10 Kg/(T of steel) soluble Al decreased to such low level that no further loss takes place. But C_S increases continuously. That is increase in $(\eta_S^*)_o$ occurs at Y_C above 10Kg/(T of Steel).

3.2.1.2 **Phosphorus:**

For phosphorus removal the synthetic slag composition chosen is 55% CaO-23%FeO-22%CaF_2. Mass of synthetic flux, mass of carried-over slag and the average composition of carry-over slag are same as in the section 3.2.1.1. $a_{\underline{O}}$ is evaluated as per the procedure given in appendix-4. C_P is evaluated from optical basicity correlation (see table 2.3). $(\eta_P^*)_o$ is computed from equation 2.55. η_P^* is computed to be 50. $(\eta_P^*)_o$ as a function of τ is plotted in Fig. 3.12 for various values of Y_C. $(\eta_P^*)_o$ is more than that of synthetic flux along and like sulphur $(\eta_P^*)_o$ increases with carry-over mass. This is just opposite to the partition coefficient of sulphur variation in the present of carry-over

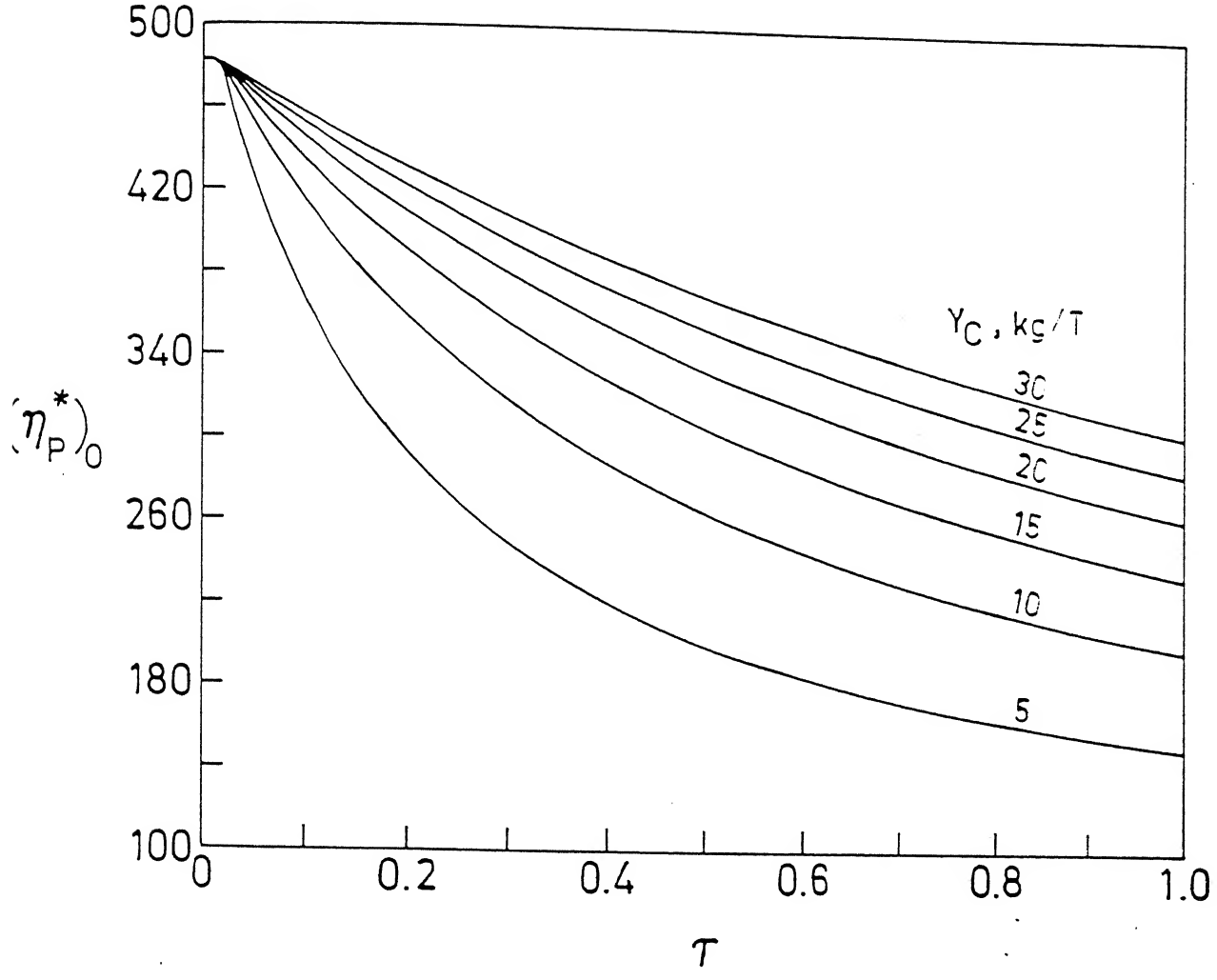

Fig. 3.12 Variation of $(\eta_P^*)_o$ as a function of time for various values of carry-over slag mass.

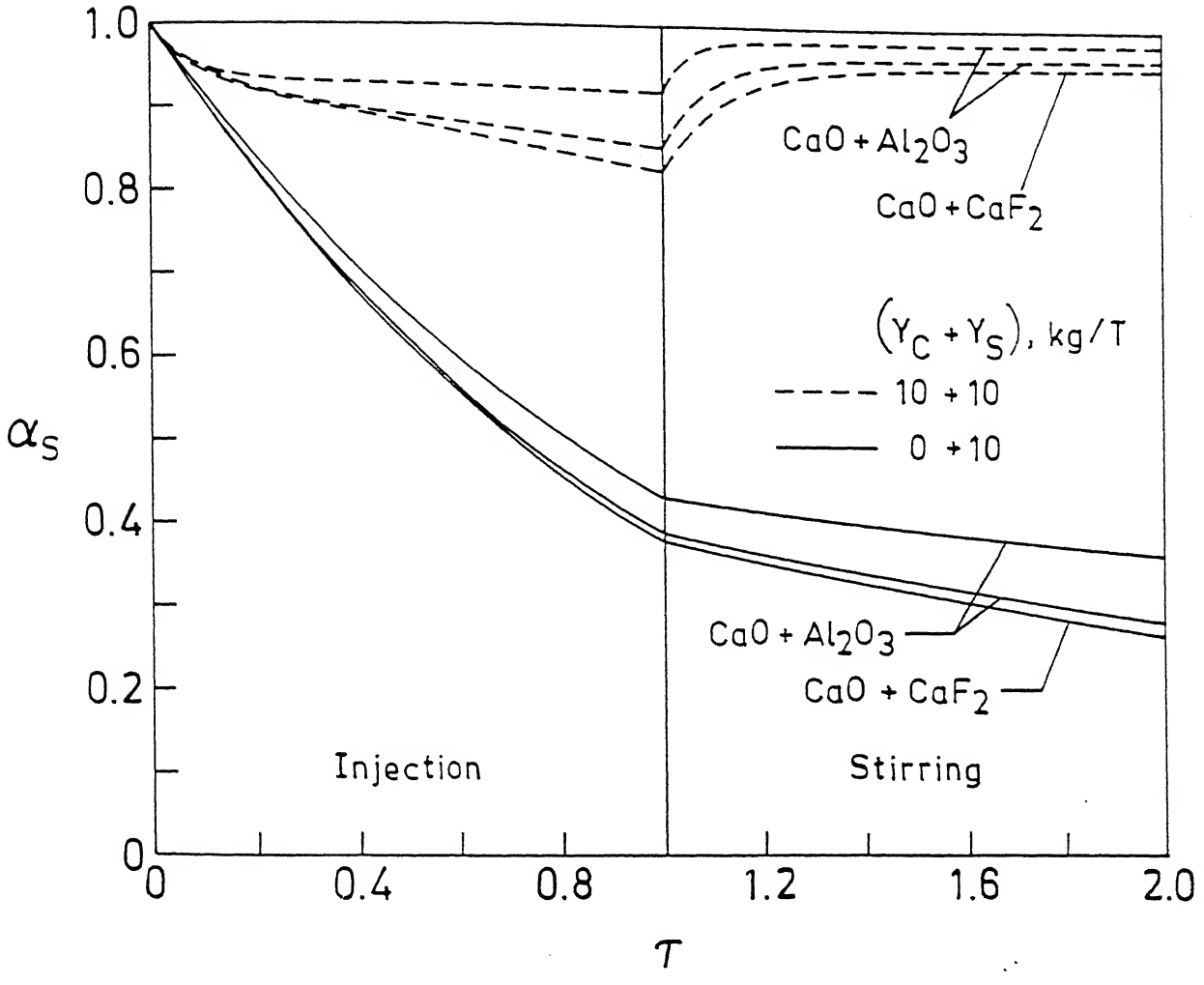

Fig. 3.13 α_S vs τ for $CaO-Al_2O_3$, $CaO-CaF_2$ slag systems in the presence of slag carry-over

slag. The increment in $(\eta_P^*)_o$ is due to both C_P and $a_{\underline{O}}$.

3.2.2 Concentration vs. time plots:

Appearance of η_o^* and Y_C in equation 2.24 forced to chose specific parameters, as input to modern, to discuss about slag carry-over effect on powder injection refining. As discussed in section 3.2.1 slag carry-over affects deS and deP during powder injection, in opposite manner. That is why, here also, they are separated.

3.2.2.1 α vs τ plots for sulphur:

In the fig. 3.13 the variation of sulphur as a function of time is shown for three different types of synthetic fluxes namely $60CaO-40Al_2O_3$, $70CaO-30Al_2O_3$, $70CaO-30CaF_2$ in the presence and in the absence of carried-over slag. The selected synthetic fluxes have η_S^* 276, 310 and 500 respectively for 0.03% sol. Al in liquid steel. In all the cases mass of synthetic flux is 10 Kg/(T of steel), mass of carried-over slag is 10 Kg/(T of steel), synthetic flux injection rate is 1 Kg/(T of steel) and selected B_P, B_T values are 0.4, 0.6 respectively. Melt concentration as a function of time is evaluated from the equation (2.24). It can be seen from the figure that slag carry-over deteriorates, considerably, the removal of sulphur both in injection and stirring regions. This is due to the reversion of Sulphur from slag to melt.

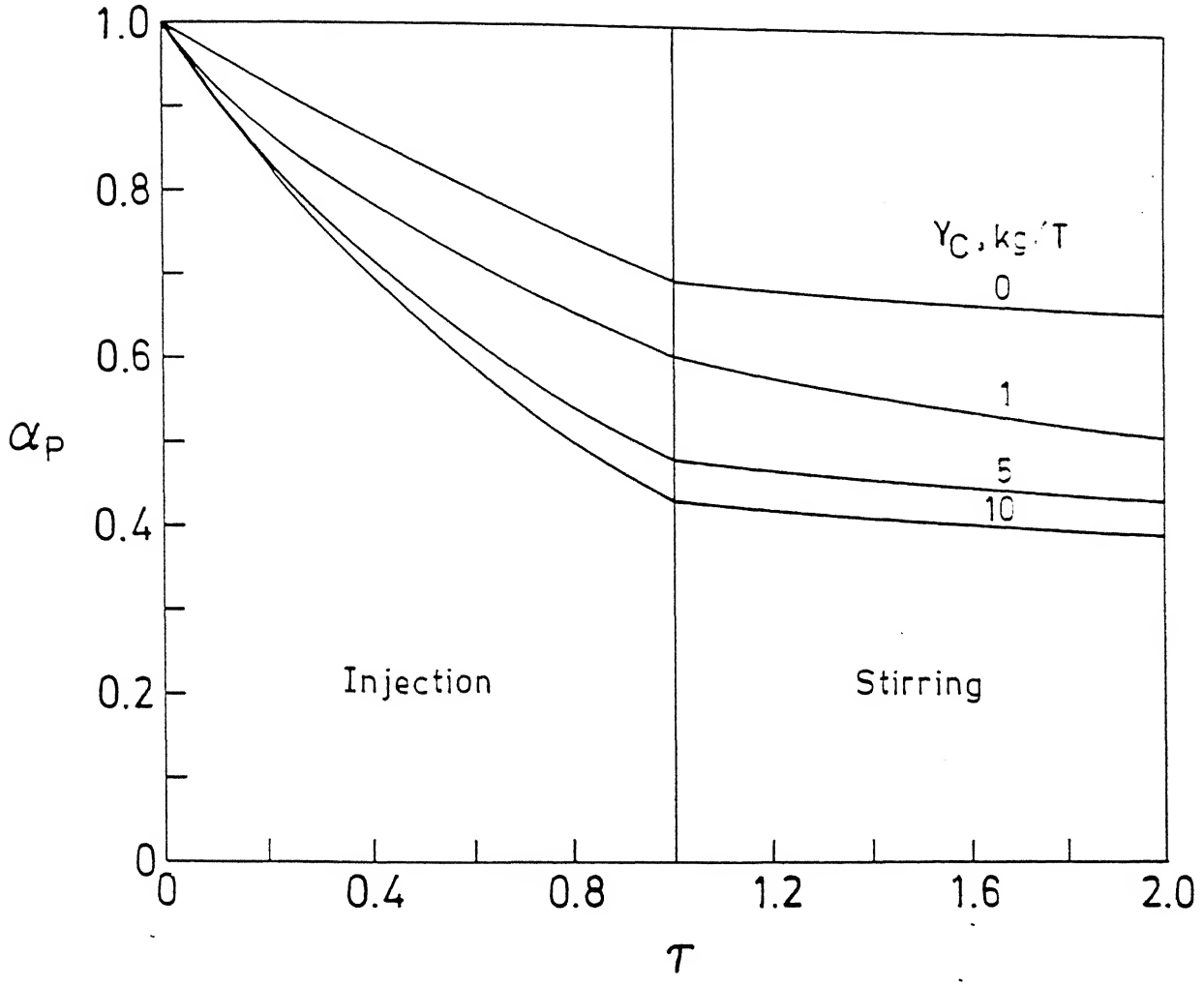

Fig. 3.14 α_P vs τ as function of carry-over slag mass

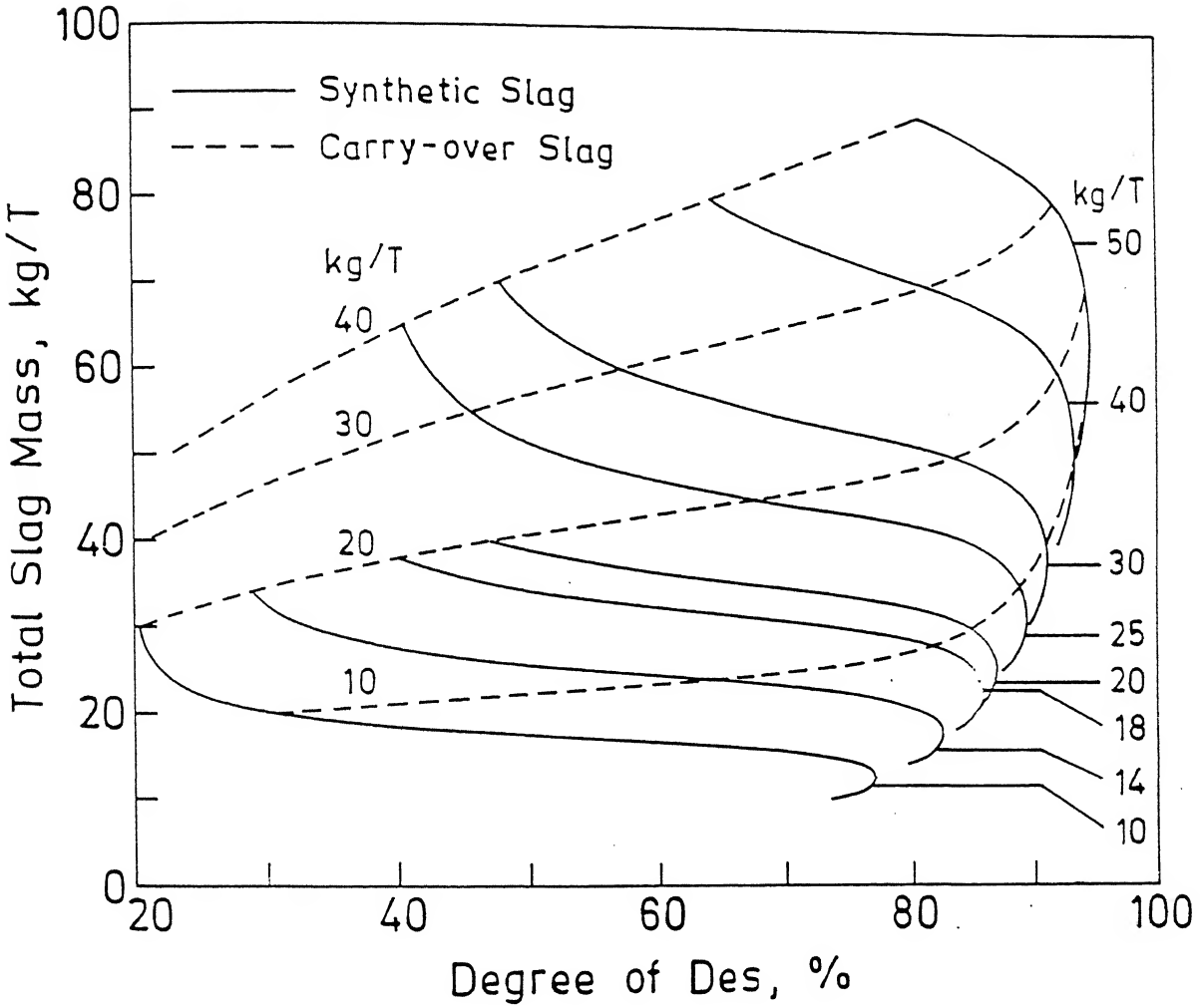

Fig. 3.15 DeS degree variation with synthetic and carry-over slag mass.

3.2.2.2 α vs τ plots for phosphorus:

In Fig. 3.14 the variation of phosphorus as a function f time is shown for the synthetic flux of composition 55%CaO-23%FeO-22%CaF_2 in the presence and in the absence of carried-over slag. Three values of Y_C are chosen. Calculation of $a_{\underline{o}}$ and C_S is same as in section 3.2.1.2. It seems from this figure that carry-over slag is beneficial for deP. But if synthetic slags partition coefficient is greater than that of carried-over slag (this conditon is similar to that in deS with slag carry-over) rephosphorisation will occur for high value of B_T.

Because of the reasons discussed above the negative effect of slag carry-over is observed, mostly, in deS by powder injection.

3.2.3 DeS and DeP efficiency:

Efficiency of impurity removal is defined by

$$\eta = \left[1 - \frac{[x]}{[x_o]}\right] \times 100 \qquad (3.5)$$

$[x_{eq}]$ depends η_o^* as per equation (2.29). Degree of deS is shown in Fig. 3.15 with total slag weight, consists of synthetic and carry-over slags, as a variable. Slag system chosen is 60% CaO-40%Al_2O_3 and initial soluble Al of melt is 0.03%. In this figure. iso synthetic slag mass lines and iso carry-over slag masslines are shown. Along each iso Y_S line initial increase in degree of deS with a small increase in carry-over slag mass and a drastic fall

are observed. The initial increase is due to rise in sulphide capacity and the drastic decrease is due to loss of

soluble Al content of the melt (see Fig. 3.13). Along each iso Y_C line the continuous increase in degree of deS' with increase in Y_S is obviously due to decrease in FeO concentration in the over-all slag. Similar to sulphur, degree of deP is also evaluated from equation (3.5) for various combinations of synthetic and carried-over slag. This is plotted in Fig. 3.16. The slag system is 55%CaO-23%FeO-22%CaF_2. With the exception of peak in Fig. 3.15, Fig. 3.16 is just opposite to Fig. 3.15, i.e. increase in Y_C, along each iso Y_S lines, increases degree of deP, but increase in Y_S, along each iso Y_C line, decreases degree of deP. This is due to the reason mentioned in the above section 3.2.2.2.

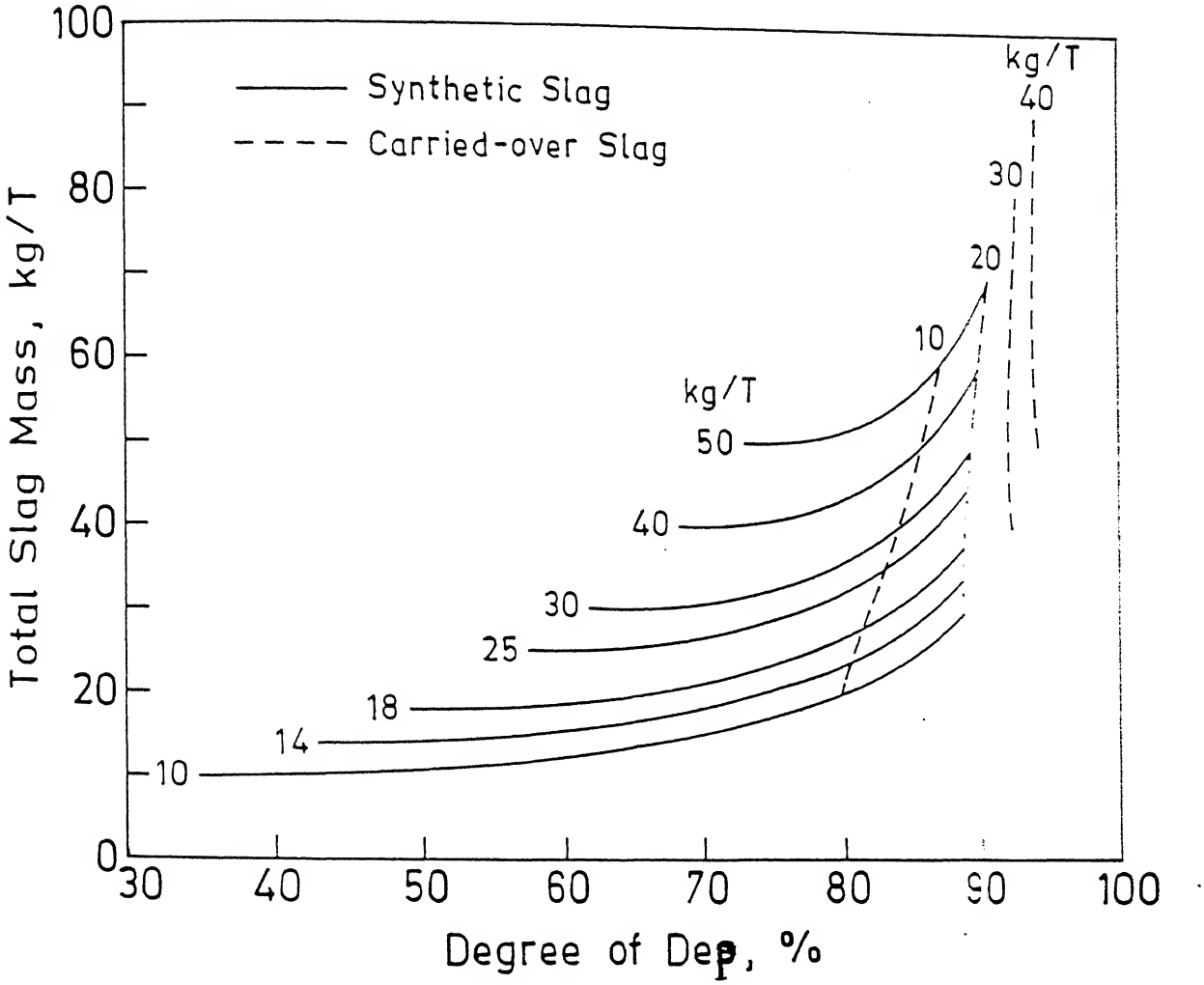

Fig. 3.16 DeP degree variation with synthetic and carry-over slag mass.

CHAPTER 4

APPLICATIONS

In this chapter the applications of the model is discussed with reference to the removal of sulphur, phosphorus and nitrogen from the hot-metal/steel without, and with carry-over of fixed amount of slag from the previous refining reactors. For this purpose the available information on the removal of the above mentioned impurities are obtained from the concentration vs time plots. From these concentration vs time plots the permanent and transitoric rate constants and their contributions towards the overall refining are evaluated, and discussed. About the organization of this chapter the rate of removal of sulphur, phosphorus and nitrogen are presented separately.

4.1 DeS:

Various research workers had investigated the removal of sulphur from hot-metal/steel by injecting suitable amount of slag forming materials. For the purpose of the present analysis deS caused by injection of binary and ternary CaO based fluxes are chosen. The details about the type of the flux, mass flow rate of the flux, carrier-gas flow rate etc., are compiled from the available literature and given in the Table 4.1. From the concentration vs time plot of each investigator the values of K_p, K_T, f and E are determined by using equations (2.15) and (2.22). The calculation procedure of the above mentioned parameters is given in Flow-chart 2 and the source code is given in Appendix-5.

The values of ϕ_S and θ_S are derived by using equations 2.15 and 2.22. (See flow chart-2 for details). η_S^* for each type of slag is determined by equation (2) of Table 2.1 and is listed in Table 4.1 as $\lambda_S(\lambda_S = \eta_S^* Y_S)$. The value of f is calculated by equation (A3.5) (see appendix-3 for detailed procedure). With the known value of ϕ_S, θ_s, λ_S and f, B_p and B_T are determined by using equation (2.14). From the known values of t_{inj}, K_p and K_T are determined from the calculated values of B_p and B_T values ($B=kt_{inj}$). The transitoric efficiency parameter is determined by equation (3.3). The calculated values of K_p, K_T, f and E are listed in Table 4.1.

Fig. 4.1 and Fig. 4.2 show the variation of α vs τ for the experimental conditions of the investigators listed in Table 4.1.

In the literataure pressumption of K_p value or evaluation of K_p by dumping experiments were done to find transitoric rate contribution, transitoric efficiency (E) etc. But as per the above procedure, with the developed model, K_p value is evaluated directly from concentration vs time plot alone. In Table 4.1 the K_p values specified by respective authors are also listed. The comparison of evaluated K_p values with the specified K_p values show a match in Sr. No. 2 (see Table 4.1), but remaining two show a large difference. Matching of the results in Sr. No. 2 (Table 4.1) is due to the fact that the permanent rate constant was specified by doing the dumping experiments under the same conditions as injection experiments i.e., same type of flux, same

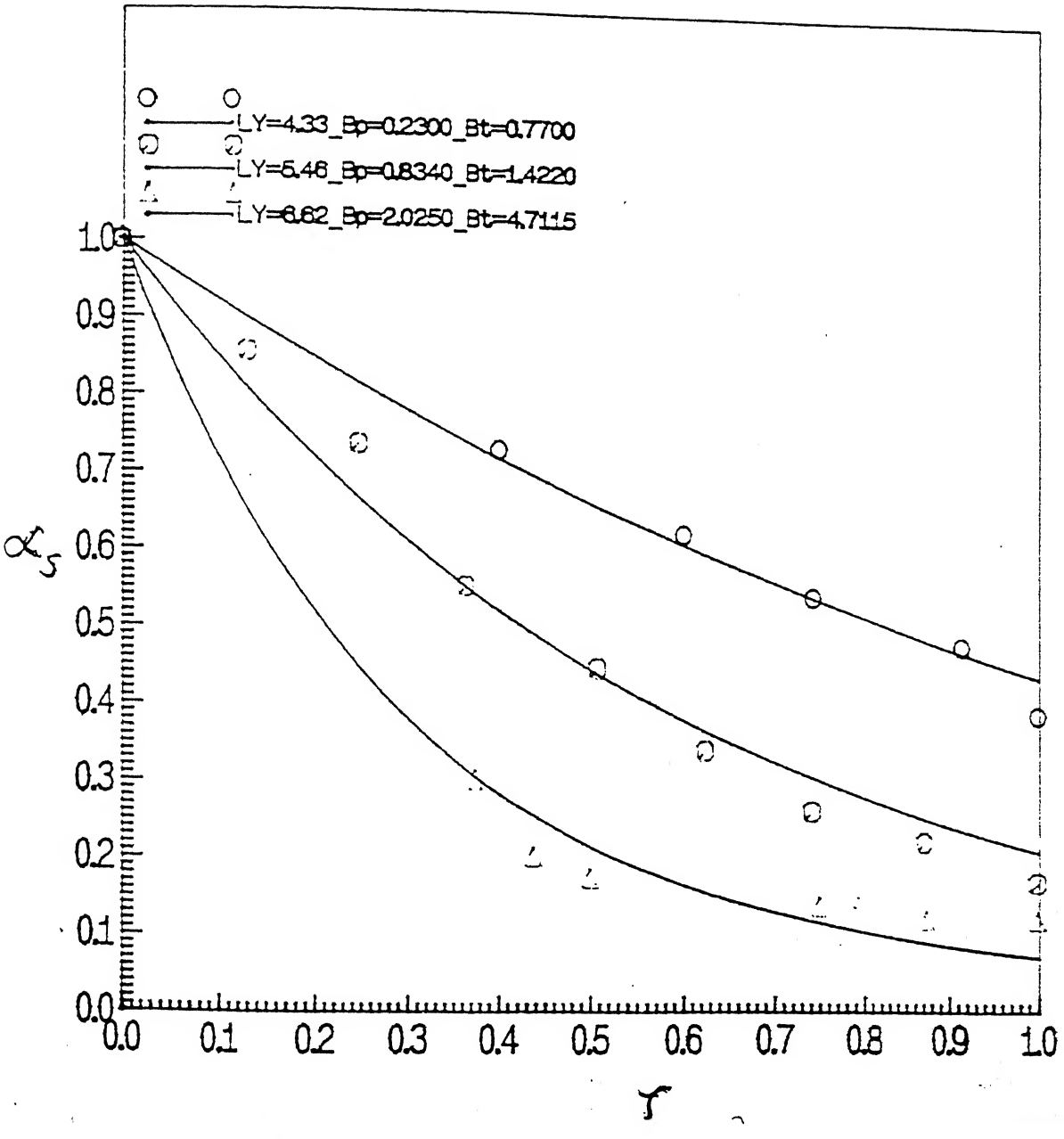

Fig. 4.1 Model parameters evaluation from concetration vs time plots for Ref. [6], [7] and [8]

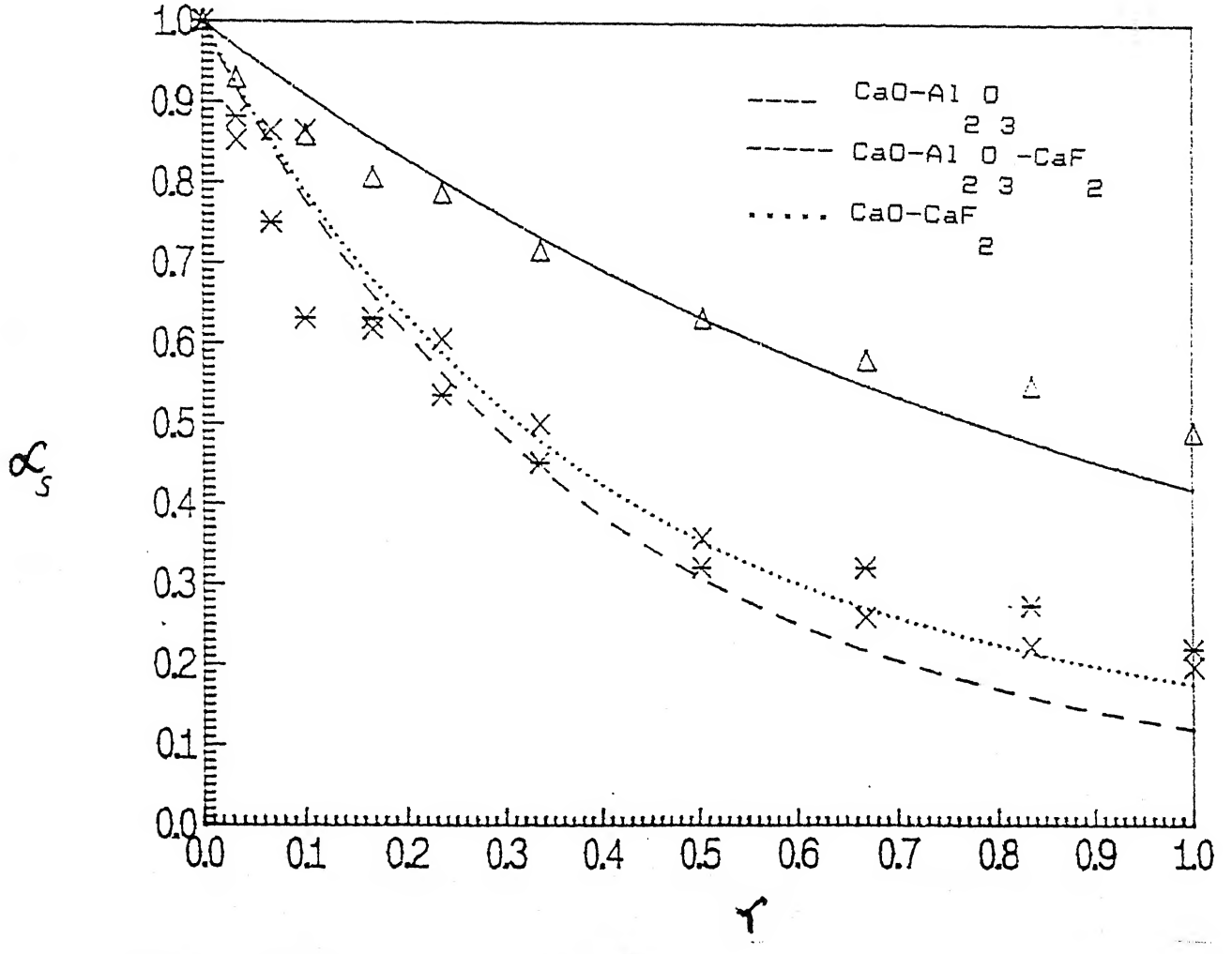

Fig. 4.2 Model parameters evaluation from concetration vs time plots for Ref.[29]

amount, same treatment time, same gas flow rate etc. In Sr. No. 1 the K_p value was assumed by the investigators. In Sr. No. 3 although K_p was specified on the basis of dumping experiments but the conditions of powder injection and dumping were not similar. For the remaining experimental conditions no rate parameters were specified. Only the concentration vs time curves with the experimental conditions were available. For those also the model parameters i.e, λ_S,K_p, K_T, f and E are evaluated.

4.2 DeP:

Similar to deS, DeP was also investigated by various research workers in hot-metal/steel by the injection of powdered fluxes under oxidizing as well as reducing conditions. The experimental conditions for some deP experiments are given in Table 4.2. For each investigators, the values of ϕ_S and θ_S are determined from their respective concentration vs. time plots and by using equations 2.15 and 2.22. The values of ϕ_S and θ_s are given in Table 4.2.

The variation of dimensionless concentration with time are shown in Fig. 4.3 and 4.4 by solid lines for CaC_2 flux and $CaO-CaCl_2-CaF_2$ flux, are obtained by using evaluated ϕ_S and θ_s values in equation 2.22. The experimental points are superimposed on the respective figures. For the investigator No. 3 in Table 4.2 the calculated values of ϕ_S and θ_S are given, but the α vs τ plot could not be given because of the lack of experimental points for comparison. For this case deP degree is calculated by the

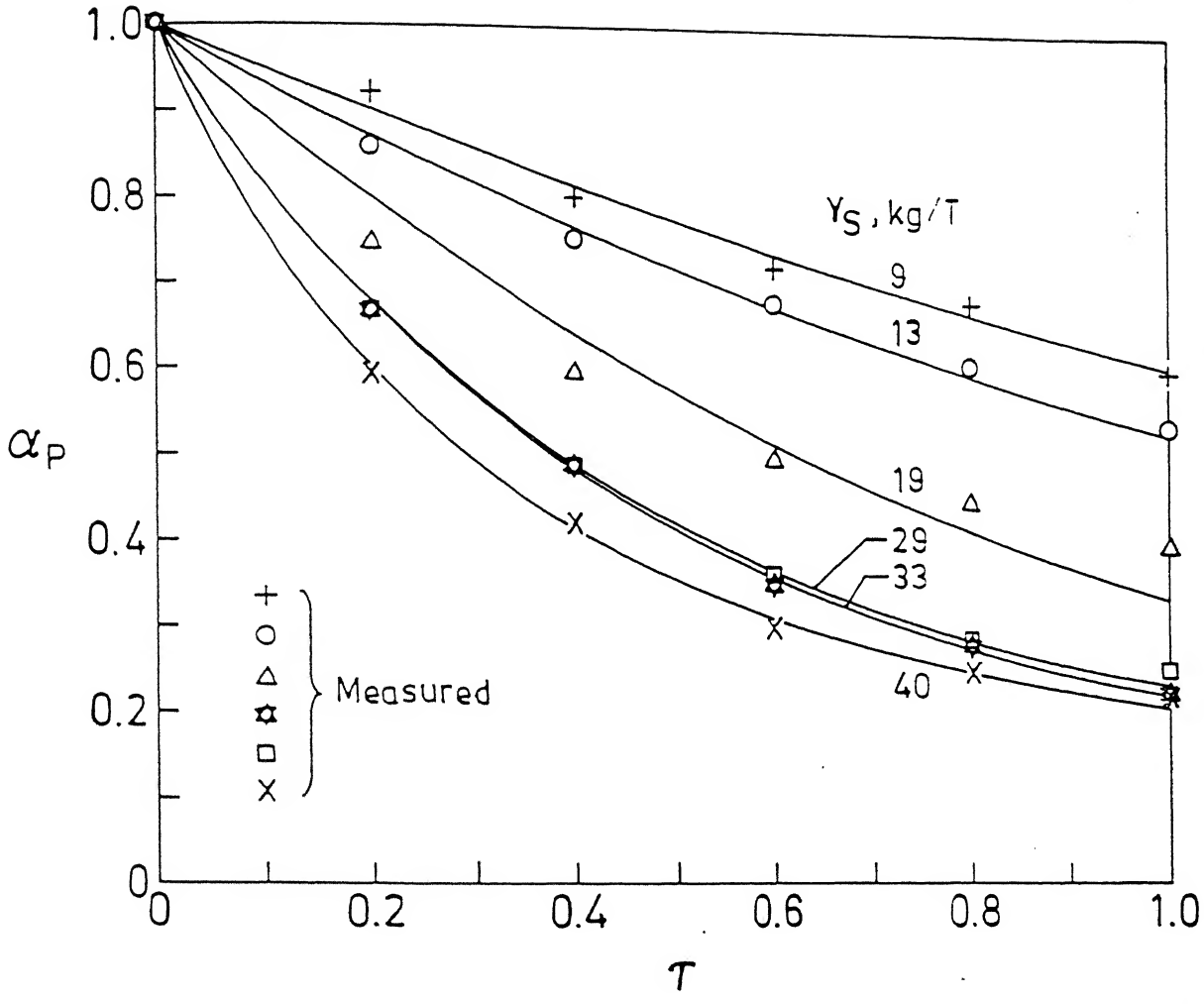

Fig. 4.3 Model parameters evaluation from concetration vs time plots for Ref. [34]

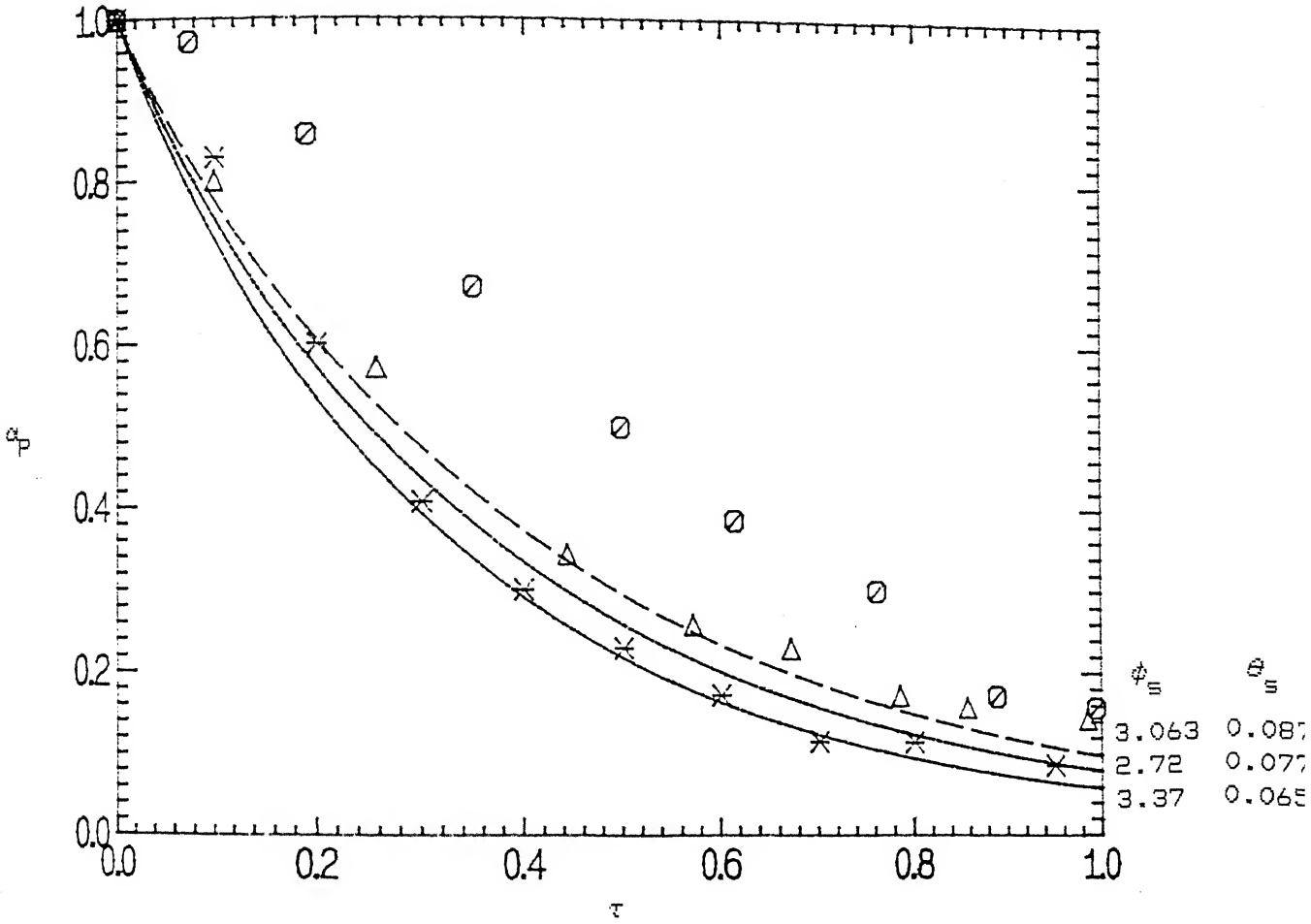

Fig. 4.4 Model parameters evaluation from the experimental conditions of Sawada's data [25]

following expression:

$$\text{deP degree} = \frac{[x_o] - [x_f]}{[x]} \times 100 \qquad (4.1)$$

The calculated values of deP degree are reported in Fig. 4.5 along with the experimental points.

4.2.1 DeP with CaC_2 flux:

From Fig. 4.3 it can be seen that the experimental data points can be reproduced well by the model equation (2.22) of the present investigaton. From their experimental result the coefficient of utilization of CaC_2 for deP is determined. The coefficient is defined by

$$\text{Utilization coefficient } (\delta) = \frac{\lambda_S}{\lambda_T} = \frac{\eta_S^* Y_S}{\eta_S^* Y_T} = \frac{Y_S}{Y_T} \qquad (4.2)$$

In equation (4.2) Y_T is the actual amount utilized inorder to decrease the concentration of phosphorus from its initial to some final value and Y_S is actually utilized among. λ_S can be calculated from the following mass balance equation

$$m_S(x_f) = m_L\left[[x_o] - [x_f]\right]_{m_S} \qquad (4.3)$$

Since $(x_f) = \eta_S^*[x_f]$ and $\frac{m_S}{m_L} = Y_S$, after some rearrangement and transformation,

$$\lambda_S = \eta_S^* Y_S = \frac{1-\alpha_f}{\alpha_f} \qquad (4.4)$$

The value of α_f is determined from the concentration vs time curve, for injection, from Ref [34]. Using this α_f valuein equation (4.4) λ_S calculated. λ_T is calculated from CaC_2 reactic with phosphorus as follows

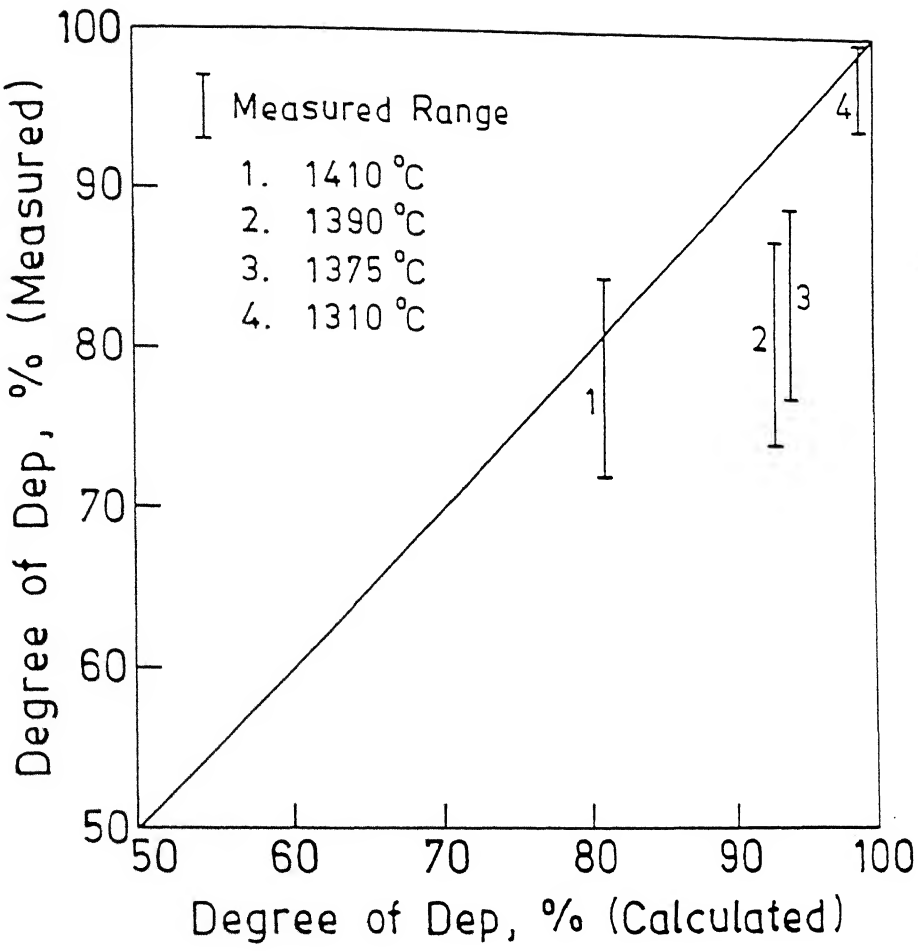

4.5 Comparison of calculated and measured deP degree

$$3CaC_2 + 2P \longrightarrow Ca_3P_2 + 6C \qquad (4.5)$$

$$\Delta G^{o}_{(4.57)} = -79.5 - 0.012T \text{ KJ/mole}$$

At 1879 K assuming $a_{CaC_2} = a_{Ca_3P_2} = 1$ and using $\Delta G^{o}_{(4.57)}$ value, we get

$$a_{\underline{P}} = 3.78 \times 10^{-2} a^{3}_{\underline{C}}$$

As carbon and phosphorus concentration are low in steel, 1 wt% standard state can be taken

$$h_{\underline{P}} = 3.78 \times 10^{-2} h^{3}_{\underline{C}} \qquad (4.6)$$

From stoichometric relation of (4.5)

$$[C_{eq}] = [C_o] + \frac{72}{62}\left\{[P_o] - [P_{eq}]\right\} \qquad (4.7)$$

From the solution thermodynamics the following relations are valid

$$\left.\begin{aligned} h_P &= f_P[\%P] \\ h_C &= f_C[\%C] \\ \log f_P &= e^{C}_{P}[\%C] + e^{Cr}[\%Cr] \\ &= 0.24[\%C] - 0.001[\%Cr] \\ \log f_C &= 0.1[\%C] - 0.036[\%Cr] \end{aligned}\right\} \qquad (4.8)$$

By solving equations (4.6), (4.7) and (4.8) simultaneously for the given initial carbon, phosphorus and chromium contents of stainless steel bath, equilibrium phosphorus ($[P_{eq}]$) content in the melt can be determined as follows.

In the selected example [Co] = 0.65%, $[Cr_o]$ 12%, $[P_o]$ is 0.03%, and $[P_{eq}]$ evaluated is6.807 ppm. Using equation (4.3), in which α_f is equal to α_{eq} [α is phosphorous], λ_T is evaluated to be

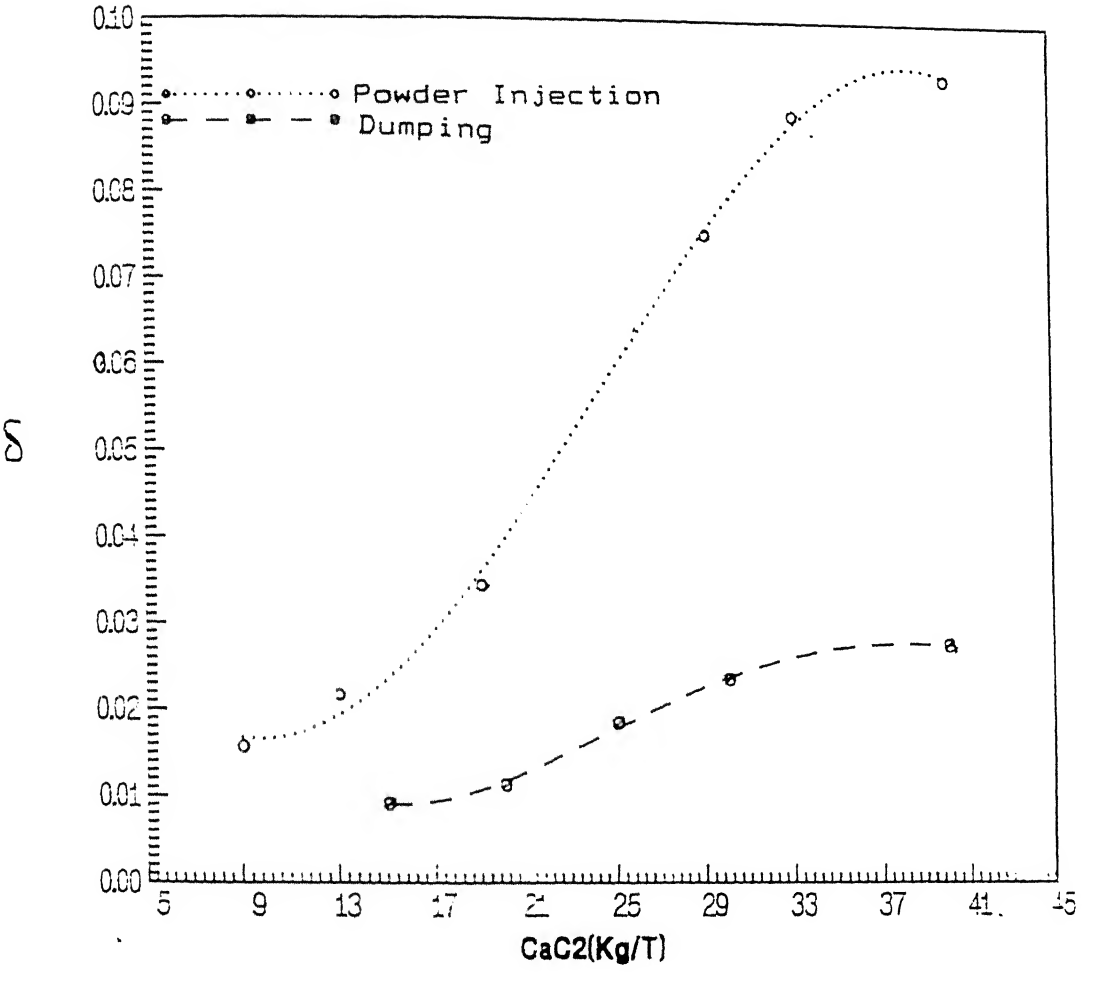

4.6 Utilisation varition of CaC_2 powder used in refining

44.5.

In the similar way λ_T is calculated for the other initial phosphorus content, and these are given in Table 4.2. By equation (4.2) δ is calculated and plotted in Fig. 4.6 against CaC_2/T injected. In this figure calculated values of δ are also shown for the case of dumping CaC_2. It can be seen in the Fig. 4.6 that the utilization coefficient lay within the range 1-2.5% for dumping experiments, whereas this value varies from 1.8 to around 9.5% for injection experiments. According to kitamura et al., [61], the maximum δ value for dumping is 2.7%, which coincides with the above calculated value for dumping. The higher δ value for injection can be explained by considering the mechanism of deP by CaC_2. CaC_2 decomposes into Ca and C. As the B.P. (Boiling point) of Ca is lower than the refining temperature, its vaporisation is bound to occur. But the vaporisation loss is decided by the partial pressure of Ca at refining temperature. Injection of CaC_2 deep into the bath decreases the partial pressure of Ca, and thus decreases the vaporization loss.

One interesting result from the model is the ratio ϕ_S upon θ_S. It is observed that this ratio is greater than the product of η_S^* and initially chosen Y_S value (see Table 4.1) for non-vaporising fluxes and much less than the same product (see Table 4.2) for vaporising fluxes. If the product is designated by λ_T, the comparison of evaluated ϕ_S/θ_S and λ_T from model suggests whether the flux is vaporising or non-vaporising.

4.2.2 DeP by $CaO-CaCl_2-CaF_2$ flux:

In order to evaluate the concentration of phosphorus in the melt as a function of time by using the model, ϕ_S and θ_S values are required. To evaluate concentration vs time plot for the experimental cnditions given for deP, by using this flux, see Table 4.2, K_P, K_T and λ_S are to be computed (see flow chart-1). To calculate K_P and K_T from the given experimental conditions, selected equations in Chapter 2 are used. To calculate λ_S, precisely η_P^*, regular solution model is used because of the inability of equations listed in Table 2.3, along with equations (2.55) and (2.58). $\nu_{PO_{2.5}}$ (see equation (2.58)) is calculated by the regular solution model as follows

$$RT\ln\nu_{PO_{2.5}} = \alpha_{Ca^{2+}-P^{5+}}\,(X_{CaO}^2 + X_{CaCl_2}^2 + X_{CaF_2}^2) \qquad (4.9)$$

$$\alpha_{Ca^{2+}-P^{5+}} = -250000 - 127000\left[10X_{CaF_2}/X_{CaO}\right]^{1/2} - 23350\left[10X_{CaF_2}/X_{CaO}\right]^{2} \text{ (J/mole)} \quad [62] \qquad (4.10)$$

For exmaple, for $X_{CaO} = 0.8991$, $X_{CaCl_2} = 0.0419$, $X_{CaF_2} = 0.059$

$$\alpha_{Ca^{2+}-P^{5+}} = -358560.31 \text{ (J/mole)}$$

$$\nu_{PO_{2.5}} = 4.08\times10^{-10}$$

The value of equilibrium constant (K) from equation (2.57) is 100.3226. In carbon saturated iron the average value of a_o is 6×10^{-5} (see section 2.4.1.1), by considering carbon and oxygen equilibrium in the melt.

Thus $\log C_P$ from equation (2.58) is 13.087 and η_P^*, from

equation (2.55), is 1367.4, and λ_P is 32.27. (Y_S= 0.0236).

The calculated value of K_P, from equation (2.77), is 0.14 min^{-1}. Stirring energy is evaluated from the equation (2.79). To calculate K_T, β_T and A_T are needed. A_T is computed from the equation (2.74), by wing equation (2.75) and (2.76) to evaluate t_R. The calculated value of t_R and A_T are 0.163 sec. and 3846.8 cm^2 respectively. β_T is evaluated from equation (5) of table 2.4 along with equations (2.72) and (2.73). It is 0.051 cm/sec.

For particle diameter of 0.1mm, usually used in powder injection refining, the computed K_T is 0.0135 min^{-1}. With t_{inj} is 20 min. B_P and B_T are 2.8 and 0.11 respectively. Similarly λ_S, B_P and B_T can be evaluated for other conditions given in Table 4.2 for this flux.

4.2.3 DeP by CaO-FeO-CaF_2-Fe_2O_3 flux:

The values of ϕ_S and θ_S are evaluated from the experimental conditions through the calculation of B_P, B_T and λ_S in the same way as discussed above. The calculated values are given in Table 4.2. Melt concentration at the end of injection is calculated, and deP degree from equation (4.1) is calculated. Calculated and measured deP degree are shown in Fig. 4.5 with 45° line. η_P^* for the above system is computed from the equation (2.55) by using optical basicity equation (equation (2), Table 2.3) for C_P calculation. Theoretical optical basicities of oxides and fluorides are given in Table 2.2 and the evaluation of optical basicity of slag-system is explained in section 2.4.1.

For the given flux composition say 45-56%CaO, 14.8%FeO, 34.62%Fe_2O_3 and 5.02%CaF_2, $\log C_p$, calculated from the optical basicity correlation given in Table 2.2, is 7.07. $\log a_{\underline{o}}$ is calculated to be 11.496 and η_p^*, calculated from equation (2.55) is 466. With the given mass fraction of slag 0.02468, λ_S is evaluated to be 11.496. Permanent rate constant is calculated from the equation (2.77) is 0.1222 min^{-1} and transitoric rate constant, calculated same as the procedure given in section 4.2.2, is 0.046 min^{-1}. To calculate B_P and B_T, K_P and K_T are to be multiplied with t_{inj} (in this example it is 22 min.). But it was reported that deP proceeds then only when deSi rate is practically ended. In the present experimental conditions given in Table 4.2 initial Si content of the bath is less than 0.1%. Kawasaki et al, [60] reported that deSi rate depends on

(a) rate of supply of oxygen when initial silicon is greater than 0.1%.

(b) Silicon transportation rate in hot-metal when initial silicon is less than 0.1%.

Thus from various experimental results analysed deSi can be taken as first order rate reaction when initial silicon content of the bath is less than 0.1%. Then onwards deP is active. Therefore the time taken for silicon removal from initial to 0.01% is found. It is deducted from total treatment time and thus deP degree was found.

When initial Si content is less than 0.1%,

$$\frac{d[\%Si]}{dt} = - K_T [\%Si] \qquad (4.11)$$

On integration of the above equation

$$\ln \frac{[\%Si_f]}{[\%Si_o]} = -K_T t \qquad (4.12)$$

K_T can be evaluated in the same way as given in section (4.2.2).

In the above chosen exsample initial silicon content is 0.08% and calculated K_T is 0.2234 min^{-1}, and thus time taken to reduce Si from 0.08 to 0.01% from equation (4.12) is 9.31 min. Thus deP proceeds in the remaining time i.e., 12.69 min. Hence B_P and B_T are 1.55 and 0.584 respectively. Final concentration of the melt can be calculated from the equation (2.22) as per the procedure shown in flow-chart 1 and deP degree is evaluated from the equation (4.1). Fig. 4.5 shows that the predicted deP degree is fairly well at 1310°C and 1410°C. Slightly lower deP degree was predicted at 1390°C and 1375°C.

4.3 DeN:

DeN by slag/metal refining is the new concept and not investigated as rigorous as deS and deP. The experimental conditions available in the literature are restricted to only dumping the flux as the top of the melt. From Fig. 2.4 it can be seen that the magnitude of partition coefficient of deN flux is much lower than that of deP and deS. it was identified that $BaO-TiO_2-Al_2O_3$ type fluxes are good for deN. The experimental conditions for deN, taken from ref. [38].

To evaluate the concentration vs time for the given

conditions under dumping experiments, the differential equation (2.10) is to be modified by putting the conditions $B_T = 0$ and by putting $t = t_{inj}$. The resultant differential equation is

$$-\frac{d[x]}{dt} = K_P\left[[x] - \frac{[x] - [x]}{\eta_S^* \gamma_S}\right] \qquad (4.13)$$

By integrating the equation (4.13), we get

$$\alpha = \frac{1 + \lambda_S \exp\left[-\frac{1+\lambda_S}{\lambda_S} K_P t\right]}{1+\lambda_S} \qquad (4.14)$$

As there is no equation available for calculation of nitride capacity of the slag system, measured value of C_N^{s-} is taken for the slag systems in Table 4.2, and η_N^* is evaluated from equation (2.69). For C_N^{s-} values as a function of composition at 1873K (see Fig. 2.2 and 2.3). With the given equilibrium Al content and the C_N^{s-} values η_N^* is evaluated. For example for the slag system containing 10%CaO-35%BaO-45%Al_2O_3-10%TiO_2, η_N^* is calculated to be 72.85 with the equilibrium Al content of the melt 0.15%. In induction stirring β_P varies from 0.02-0.03 Cm/sec [38]. Slag/metal interfacial area, in induction stirring, is the reactor cross-sectional area. Taking β_P is 0.02 Cm/sec and interfacial area, for the above example is calculated from the crucible inner dia, 86.6 Cm^3 and V_m is 1282.03 Cm^3(for 10 Kg melt), K_P is calculated to be 0.081 min^{-1}. Dimensionless concentration of the melt at time t is evaluated from equation (4.14) and shown as solid line in Fig. 4.7 with the experimental points. The close approximation of calculated and experimental points suggest that the model prediction is fairly well.

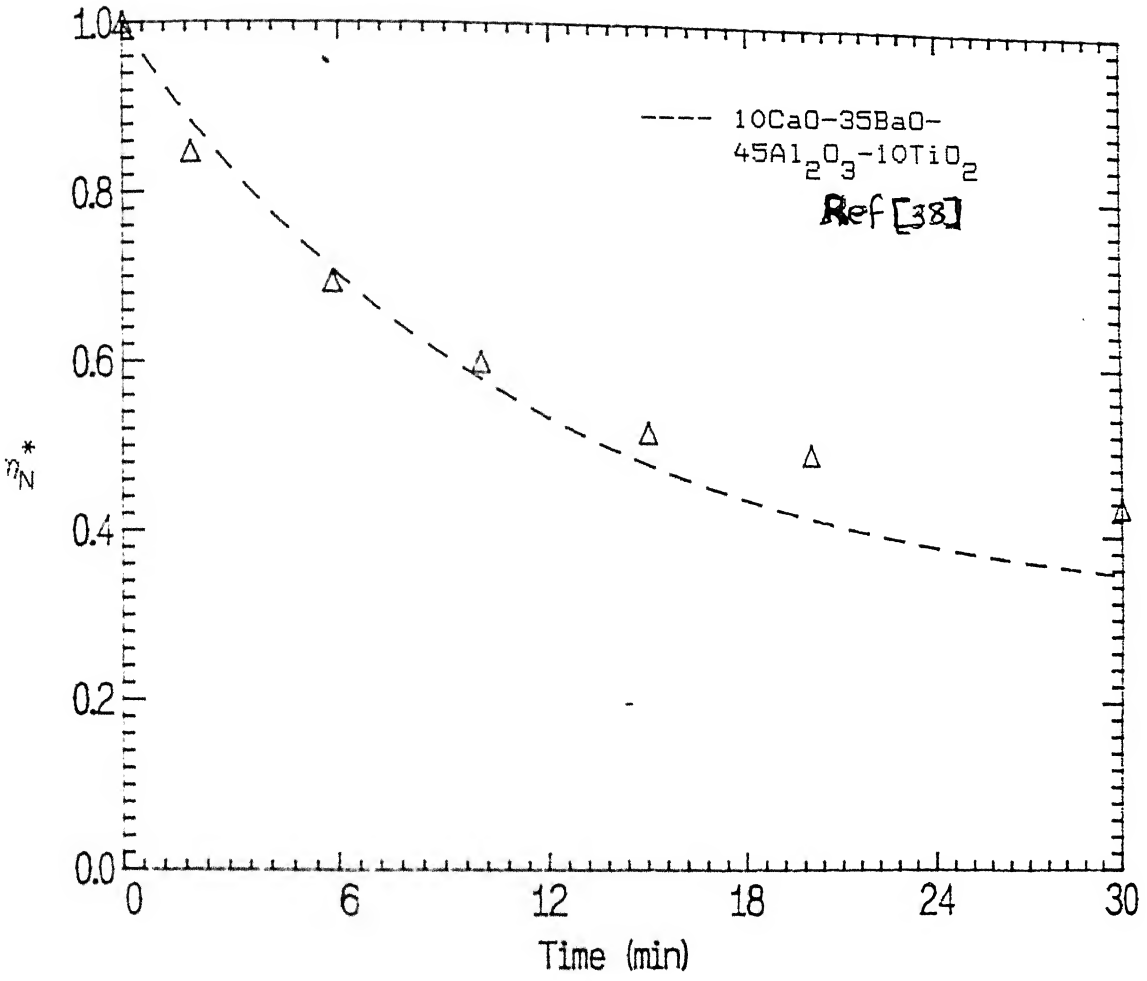

Fig. 4.7 DeN concetration vs time curve by slag/metal refining

CHAPTER 5

CONCLUSIONS AND SUGGESTIONS FOR FUTURE WORK

As a result of the present work, the following conclusions are made:

1. Mathematical model, developed in the present work, can be used as a tool to study the influence of powder injection parameters in impurity extraction from the melt.
2. Transitoric rate contribution in the overall refining process depends on the magnitude of B_P, B_T and λ_S.
3. The model demonstrates the deleterious effect of slag carry-over on powder injection refining process, especially with respect to deS.
4. Model is the mediator between powder injection refining parameters and melt concentration as a function of time, i.e., by using concentration vs. time curves powder injection refining parameters can be obtained or vice versa.

From the analysis of the model and the equations available in literature to calculate model parameters the following suggestions for further work are made:

1. Thorough analysis of critical stirring energy required for the emulsification of slag into melt, emulsified mass, drop diameter as a function of stirring energy are needed to evaluate K_P.
2. Investigation on injected powder - melt contact area is desirable.

REFERENCES

1. T. Tsukada et al. Tethu-to-Hagame. 68(1982), pp.S459.
2. T. Emi et al, Scaninject III, Part II, (1983), pp. 1:1-1:31.
3. R. Nemoto, Proc. Symp. Japan Inst. Metals, (Dec. 12, 1982, Tokai Bounch), pp. 10
4. K. Uchida et al., Tetsu-to-Hagane, 67(1981), pp. S573.
5. H. Schenck, Stahl U. Gzen, (1964), 84, pp. 311
6. Robertson et al., 11(1984), No. 5, pp.262-273.
7. Y. Haru et al., Scaninjeu IV, Part I, (1986), pp. 18:1 - 18:24.
8. Xu Chustao et al., ISIJ International, 32(1992), 10, pp. 1081-1083.
9. Haru-JÜrgen ergell, Steel Research, 59(1988), No. 12, pp. 527-531.
10. V. A. Kudiin, Scaninject IV, Part II, pp. 10:1-10:9.
11. E.T. Tuskdogan, Ironmaking and Steelmaking, 15(1988)6, pp. 311-317.
12. Xu Chushao et al., ISIJ International, Vol. 32, 1992, No. 10, pp.1081-1087.
13. Anders Werme et al., Scaninject IV, part I, pp. 22, (1986).
14. Akihide Hikoscaka et al., Pretretment of B/F molten iron, Iron and Steel Society, pp. 11 (1987).
15. J. Kolsi, Scand. Jr. metl (1990), pp. 110-115.
16. Dieter Janke, Pretreatment of B/F molten iron, Iron and Steel Society, pp. 129 (1987).
17. Keizo Taoka et al., Pretreatment of B/F molten Iron, Iron and Steel Society, pp. 49 (1987).

18. John Olof Edstrom et al., Pretreatment of B/F Molten iron, Iron and Steel Society, pp. 145 (1987).

19. Y. Nakajima et al., Pretreatment of B/F molten iron, Iron and Steel Society, pp. 87 (1987).

20. Shozo Kawara ki et al., Scaninject IV, Part I, pp. 20 (1986).

21. J.P. Reboul et al., Pretreatment of B/F molten iron, Iron & Steel Society, pp. 79(1987).

22. O. Haida et al., Scaninject II, 1980, pp. 20.

23. J. C. Niedringhaus et al., Pretreatment of B/F molten Iron, Iron and Steel Society, pp. 79(1987).

24. J. H. Kaminski et al., Pretreatment of B/F molten iron, Iron and Steel Society, pp. 3 (1987).

25. I. Sawada et al., Scaninject IV, Part I, pp. 12, (1986).

26. D.G.C. Robertson et al., ladle metallurgy Principles and Practices, pp. 67.

27. Y. Hera et al. Scaninject IV, Part I, pp. 18, (1986).

28. G. Repari et al., Scaninject III, Part II, pp. 44(1983).

29. A. Moria et al., Scaninject III, Part II, pp. 32 (1983).

30. T. Usui et al., Scan inject II, pp. 12 (1980).

31. Yuraka Yoshi et al., HSLA Steels Technology and Applications, American Society of Metals, pp. 380, (1983).

32. D. V. Moghe et al., Scan inject III, Part I, pp. 16, (1983).

33. Kikuch et al., Scaninject III, Part I, pp. 13, (1986).

34. Carlos Leal et al., Scaninject IV, Part II, pp. 17 (1986).

35. V. Presern et al., Scaninject IV, Part II, pp. 3 (1986)

36. Guo Deje et al., Scaninject II, Part II, pp. 37(1980).

37. Christian Marique, Scaninject IV, Part II, pp. 25(1986).

38. R. J. Freuhan et al., Metallurgical Transactions, 22B, 1941, pp. 783-790.

39. TSao et al., Transactions of JSIJ, 26 (1986), pp.717-723.

40. R.W. Young et al., Ironmaking and Steelmaking, 19(1992), No. 3, pp. 201-639.

41. H. Gaye et al., 5th International Iron and Steel Congress, Vol. 6, 1986, pp. 631-639.

42. J.A. Duff et al., J. Chem. Soc. Faraday Metals, I 74(1971), pp1410-1419.

43. A. S. Venkatadri et al., J. Iron and Steel Inst., 207(1969), pp. 1110-1113.

44. K. P. Abraham et al., J. Iron and Steel Inst., 196 (1960), pp. 313-319.

45. B. Oztusk et al., Metal Science, 18(1984), pp. 299-305 and 306-310.

46. Banya et al., 3rd International Conference on Slags anf Fluxes, 1989, pp. 24.

47. Suito et al., Transactions of ISIJ, 24 (1984), pp. 47.

48. F.H. Garner et al., A.I.ch.E. Jl, 6(1968), pp. 579.

49. D. M. Ward et al., Can. Jl. Chem. Engg., 40(1962), pp. 164.

50. Hugmark, Ind. Engg. Chem. Fundam., 6(1967), pp. 408.

51. G. S. Laddha, Transport Phenomena in liquid expaction, Tata McGraw-Hill,Publishing Co. Ltd., 1976, pp. 199.

52. Gainer Et al., Jl. Appl. Chem, 9(1959), pp. 315.

53. Heinrich Schlak et al, Steel Research, 56(1985), No. 1, pp. 15-18.

54. Asai et al., Scaninject III, Part I, 1983, pp.12:1.

55. Ikuo Sawada et al., Scaninject IV, Part I, 1986, pp. 12:1-12:24.

56. Y. Kikuchi et al, Scaninject III, Part I, 1983, pp. 13:1.

57. E.T. Turkdogan, Scaninject IV, part I, 1986, pp. 1:1-1:59.

58. R.J. Freuhean, Pretreatment of B/F iron, Iron & Steel Society, 1987, pp. 950-1102.

59. X. F. Zhang et al ISS Trans. 6 (1985), pp. - 27

TABLE 1.1 : Refining conditions of Hot Metal

Sr. No.	Ref.	Melt Wt. (tons) Composition	Flux used					Impurity	Treatment Time (min)	Efficiency $= \frac{[x_0]-[x_f]}{[x_0]} \times 100$	Miscellaneous
			Amount (Kg)	Rate (Kg/min)	t_{inj} (min)	Composition	Carrier gas (Nm^3/min)				
1	[11]	90	600	60	10	$CaO+5\%CaF_2$	Ar=0.09	S	10		$Kp = 6.49 \times 10^{-4}$ sec^{-1}
2	[12]	0.25	2.5-5		18	35%CaO 30%Na_2CO_3 21%$CaCO_3$ 8%CaF_2	Ar=?	S P	18		Melt depth = 400mm Lance immersion depth=350-400mm
3	[13]	80-90	5.8 Kg/T	70-120	5	Na_2CO_3	N_2 = 2.2-4.7	S	5		Lance immersion depth=1100-2000mm deP preceds deS, and deP slag is not removed. Flux used in deP 43% CaO, 43%scale, 14%CaF_2
4	[14]	50.8		26-40	12	75%CaO 15%$CaCO_3$ 10%CaF_2	0.33	S	24	68-80	
5	[15]	0.05	1-2.5	0.1-0.4	25	20%CaO 50%CaF_2 30%Fe_2O_3	50% Ar-50%O_2 =0.01	P	25		Inner dia. of lance =6mm Immersion depth = 200mm
6	[16]	350	2.9Kg/T	90-150	17-25*	35%$CaCO_3$ 57%CaO 3%CaF_2 5%C	N_2 = 0.5-0.7	S	17-25*	57.14	Lance immersion depth=1.6-2.0m Torpedo car
			5.1Kg/T			92% CaC_3 3%CaF_2 5%C		S		57.14	
			4.4Kg/T			70%$CaCO_3$ 22%CaO 3%CaF_2 5%C		S		57.14	

Sr. No.	Ref.	Melt Wt. (tons) Composition	Flux used					Impurity	Treatment Time (min)	Efficiency $= \frac{[x_o]-[x_f]}{[x_o]} \times 100$	Miscellaneous
			Amount (Kg)	Rate (Kg/min)	t_{inj} (min)	Composition	Carrier gas (Nm^3/min)				
7	[17]	240-300	1.8Kg/T	20-50	10	CaC_2-CaO	N_2 = 4-6	S	10		Lance immersion depth =1000-1500mm
8	[18]	6	30	15.8	8	Na_2CO_3	Air=0.8	P S	8	P:96% S:60%	O_2 = 5.1 m^3/T P_o = 0.5%, S_o = .05%
			41	17.1	10	52%CaO 23%CaF_2 25%Fe_2O_3	Air=0.8	P S	10	P:90% S:60%	O_2 = 5.1 m^3/T P_o = 0.5%, S_o = .05%
9	[19]	0.17		0.25	20	Na_2CO_3	O_2 = 0.06 Ar = .024	P S	20	P:89.3% S:83.3%	Bath Height = 400mm Inner Dia. Furnace=300mm Si_o = 0.21%
				.195 & .36		80%CaO 20% CaF_2	O_2 = 0.08	P			Si_o <0.06% Bottom injection Powder particle size = 340 micron
				.333 & .55		40%CaO 10%CaF_2 50%Scale	O_2 =.08	P			
10	[20]	80	33.2Kg/T		10	43%CaO 43%scale 14%CaF_2	N_2 = ?	P	10	65%	
			5.1Kg/T		5	Na_2CO_3	N_2 = ?	S	5	71%	
11	[21]	6	20Kg/T		18	Na_2CO_3	N_2 = ?	P	18	90%	Si_o = 0.1% O_2 top blowing = 0.4m^3/(min. T)

Sr. No.	Ref.	Melt Wt. (tons) Composition	Flux used					Impurity	Treatment Time	Efficiency $\frac{[x_0]-[x_f]}{[x_0]} \times 100$	Miscellaneous
			Amount (Kg)	Rate (Kg/min)	t_{inj} (min)	Composition	Carrier gas (Nm^3/min)		(min)		
12	[22]	260-340		150		55%CaO 5%CaF_2 25%$CaCO_3$ 15%C	N_2 = 1.5	S			Lance angle = 65 - 70° (below Horizontal) Gas/Solid = 10 Nl/Kg
13	[23]	0.005	0.5			50%CaF_2 20%CaO 30%Fe_2O_3		P S	25	P:94.3% S:90%	Inductively stirred
						80%Na_2CO_3 10%SiO_2 10% MnO_2		P S	25	P:87% S:94%	Inductively stirred
						75%Fe_2O_3 25%CaO		P S	25	P:70.8% S:35%	Inductively stirred
						75%Fe_2O_3 25%CaO 10%Al_2O_3		P S	25	P:70% S:20%	Inductively stirred
						45%Fe_2O_3 35%CaO 20%Al_2O_3		P S	25	P:42% S:26%	Inductively stirred
14	[24]	6	45Kg/T			32%CaO 58%Fe Ore 5%CaF_2 5%Na_2CO_3		P	20 15	90% 51%	$[Si_0]$ = 0.1% Total Oxygen = $10m^3$/THM (Gaseous + Iron Ore)
			20Kg/T			Na_2CO_3		P	25	90%	$[Si_0]$ = 0.25% Oxygen blown = $0.4m^3$/(min.T)

Sr. No.	Ref.	Melt Wt. (tons) Composition	Flux used					Impurity	Treatment Time (min)	Efficiency $\frac{[x_o]-[x_f]}{[x_o]} \times 100$	Miscellaneous
			Amount (Kg)	Rate (Kg/min)	t_{inj} (min)	Composition	Carrier gas (Nm^3/min)				
15	[25]	0.0065	0.1			CaO		S	100		Ar Stirring : 1400Cm^3 9Cm I.D. Graphite Crucible
						CaO Al(.001-.55%)		S	100		Ar Stirring : 1400Cm^3 9Cm I.D. Graphite Crucible
						CaO CaF_2(0-20%)		S	100		Ar Stirring : 1400Cm^3 9Cm I.D. Graphite Crucible
16	[26]			0.8Mg 1.55CaO (lbs/min/T)	7	CaO 95%Mg	0.08Scf/min/T	S	7		$Ln[S_o/S_f]$[NTHM/lbs Mg/24.3]=38.7
				0.13Mg 0.53CaC_2 (lbs/min/T)	6.7	CaC_2-Mg		S	6.7		$Ln[S_o/S_f]$[NTHM/lbs Mg/24.3]=48
17	[27]	6		6.84-7.08	20	84%CaO 8%$CaCl_2$ 8%CaF_2	O_2=2.22-3.42	P S	20		Lance immersion depth =250-550mm
				6.78	30	85%CaO 7.5%$CaCl_2$ 7.5%CaF_2	O_2 = 1.14	P S	30		Lance immersion depth=550mm
		100	4278-10450		22-57	45%CaO 5-9%CaF_2 4-15%FeO 35-45%Fe_2O_3	O_2=15.3-20.14	P	22-57	75-90%	
18	[28]	.003 (4.35wt% C-Iron)	0.18	0.017	10.5	30%CaO 20%CaF_2 20%$CaCl_2$ 30%Fe_2O_3	Ar=.003	P S	33.33		Lance immersion depth = 4Cm $[Si_o]$ = .13% Flux is premelted

TABLE 1.2 : Refining conditions of Steel

Sr. No.	Ref.	Melt Wt. (tons) Composition	Flux used					Impurity	Treatment Time (min)	Efficiency $\frac{[x_0]-[x_f]}{[x_0]} \times 100$	Miscellaneous
			Amount (Kg)	Rate (Kg/min)	t_{inj} (min)	Composition	Carrier gas (Nm^3/min)				
1	[29]	AlSi killed steel 150	720	90	8-9	70%CaO 30%CaF_2	2.3	S	8		
2	[30]	DX-65 HSLA Steel 0.15%C, 1.6%Mn 1.6% Mn (max.) 0.5%Si (max.) 0.08%V 0.1%Nb(max.) (180T)	400Kg CaSi; & 100Kg misture (2.85-2.9Kg/T)	52.6-61.5	8-9	CaSi+ mixture (85%CaO + 15%CaF_2) + top slag (CaO-CaF_2 - SiO_2-FeO - Al_2O_3)	N_2:0.8	S	8-9.5	23.1%	Top slag thickness =7-8Cm
			320Kg CaSi & 180Kg Mixture (2.9 Kg/T)	55.5	9	"	"	S	9	31.3%	Top slag thickness = 5 Cm
			250Kg CaSi & 250Kg Mixture (2.9-3.1 Kg/T)	50-51.5	9.7-10.0	"	"	S	9.7-10.0	40.7%	Top slag thickness = 15-20 Cm
			80Kg CaSi & 420Kg Mixture (2.9 Kg/T)	45.9	10.9	"	"	S	10.9	34.5	Top slag thickness = 20 Cm

Sr. No.	Ref.	Melt Wt. (tons) Composition	Flux used					Impurity	Treatment Time (min)	Efficiency $= \frac{[x_0]-[x_f]}{[x_0]} \times 100$	Miscellaneous
			Amount (Kg)	Rate (Kg/min)	t_{inj} (min)	Composition	Carrier gas (Nm^3/min)				
2	[30]	DX-65 HSLA Steel 0.15%C, 1.6%Mn 1.6% Mn (max.) 0.5%Si (max.) 0.08%V 0.1%Nb(max.) (180T)	350 - 500	44.7-56.8	6.2-10.3	100% CaSi+ top slag ($CaO-CaF_2-SiO_2-FeO-Al_2O_3$)	N_2:0.8	S	6.2-10.3	23.5-36.3	Top slag thickness =8-30Cm
3	[31]	C=0.16%, Si=0.27% Mn=1%; P=0.013% S=0.01%; Sol. Al =0.03% (2.5Kg)	0.0375		30	48%CaO-32% Al_2O_3 - 20%CaF_2 90%CaO - 10%CaF_2 53%CaO- 47%Al_2O_3		S	30		Dia. of crucible = 77mm
			(2.9-3.1 Kg/T)								
			80Kg CaSi & 420Kg Mixture (2.9 Kg/T)	45.9	10.9	"	"	S	6.2-10.3	23.5-36.3	Top slag thickness = 15-20 Cm

Sr. No.	Ref.	Melt Wt. (tons) Composition	Flux used					Impurity	Treatment Time (min)	Efficiency $\frac{[x_0]-[x_f]}{[x_0]} \times 100$	Miscellaneous
			Amount (Kg)	Rate (Kg/min)	t_{inj} (min)	Composition	Carrier gas (Nm^3/min)				
4	[32]	250T	13-15 Kg/T		20	65%CaO-15%CaF_2 20%Al_2O_3	1.5-7.2	S	20		
5	[33]	HSLA Steel ($\underline{O}$ = 100ppm) 150*		80-120 (0.7Kg/T/min)	6	80%CaO - 15%CaF_2	5	S	6		
6	[34]	En-31 steel 0.01	20-40 Kg/T	0.050--0.1	4-5	40%CaO - 60%CaF_2	N_2:0.065	S	4-5	45.9%-91%	150-105 m particle size 105-75 m particle size Lance dia. = 8 mm
7	[35]	$1x10^{-3}$ C<0.04% Mn<0.1% P=0.03-0.27%	30-100g		20-30	40-60%CaO + 15-30%CaF_2 25-40% $(FeO)_t$	Ar:0.5Nl/min	$\underline{P}$	20-30		
		50	1-5Kg/T		2.5-7.0	"	?	$\underline{P}$	2.5-7	58%	K_p=0.084-0.106min^{-1}
		250	11.1-18.8Kg/T		50-60	"	?	$\underline{P}$	50-60	55-94	K_p = 0.035-0.084 min^{-1} Stirred with Ar:0.5-1.6
8	[36]	0.015 (Stainless Steel 12%Cr)	9-40 Kg/T		10	CaC_2	?	$\underline{P}$ S	10	40-80%	
			15-40 Kg/T			"		$\underline{P}$ S	10	29-53%	Dumping

* Calculated

Sr. No.	Ref.	Melt Wt. (tons) Composition	Flux used					Impurity	Treatment Time (min)	Efficiency $= \frac{[x_o]-[x_f]}{[x_o]} \times 100$	Miscellaneous
			Amount (Kg)	Rate (Kg/min)	t_{inj} (min)	Composition	Carrier gas (Nm^3/min)				
9	[37]	DX-65HSLA Steel (0.15%C, 1.6%Mn, 0.5%Si(max), 0.08%V(max) 0.1%Nb)				$CaO-CaF_2$ SiO_2-FeO-Al_2O_3	N_2 purging ?	S	4.5	7.4%	Slag Thickness= 10Cm(1.5%FeO) CaO/SiO_2 = 2.33
						"	Ar purging ?	S	3		Slag Thickness= 15Cm CaO/SiO_2 = 2.83
10	[38]	60*	1.5-1.8 Kg/T	15-25	4-7	CaSi	Ar:0.4-0.6	S	4-7	72-90	
11	[39]	C=0.22-1.85% Cr=5.3-20.24% P=0.021-0.051% Si=0.09-0.68%	15-45 Kg/T of CaF_2 0.40% CaF_2 powder	18.1-66.7	3-8	CaC_2(75-80% PPm)-CuF_2 (95%PPm)	Ar ?	P	3-8	18.2-61.9%	Lance dia. = 13-20 mm Lance immersion depth = 250-400mm 3T basic EFF
12	[40]	75 (C=0.06%, Mn=0.506% Al_t=0.078% Si=0.01% S=0.06%)	60-85	12-20		CaSi(30%Ca)	1-.33	S		40%	Lance nozzle dia.>9mm (one hole) 0-1mm Size distribution of particles
		195	120-300	27-30		Metallic Ca powder (40% Ca) synthetic slag	0.75	S		<25%	Lance nozzle dia.=8mm (four holes) 0-1mm size distribution of particles

* Calculated

Sr. No.	Ref.	Melt Wt. (tons) Composition	Flux used					Impurity	Treatment Time (min)	Efficiency $= \frac{[x_o]-[x_f]}{[x_o]} \times 100$	Miscellaneous
			Amount (Kg)	Rate (Kg/min)	t_{inj} (min)	Composition	Carrier gas (Nm^3/min)				
12		75-80	30-200	10-30		Ca granular & the slag mixture CaO ->45%, Al_2O_3->40% CaF_2->10%		S		23-43%	Lance nozzle dia = 12mm (0.12-1.2mm is Ca Particle size range. Synthetic slag size range = 0.1-1mm (lime+CaF_2 (6-8 Kg/T)) The Mixture hot metallic Ca of 25%
13	[41]	0.01 (steel melt)	0.3			10%CaO 35%BaO 45%Al_2O_3 10%TiO_2		N	30	60%	Inductively stirred (Inner dia. of crucible=14.6 Cm)
			0.3			40%CaO 40%Al_2O_3 20%TiO_2		N	30	40%	Inductively stirred (Inner dia. of crucible=14.6 Cm)

Table 2.1 : Sulphide Capacity Correlations

Sr. No.	Ref.	C_S correlation	Remarks
1	[39]	$\log C_s = 3.44(N_{CaO}+0.1N_{MgO}-0.8N_{Al_2O_3}-N_{SiO_2})-\frac{9894}{T}+2.05$	2.5g Fe-0.12-0.15% S alloy was equilibrated with 7g slag of calcium aluminate base in a magnesite crucible at 1575, 1600 and 1650°C. SiO_2=20%; CaO=38-55%, Al_2O_3=25 & 45% and MgO=5%.
2	[40]	$\log C_S=-13.913+42.84\Lambda-23.82\Lambda^2-(\frac{11710}{T})-0.02223SiO_2-0.02275Al_2O_3$ $(\Lambda<0.8)$ $C_S=-0.6261+0.4808\Lambda+0.7197\Lambda^2+\frac{1677}{T}-\frac{2587\Lambda}{T}+0.0005144FeO$ $(\Lambda\geq0.8)$	The equations are derived from large number of experimental data of wide range of CaO based slag systems by using the optical basicity concept.
3	[41]	$\log C'_S=\frac{B}{A}+2.82-13300/T$ where, $B=5.62(\%CaO)+4.15(\%MgO)-1.15(\%SiO_2)+1.46(\%Al_2O_3)$ $A=(\%CaO)+1.39(\%MgO)+1.87(\%SiO_2)+1.65(\%Al_2O_3)$ $\log C_S=\log C'_S+\frac{936}{T}-1.375$	The equation was derived by using the correlation established by Duffy et al [42] and the data of Venkatadri and Bell [43], Abraham and Richardson [44], and Turkdogan [45].

Table 2.2 : Optical Basicity Values [40]

Slag Species	Optical Basicity Values (Λ)
FeO	1.0
SiO_2	0.46
P_2O_5	0.4
Al_2O_3	0.6
CaO	1.0
MnO	0.98
MgO	0.78
Na_2O	1.15
Fe_2O_3	0.77
BaO	1.15
TiO_2	0.65
CaF_2	0.43

Table 2.3: Phosphorus Capacity Correlations

Sr. No.	Ref.	C_S correlation	Remarks
1	[46]	$RT\ln\nu_{PO_{2.5}} = -7500X^2_{FeO_{1.5}} + 3500X^2_{FeO_{1.5}} - 60000X^2_{CaO} - 9000X^2_{MgO} + 20000X^2_{SiO_2} + 460X_{FeO}X_{FeO_{1.5}} + 60000X_{FeO}X_{CaO} - 24500X_{FeO}X_{MgO} + 22500X_{FeO}X_{SiO_2} - 33600X_{FeO_{1.5}}X_{MgO} - 4800X_{FeO_{1.5}}X_{MgO} + 15700X_{FeO_{1.5}}X_{SiO_2} - 45000X_{CaO}X_{MgO} - 8000X_{CaO}X_{SiO_2} + 27000X_{MgO}X_{SiO_2}$	$\underline{P}+2.5\underline{O}=(PO_{2.5})$ $\log K_P = 17060/T - 8.51$ Slags System: $FeO-Fe_2O_3-P_2O_5-SiO_2-CaO-Mg$ (from 1380-1680°C)
2	[40]	$\log C_P = -18.184 + 35.84\Lambda - 22.35\Lambda^2 + \frac{22930\Lambda}{T} - 0.06257FeO - 0.04256MnO + 0.359P_2O_5^{0.3}$ $\left[C_P = \frac{(\%P)}{f_P[\%P]a_O^{5/2}}\right]$	Derived from literature data and then tested by performing experiments. Recommended optical basicity values are to be used.
3	[47]	$\log C_P = 0.51(23N_{CaO} + 17N_{MgO} + 8N_{Fe_tO} + 42N_{BaO} + 20N_{CaF_2} + 13N_{MnO} - 26N_{P_2O_5})^{\frac{2}{3}} + 29920/T - 19.28 + \log[(\%P)/N^{1/2}_{P_2O_5}]$ $\log \frac{(\%P)}{N^{1/2}_{P_2O_5}} = 0.478 \log N_{P_2O_5} +$ 1.955 for $CaO-FeO-SiO_2-P_2O_5$- $(CaO/SiO_2=3\ Fe_tO=20\%)$ $=0.479\log N_{P_2O_5} + 1.813$ for CaO- $Fe_tO-CaF_2-P_2O_5$ $(CaO/CaF_2=1;\ Fe_tO=20\%)$ $\left[C_P = \frac{(\%P)}{f_P[5P]a_O^{5/2}}\right]$	7-13%Na_2O & 4%BaO additions are done. P_2O_5 < 1 wt% Experiments are done at 1550°C Using ΔG° for the followin equation $2P+5\underline{O} = (P_2O_5)$, the following relationship is derived. $\log C_P = -\frac{\Delta G^\circ}{2RT} - \frac{1}{2}(\log \nu_{P_2O_5}$ $\log \left(\frac{(\%P)}{N^{1/2}_{P_2O_5}}\right)$ and $\log \nu_{P_2O_5}$ is taken from Turkdogan's treatment.

Table 2.4: Mass transfer coefficient relations for drops

Sr. No.	$(N_{Sh})_C = f[(N_{Re})_C, (N_{Sc})_C]$	Remarks	Ref.
1	$(N_{Sh})_C = 2 + 0.95 (N_{Re})^{1/2} (N_{Sc})_C^{1/4}$	Solid spheres. Rigid Liquid drops.	[48]
2	$(N_{Sh})_C = 0.98 (N_{Pe})^{1/3}$	For non-circulating drops	[49]
3	$(N_{Sh})_C = 0.61 \left(\frac{\mu_d}{\mu_c + \mu_d}\right) (N_{Pe})^{1/2}$	$N_{Pe} > 2.8 \left(\frac{\mu_d + \mu_c}{\mu_d}\right) \left(\frac{12\mu_c + 9\mu_d}{\mu_d}\right)^2$ for circulating drops	[49]
4	$(N_{Sh})_C = 2 + 0.084 \left[(N_{Re})_C^{0.484} (N_{Sc})^{0.339} \left(\frac{d_p g^{1/3}}{D_C^{2/3}}\right)^{0.072} \right]^{1.5}$	For oscillating drops	[50]
5	$\beta_T = 2 \left(\frac{D_C u_T}{\pi d_p}\right)^{1/2}$	For circulating & oscillating drops (Penetration theory)	[51]
6	$(N_{Sh})_C = 50 + 0.0085 (N_{Re})_C \left(\frac{\mu_C}{\rho_C D_C}\right)^{0.7}$		[51]
7	$\beta_T = 0.023 u (N_{Sc})_C^{-1/2}$	Single file droplets	[51]
8	$\frac{\beta_T}{u} \left(\frac{\mu_C}{\rho_C D_C}\right)^{0.58} = 1.3 \left(\frac{d_p u \rho_C}{\mu_C}\right)^{-1/2}$	For circulating drops	[52]
9	$(N_{Sh})_C = 2 + 0.0511 (N_{Re})^{0.724} (N_{Sc})^{0.7}$		[53]

Table 2.5: Slag-Systems and the evaluated rate constants

Sr. No.	Slag System	$K_P (min^{-1})$
15	$65\%Fe_2O_3$-2.5%CaO-$10\%Al_2O_3$ (Inductively stirred)	
	→ Sulphur	0.0273
	→ Phosphorus	0.06634
16	$75\%Fe_2O_3$-25%CaO (Inductively stirred)	
	→ Phosphorus	0.033
17	Na_2CO_3 (1400°C) ($\dot{\varepsilon}$=76W/T)	
	→ Sulphur [Si_o=0.017]	0.2283
	→ Sulphur [Si_o=0.13]	0.2283
	→ Phosphorus [Si_o=0.01%]	0.0691
	→ Phosphorus [Si_o=0.13%]	0.05066
18	Na_2CO_3 (1300°C) ($\dot{\varepsilon}$=76W/T)	
	→ Sulphur [Si_o=0.01%]	0.0723
	→ Phosphorus [Si_o=0.01%]	0.0146
19	31%CaO-33%SiO_2-17%Al_2O_3-19%$CaCl_2$ (Al-deoxidized 1350°C)	0.2533
20	Na_2CO_3 [Pellets]	0.2533
	[Powder]	0.194
21	(40.60%CaO)-(15-30%CaF_2)- (25-40%$(FeO)_t$) → (deP) (250T arc process)	0.035 0.084

Table 2.5: Slag-Systems and the evaluated rate constants

Sr. No.	Slag System	K_p (min^{-1})
22*	$6T.\dot{V}_{Ar}$=1.2, B=1.73	0.39
	$6T.\dot{V}_{Ar}$=1.8, B=1.96	0.55
	$5T.\dot{V}_{Ar}$=0.9, B=2.43	0.45
	$5T.\dot{V}_{Ar}$=1.1, B=2.75	0.44
	$4.5T.\dot{V}_{Ar}$=0.075, B=? (Si-deox)	0.028
	$4.5T.\dot{V}_{Ar}$=0.075, B=? (Al-deox)	0.042
	$150T.\dot{V}_{Ar}$= ?, B= 3 (Al-deox)	0.066
23	80%Na_2CO_3-13.3%SiO_2-6.67%Fe_2O_3	0.5

* K_p values are taken from the ref.

$\dot{V}_{Ar}$ in $\frac{dm^3n}{t.sec}$; $B = \left[n_{CaO} + n_{CaF_2}\right] / \left[n_{SiO_2} + n_{Al_2O_3}\right]$

Table 2.6: Evaluated parameters for hot metal experimental conditions

Sr. No.	$\dot{\varepsilon}$ (W/T)	Loading Ratio (Kg/m^3)	Y	η^*	K_T (min^{-1})	State of slag at hot metal temperature (1623K-1673K)
1	6.22	666.67	0.0067	1060	0.245	Solid
2			0.01-0.02	542-1.35		
3	248.77	15-55	0.0058	$[S_{eq}]$= .05ppm	.0374 - .056	
4	35	78.8-121.2	.00614 - .0095	405.5	.068 - .1044	
5	255	10-40	.02-.05	25	.0257-.1026	Liquid
6	12.25-17.14	128.57-300	.0029-.0051	1507	.0734-.1458	
				1167	.0734-.1458	
				1336.6	.0734-.1458	Solid
7	120-180	3.33-12.5	.0018		.006 - .0183	
8	400	19.725	.005	$[S_{eq}]$= .05ppm	.0612	
		21.375	.041		.0662	Liquid
9	850	4.17	.0294	$[S_{eq}]$= .05ppm	.0155	
	340	10.42	.0294	$[S_{eq}]$= .05ppm	.025	
	1130				.0104-.02	
	1130			177	.0178-.03	Liquid
10			.0332	177		Liquid
			.0051	$[S_{eq}]$= .05ppm		Liquid

Conttd.

Table 2.6: Evaluated parameters for hot metal experimental conditions

Sr. No.	$\dot{\varepsilon}$ (W/T)	Loading Ratio (Kg/m^3)	Y	η^*	K_T (min^{-1})	State of slag at hot metal temperature (1623K-1673K)
11			.02	$[S_{eq}]$= .05ppm		
12	41.4	100		.862	.0876	Solid
16		450	.00224	$[S_{eq}]$= .07ppm		
17	1165.6-1795.66	2-3.2	.0228-.0236		.01244-.01612	Solid
	600	6	.00113		.02183	Solid
	976.35-1285	10.52	.0428-.1045	500-1100	.02542-.0717	Liquid
18	274	5.76	.06		.0252	Liquid

Note: Sr. No. in this Table is same as that in Table 1.1.

Table 2.7: Evaluated parameters for Steel experimental conditions

Sr. No.	$\dot{\varepsilon}$ (W/T)	Loading Ratio (Kg/m^3)	Y	η^*	K_T (min^{-1})	State of slag at steel making temperature (1873°K)
1	121.42	39.13	.0048	1555.47	.06474	Partially Liquid
2	36.77	65.75-78.125	.0028		.061-.0724	Partially Liquid
		69.375	.0028		.06428	Partially Liquid
		62.5-64.375	.0028		.058-.06	Partially Liquid
		57.375	.0028		.05316	Partially Liquid
		55.875-71	.002-.003	$[S_{eq}]$= .23ppm	.052-.066	
3			.015	113.82		Liquid
				2103.35		Solid
				131.2		Liquid
4	53.6-78.6	73.86-125	.013-.015	575	.0975-.137	Liquid + CaO
5	264	21	.0042	300	.0384-.0577	Solid
6		.77-1.54	.02-.04	300	.011-.022	Liquid
7	106	60-200	.03-.1	46.13	.0082-.0272	Liquid (40-50% CaO) Liquid + CaO (>50%)
			.001-.005	46.13		Liquid (40-50% CaO) Liquid + CaO (>50%)
8			.01-.04	$[P_{eq}]$= 8.2ppm		
10	42-63	37-42	.0015-.0018	$[S_{eq}]$= .23ppm	.04-.052	

Table 2.7: Evaluated parameters for Steel experimental conditions

Sr. No.	$\dot{\varepsilon}$ (W/T)	Loading Ratio (Kg/m^3)	Y	η^*	K_T (min^{-1})	State of slag at steel making temperature (1873°K)
11			.015- .045	$[P_{eq}]$= 8ppm		
12	29.35- 88.94	20-36	.0008- .0011	$[S_{eq}]$= .23ppm	.0313- .03	
	32.43	36-40	.00062- .00154		.14- .35	
	43.4- 115.42	20-23	.0004- .0026		.021- .0374	Liquid

Note: Sr. No. in this Table is same as that in Table 1.2.

Table 4.1: DeS Evaluation

Sr. No.	Melt Wt. (tons) and Composition	Type	Flux used			Evaluation by the present model							Specified K_p (min^{-1})	Investigator
			Rate (Kg/min)	t_{inj} (min)	Carrier gas Flow (Nm^3/min)	Ω_S	θ_S	λ_S	K_S	K_T	f	E		
1	3.54Kg Hot-metal	20CaO-60CaF_2 - 20Al_2O_3	0.0065	16	0.0068	1.8882	0.1276	3.4644	0.052	0.08875	0.748	0.218	0.18*	Robertson etal.,[6]
2	150T Al-Si killed steel	70CaO-30CaF_2	90	8	2.3	4.03	0.183	6.624	0.253	0.5875	0.94	0.426	0.283	Y. Hara etal.,[7]
3	90T Hot-metal	95CaO-5CaF_2	60	10	0.09	0.8712	0.046	4.3333	0.023	0.077	0.82	0.155	0.036	Chushao [12]
4	2.5Kg Sol. Al. 0.03	48%CaO-32%Al_2O_3-20%CaF_2	0.00125	30	?	3	0.189	5.143	0.05	0.1044	0.893	0.394	---	Moriya etal., [29]
		90%CaO-10%CaF_2	0.00125	30	?	3.82	0.576	4.74	0.105	0.042	0.566	0.23	---	
		58%CaO-47%Al_2O_3	0.00125	30	?	1.3627	0.4236	1.97	0.033	0.021	0.6	0.27	---	

* Calculated

Table 4.1: DeP Evaluation

Sr. No.	Melt Wt. (tons) and Composition	Type	Flux used			Evaluation by the present model							Investigator
			Rate (Kg/min)	t_{inj} (min)	Carrier gas Flow (Nm^3/min)	α_S	β_S	λ_S	K_S	K_T	f	E	
1	15Kg Stainless Steel (0.03%P, 0.65%C, 12%Cr)	CaC_2	0.0135	10	?	0.7665	0.45	---	---	---	---	---	Carlos Leal etal.,[34]
			0.0195	10	?	1.028	0.487	---	---	---	---	---	
			0.0285	10	?	1.188	0.0586	---	---	---	---	---	
			0.0435	10	?	3.926	0.8985	---	---	---	---	---	
			0.0495	10	?	3.478	0.6951	---	---	---	---	---	
			0.06	10	?	10.17	2.414						
2	6T Hot-metal (Avg. Composition 4.2%C, 0.1%P, 0.03%S, 0.025%Si, 0.08%Mn)	84.54%CaO, 7.73%$CaCl_2$, 7.73%CaF_2	7.08	20	3.42	3.063	0.087	32.27	0.14	0.0133	0.1	0.01	Sawada etal.,[25]
		84.11%CaO, 7.945%$CaCl_2$, 7.945%CaF_2	6.84	20	2.22	2.72	0.077	31.176	0.12	0.016	0.133	0.01	
		84.52%CaO, 7.74%$CaCl_2$, 7.74%CaF_2	6.78	30	1.14	3.37	0.065	41.72	0.09	0.0226	0.225	0.016	
3	100 T Hot-metal (4.4%C, 0.12%P, 0.13%S, 0.32%Mn) $[Si_0]$=0.08%	45.56%CaO, 14.8%FeO, 34.62%Fe_2O_3, 5.03%CaF_2	194.5	22	20.14	3.63	0.23	11.5	0.1245	0.046	0.383	0.086	Sawada etal.,[25]

Sr. No.	Melt Wt. (tons) and Composition	Type	Flux used			Evaluation by the present model							Investigator
			Rate (Kg/min)	t_{inj} (min)	Carrier gas Flow (Nm^3/min)	α_S	β_S	λ_S	K_S	K_T	f	E	
3	$[Si_0]$=0.06%	44.64%CaO, 6.70%FeO, 39.74%Fe_2O_3, 8.92%CaF_2	196.5	30	15.3	4.8	0.104	31.04	0.1	0.053	0.4	0.051	
	$[Si_0]$=0.07%	43.82%CaO, 3.37%FeO, 44.04%Fe_2O_3, 8.77%CaF_2	193.82	28	18.18	4.6	0.1	33.24	0.118	0.048	0.348	0.0384	
	$[Si_0]$=0.05%	43.06%CaO, 5.98%FeO, 43.3%Fe_2O_3, 7.66%CaF_2	183.33	57	14.6	8.85	0.057	105.3	0.106	0.051	0.376	0.027	

APPENDIX - 1

General solution for powder injection refining without slag carry-over:

Governing differential equation for concentation change of impurity in the melt with time during the powder injection when slag is not carried-over is (see equation (2.15))

$$\frac{d(\alpha-1)}{d\tau} + (\alpha-1)\left\{\phi_S + \frac{\theta_S}{\tau}\right\} = -\phi_S \qquad (2.15)$$

It was already discussed in the section (2.2.1) that the form of equation (2.15) is similar to that of Leibnitz's linear equation.

$$\frac{dY}{dx} + Yf(x) = C \qquad (2.21)$$

The general solution of equation (2.21) is given by

$$Y = e^{-\int f(x)dx}\left\{C \int e^{\int f(x)dx}\, dx + C_1\right\} \qquad (A1.1)$$

where C_1 is integration constant.

By putting similar term from equation (2.15) into equation (A1.1), we get

$$(\alpha-1) = e^{-\int(\phi_S + \frac{\theta_S}{\tau})\, d\tau}\left\{(-\phi_S)\int e^{\int(\phi_S + \frac{\theta_S}{\tau})d\tau}\, d\tau + C_1\right\} \qquad (A1.2)$$

$$\int e^{-(\phi_S\tau + \frac{\theta_S}{\tau})}\, d\tau = \int e^{-(\phi_S\tau + \theta_S \ln\tau)} \qquad (A1.3)$$

$$\int e^{-(\phi_S\tau + \theta_S\ln\tau)} = \int e^{\phi_S\tau}\, \tau^{\theta_S}\, d\tau$$

$$= \tau^{\theta_S}\left[1 + (\phi_S\tau) + \frac{(\phi_S\tau)^2}{2!} + \ldots\ldots\right]d\tau$$

$$= \frac{\tau^{(\theta_S+1)}}{(\theta_S+1)} + \frac{\phi_S\tau^{(\theta_S+2)}}{(\theta_S+2)} + \frac{\phi_S^2\tau^{(\theta_S+3)}}{2!(\theta_S+3)} + \ldots\ldots$$

$$= \sum_{m=0}^{\infty} \frac{(\phi_S\tau)^m\, \tau^{(\theta_S+1)}}{m!\ (1+\theta_S+m)} \qquad (A1.4)$$

Combining equations (A1.2), (A1.3) and (A1.4)

$$(\alpha-1) = e^{i\phi_S\tau}\,\psi^{-\theta_S}\left\{-\phi_S\sum_{m=0}^{\infty}\frac{(\phi_S\tau)^m\,\tau^{(\theta_S+1)}}{m!\;(1+\theta_S+m)} + C_1\tau^{-\theta_S}\right\} \qquad \text{(A1.5)}$$

I.C. at $\tau = 0$, $\alpha=1$

i.e., $C_1 = 0$

Thus,

$$\alpha = 1 - (\phi_S\tau)\exp(-\phi_S\tau)\sum_{m=0}^{\infty}\frac{(\phi_S\tau)^m}{m!\;(1+\theta_S+m)} \qquad \text{(2.22)}$$

Equation (2.22) is the obtained general solution.

APPENDIX - 2

Numerical solution for powder injection refining with slag carry-over.

Governing differential equations for concentration change of impurity with time during powder injection refining with slag carry-over from BOF is (see equation 3.20)

$$-\frac{d(\alpha-1)}{d\tau} = \left\{\phi_S + \frac{\theta_S}{\tau}\left[\frac{1}{\frac{\eta_o^*}{\eta_S^*}\left[1+\frac{Y_C}{Y_S\tau}\right]}\right]\right\}(\alpha-1) + {}_S\phi \qquad (2.20)$$

By using crank-Nicholson's FDM

$$-\frac{(\alpha_{j+1}-\alpha_j)}{\Delta\tau} = \left\{\phi_S + \frac{\theta_S}{\frac{(\tau_{j+1}+\tau_j)}{2}}\left[\frac{1}{\frac{[(\eta_o^*)_{j+1}+(\eta_o^*)_j]}{2\eta_S^*}\left[1+\frac{\tau_C}{\tau_S\left[\frac{\tau_{j+1}+\tau_j}{2}\right]}\right]}\right]\right\} \times$$

$$\left[\frac{\alpha_{j+1}+\alpha_j}{2}-1\right] + \phi_S \qquad (A2.1)$$

Defining $(\tau_{av})_{j+1} = (\tau_{j+1}+\tau_j)/2$

$$\left[(\eta_o^*)_{av}\right]_{j+1} = \left[(\eta_o^*)_{j+1}+(\eta_o^*)_j\right]/2 \qquad (2.25)$$

$$\frac{\alpha_j-\alpha_{j+1}}{\Delta\tau} = \left\{\phi_S + \theta_S\left[\frac{\eta_S^*}{[(\eta_o^*)_{av}]_{j+1}\ [(\tau_{av})_{j+1}+\frac{Y_C}{Y_S}]}\right]\right\}\left[\frac{\alpha_{j+1}+\alpha_j}{2}-1\right]+\phi_S$$

(A2.2)

After rearrangement

$$(\alpha_{j+1}-1)[1+T] = (\alpha_j-1)[1-T] - \phi_S\Delta\tau \qquad (2.24)$$

T is defined in equation (2.15)

Equation (2.24) is the obtained numerical solution.

APPENDIX 3

Transitoric Rate Contribution (f)

f is rate contribution of injected flux in the overall refining process. Therefore f is the ratio of area under transitoric rate curve to area under total rate curve.

$$f = \frac{\int_{\tau=0}^{\tau=1} (Rate_T)\, d\tau}{\int_{\tau=0}^{\tau=1} (Rate)\, d\tau} \qquad (A3.1)$$

Considering the equals time interval $d\tau$, (A3.1) can be reqritten as

$$f = \frac{\sum_{\tau=0}^{\tau=1} (Rate_T)_{\tau+d\tau}}{\sum_{\tau=0}^{\tau=1} (Rate)_{\tau+d\tau}} \qquad (A3.2)$$

From equation (2.15)

$$Rate = (\alpha-1)\left\{\phi_S + \frac{\theta_S}{\tau}\right\} + \phi_S \qquad (A3.3)$$

From equation (2.12)

$$Rate_T = \alpha(\phi_S - \lambda_S\theta_S) \qquad (A3.4)$$

Then,

$$f = \frac{\sum_{\tau=0}^{1} \alpha\ (\phi_S + \lambda_S\theta_S)}{\sum_{\tau=0}^{1} [(\alpha-1)\left\{\phi_S + \frac{\theta_S}{\tau}\right\} + \phi_S]} \qquad (A3.5)$$

α depends as ϕ_S, θ_S; ϕ_S and θ_S depend on B_P, B_T, λ_S and f. Therefore f depends on only B_P, B_T and λ_S.

$$\text{Thus } f = f((B_P, B_T, \lambda_S) \qquad (A3.6)$$

APPENDIX 4

Calculation procedure of $a_{\underline{O}}$:

If the slag in contact with the melt contains the components CaO, MgO, FeO, MnO, SiO_2, Al_2O_3, P_2O_5 then the mole fraction of oxygen ions of the slag melt is determined as follows,

$$n_{O^{2-}} = n_{CaO} + n_{MgO} + n_{FeO} + n_{MgO} - 2n_{SiO_2} - n_{Al_2O_3} - 3n_{P_2O_5} \quad (A4.1)$$

$$X_{O^{2-}} = \frac{n_{O^{2-}}}{n_{SiO_2} + 2n_{Al_2O_3} + 2n_{P_2O_5} + n_{O^{2-}}} \quad (A4.2)$$

Relation between $X_{O^{2-}}$ and activity coefficient of FeO is [59]

$$\log \nu_{(FeO)} = 2.02 - 1.34 X_{O^{2-}} - \frac{1475}{T} \quad (A4.3)$$

$$\log \frac{a_{\underline{O}}}{a_{(FeO)}} = - \frac{6150}{T} + 2.604 \quad (A4.4)$$

Thus activity of oxygen in melt can be determined frome equation (A4.4) for the given slag composition of the slag.

E.T.Turkdogan [11] suggested the following solubility product relation for the Al-O equilibrium for Al killed steels

$$[Al]^2[O]^3 = 1.2 \times 10^{-13} \quad (A4.5)$$

Final Al content of the melt when the initial Al ($\underline{Al}_o$) and initial O ($\underline{O}_o$) are given, is

$$\underline{Al}_f = \underline{Al}_o - \frac{54}{48}\left[\underline{O}_o - 4.9324 \times 10^{-5}\, \underline{Al}_f^{\frac{2}{3}}\right] \quad (A4.6)$$

```
while (factor >= 0.0001)
{
div = fact1 = 0.0;
if (m > 0)
for (k = 1.0; k <= m; k++)
{
fact1 += log(k)-5.0;
div += 5.0;
}
fact = exp(fact1);
factor = exp(m*log(phi*t))*exp(-div)/(fact*(theta+1.(
sum += factor;
m++;
fact = 1.0;
}
x[i][point] = 1.0-phi*t*exp(-phi*t)*sum;
xinj = x[i][point];
rate[i][point] = x[i][point]*(phi+theta/t)-theta/t;
rate_per[i][point]=x[i][point]*theta*(lamda[i]+1.0/t)
rate_tra[i][point] = x[i][point]*(phi-theta*lamda[i])
sum_rate_tra += rate_tra[i][point];
sum_rate += rate[i][point];
}
fra = sum_rate_tra/sum_rate;
printf("fra = %f\n",fra);
number = point;
}
printf("phi = %f\ttheta = %f\n",phi,theta);
for (t=1.01,point=number;t<=max_time;t+=time_interval,
{
dummy1 = (1.0+lamda[i])*kp[i]*tinj*(t-1.0)/lamda[i];
dummy2 = 1.0-xinj*(1.0+lamda[i]);
x[i][point] = (1.0-dummy2*exp(-dummy1))/(1.0+lamda[i]);
rate_per[i][point] = kp[i]*tinj*(x[i][point]*
                     (1.0+lamda[i])-1.0)/lamda[i]
                     (1.0+lamda[i])-1.0)/lamda[i];

rate[i][point] = rate_per[i][point];
}
}

if (equ_super == 'y')
{
no_lamdas = 1;
ly[no_curves] = lamda[0];
if ((no_curves >1) && (no_curves == 2))
{
i = 0;
no_lamdas = ((lamda[i] > lamda[i+1]) || (lamda[i] <
                lamda[i+1])) ? (no_lamdas+1):no_lamdas;

ly[no_curves+no_lamdas-1] = ((lamda[i] > lamda[i+1]) ||
                (lamda[i]<lamda[i+1])) ? lamda[i+1]:lamda[i

}
else if (no_curves >2)
for (i = 0; i <= no_curves - 2; i++)
```

```
{
no_lamdas = ((lamda[i] > lamda[i+1]) || (lamda[i] <
                    lamda[i+1])) ? (no_lamdas+1):no_lamdas;

ly[no_curves+no_lamdas-1] = ((lamda[i] > lamda[i+1]) || (lamda[i]
                          < lamda[i+1])) ? lamda[i+1]:lamda[i];


}
}
else if (equ_super == 'n')
no_lamdas = 0;

ifp = fopen("KINETIC_DATA","w");
no_points = fabs(max_time/time_interval)+1;
if (type_of_graph == 1)
{
fprintf(ifp,"%i\n",no_curves+no_lamdas);
for (i = 0; i <= no_curves - 1; i++)
{
fprintf(ifp,"%i\n",i+1);
fprintf(ifp,"%i\n",no_points);
fprintf(ifp,"LY=%3.2f_Bp=%5.4f_Bt=%5.4f\n",lamda[i],kp[i]*tinj,
                                                kt[i]*tinj);

for (t = 0.0, j = 0; t <= max_time; t += time_interval, j++)
fprintf(ifp,"%f\t%f\n",t,x[i][j]);
}

for (i = no_curves; i <= no_curves+no_lamdas - 1; i++)
{
fprintf(ifp,"%i\n",i+1);
fprintf(ifp,"%i\n",no_points);
fprintf(ifp,"LY=%3.2f\n",ly[i]);
for (t = 0.0; t <= max_time; t += time_interval)
if (t < 1.008)
fprintf(ifp,"%f\t%f\n",t,1.0/(1.0+ly[i]*t));
else if (t > 1.008)
fprintf(ifp,"%f\t%f\n",t,1.0/(1.0+ly[i]));
}
fclose(ifp);
graph_settings(max_time,no_curves,no_lamdas,type_of_graph);
}
else if (type_of_graph == 2)
{
fprintf(ifp, "%i\n", 3*no_curves);
for (i = 0; i <= no_curves - 1; i++)
{
fprintf(ifp, "%i\n", i+1);
fprintf(ifp, "%i\n", no_points-1);
fprintf(ifp,"LY=%3.2f_Bp=%5.4f_Bt=%5.4f_(RATE_TOTAL)\n",
                              lamda[i],kp[i]*tinj,kt[i]*tinj);

for (t=time_interval,j=1;t<=max_time;t+=time_interval, j++)
fprintf(ifp,"%f\t%f\n",t,rate[i][j]);
}
```

```
        for (i = 0; i <= no_curves - 1; i++)
        {
        fprintf(ifp, "%i\n", no_curves+i+1);
        fprintf(ifp, "%i\n", no_points-1);
        fprintf(ifp,"LY=%3.2f_Bp=%5.4f_Bt=%5.4f_(RATE_P)\n",lamda[i],
                                                kp[i]*tinj,kt[i]*tinj);

        for (t=time_interval,j=1;t<=max_time;t+=time_interval,j++)
        fprintf(ifp,"%f\t%f\n",t,rate_per[i][j]);
        }
        no_points = fabs(1.0/time_interval);
        for (i = 0; i <= no_curves - 1; i++)
        {
        fprintf(ifp, "%i\n", 2*no_curves+i+1);
        fprintf(ifp, "%i\n", no_points);
        fprintf(ifp,"LY=%3.2f_Bp=%5.4f_Bt=%5.4f_(RATE_T)\n",lamda[i],
                                                kp[i]*tinj,kt[i]*tinj);

        for (t=time_interval,j=1;t<=1.0;t+=time_interval, j++)
        fprintf(ifp,"%f\t%f\n",t,rate_tra[i][j]);
        }
        fclose(ifp);
        graph_settings(max_time,no_curves,no_lamdas,type_of_graph);
        }
        system("gr");
        }
input()
{
        int i;

        system("clear");
        printf("\33h\33J");

        printf("\33&a2r6C DIMENSIONLESS TIME RANGE = 0.0 - ");
        scanf("%f",&max_time);

        printf("\33&a4r5C ___________________");
        printf("\33&a7r5C ___________________");
        printf("\33&a5r6C 1. [X]/[Xo] Vs t* ");
        printf("\33&a6r6C 2.     RATE Vs t* ");

        printf("\33&a3r6C TYPE OF GRAPH ? ");
        scanf("%i",&type_of_graph);

        if (type_of_graph == 1)
        {
        printf("\33&a8r6CNUMBER OF CURVES(EXCLUDING EQUILIBRIUM CURVES)?"
        scanf("%i",&no_curves);
        }
        else if (type_of_graph == 2)
        {
        printf("\33&a8r6C NUMBER OF TOTAL RATE CURVES ? ");
        scanf("%i",&no_curves);
        }
        printf("\n\n\n");
```

```
        for (i = 0; i <= no_curves - 1; i++)
        {
        printf("\tCURVE NUMBER : %i\n",i+1);
        printf("\t\tLAMDA[%i] = ",i+1);
        scanf("%f",&lamda[i]);

        printf("\t\tKp[%i] ( /min ) = ",i+1);
        scanf("%f",&kp[i]);

        printf("\t\tKt[%i] ( /min ) = ",i+1);
        scanf("%f",&kt[i]);
        printf("\n");
        }
        printf("\n\tINJECTION TIME (min) ? ");
        scanf("%f",&tinj);

        getchar();
        if (type_of_graph == 1)
        {
        printf("DO YOU WANT TO SUPERIMPOSE THE EQUILIBRIUM CURVES (y/n) ?
        scanf("%c",&equ_super);
        }
        }
graph_settings(max_time,no_curves,no_lamdas,type_of_graph)
float max_time;
int no_curves,no_lamdas,type_of_graph;
#define no_ticx_inter    10
#define no_ticy_inter    10
{
        FILE *dfp,*ifp,*ffp,*gfp,*fopen(),*ltp,*lfp,*mfp,*txtc,*titf,*out
        int i,ltype,m,no_cr;

        dfp = fopen("DATAFILE","w");
        fprintf(dfp,"KINETIC_DATA\n");
        fclose(dfp);

        ifp = fopen("XYRANGE","w");
        ffp = fopen("TIC_INTERVAL","w");
        if (type_of_graph == 1)
        {
        fprintf(ifp,"%f\t1.0\n0.0\t0.0\nm",max_time);
        fprintf(ffp,"%f\n%f\n",max_time/no_ticx_inter,1.0/no_ticy_inter)
        }
        else if (type_of_graph == 2)
        {
        fprintf(ifp,"%f\t2.0\n0.0\t0.0\nm",max_time);
        fprintf(ffp,"%f\n%f\n",max_time/no_ticx_inter,2.0/no_ticy_inter)
        }
        fclose(ifp);
        fclose(ffp);


        gfp = fopen("XYLABELS","w");
        fprintf(gfp,"%%2.1f\n%%2.1f\n");
        fclose(gfp);
```

```
lfp = fopen("LINECOLOR","w");
mfp = fopen("LINEMARKER","w");
ltp = fopen("LINETYPE","w");
m = 2;ltype = 0;
fprintf(ifp,"%i\n",m);
if (type_of_graph == 1)
no_cr = no_curves+no_lamdas;
else if (type_of_graph == 2)
no_cr = 3*no_curves;
for (i = 0; i <= no_cr-1; i++)
{
fprintf(ltp, "%i\n",ltype);
fprintf(mfp,"0\n");
if (m < 6)
m++;
else if ((m == 6) || (m > 6))
m = 2;
if (ltype < 6)
ltype += 2;
else if (ltype > 5)
ltype = (ltype == 6) ? 1:0;
fprintf(ifp,"%i\n",m);
}
fclose(lfp);
fclose(mfp);
fclose(ltp);

titf = fopen("TITLES","w");
if (type_of_graph == 1)
fprintf(titf,"t*\n[X]/[Xo]\n");
else if (type_of_graph == 2)
fprintf(titf,"t*\nRATE\n");
fclose(titf);

txtc = fopen("TEXTCOLOR","w");
fprintf(txtc,"4\n4\n");
fclose(txtc);

outf = fopen("OUTPUT_CHOICE","w");
fprintf(outf,"screen\n");
fclose(outf);
}
```

FLOW CHART 1

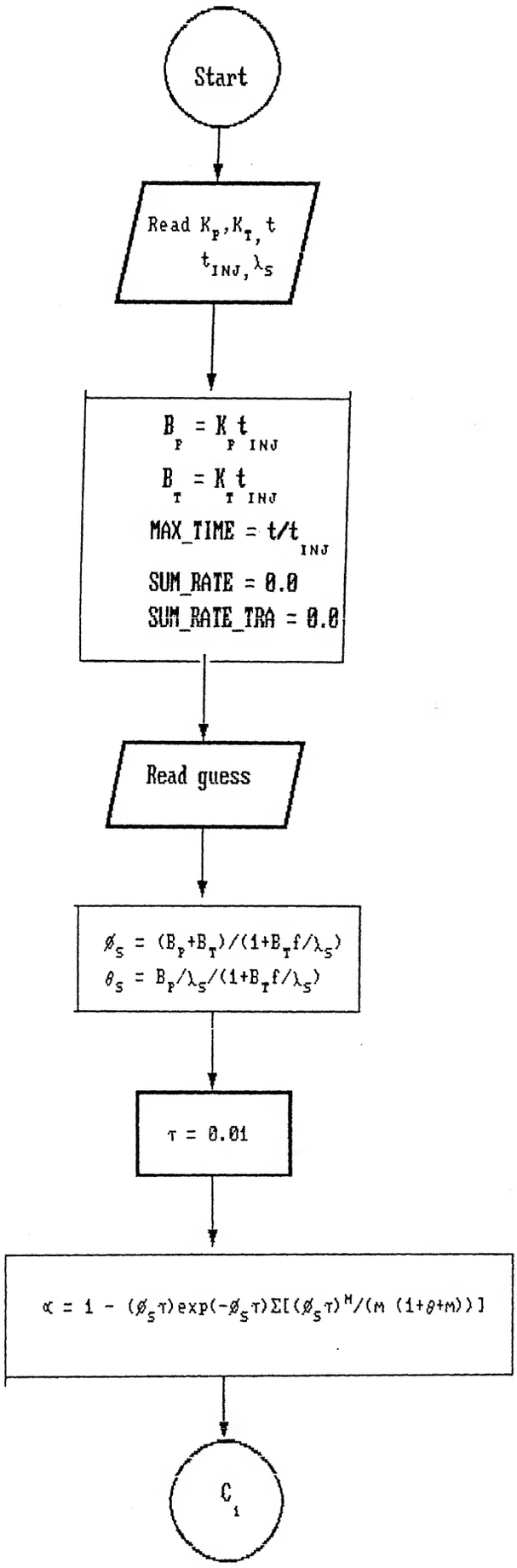
Start
Read K_P, K_T, t
t_{INJ}, λ_S
$B_P = K_P t_{INJ}$
$B_T = K_T t_{INJ}$
MAX_TIME = t/t_{INJ}
SUM_RATE = 0.0
SUM_RATE_TRA = 0.0
Read guess
$\phi_S = (B_P+B_T)/(1+B_T f/\lambda_S)$
$\theta_S = B_P/\lambda_S/(1+B_T f/\lambda_S)$
$\tau = 0.01$
$\alpha = 1 - (\phi_S\tau)\exp(-\phi_S\tau)\Sigma[(\phi_S\tau)^M/(m\ (1+\theta+m))]$
C_i

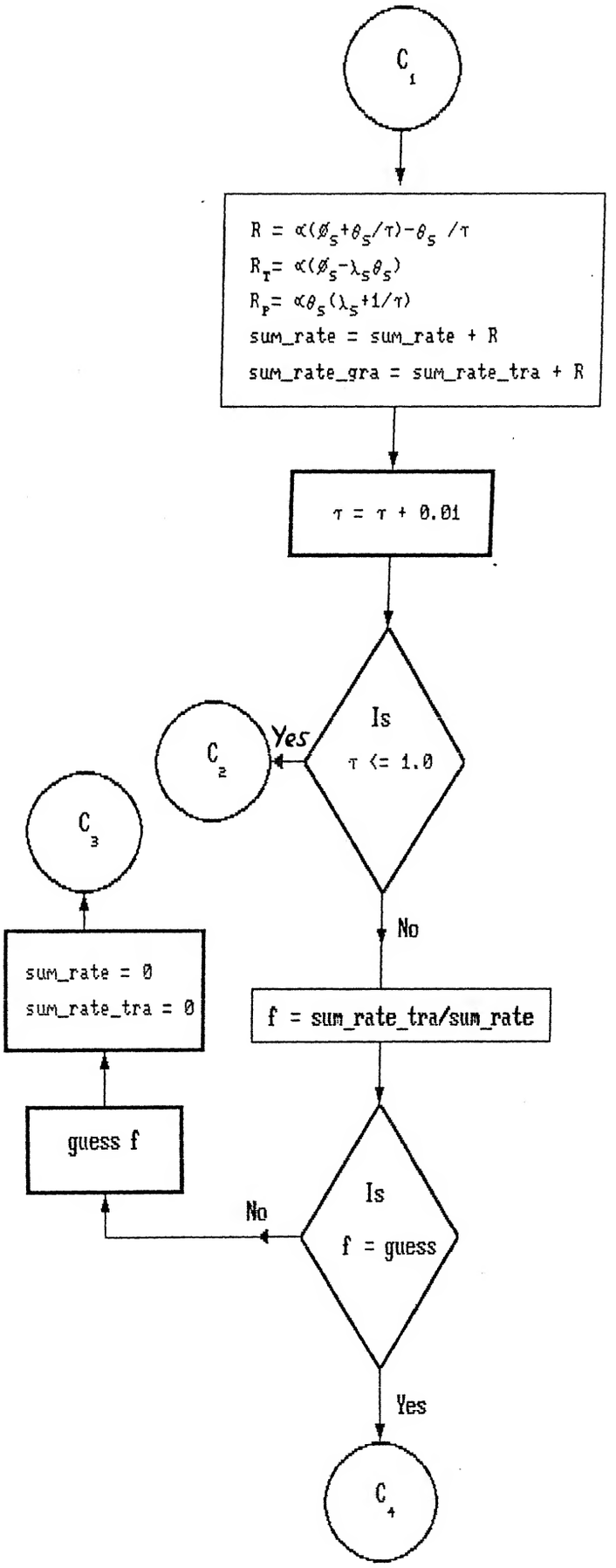
C1
R = α(Øs+θs/τ)-θs /τ
RT= α(Øs-λsθs)
RP= αθs(λs+1/τ)
sum_rate = sum_rate + R
sum_rate_gra = sum_rate_tra + R
τ = τ + 0.01
Is
τ <= 1.0
Yes
C2
No
C3
sum_rate = 0
sum_rate_tra = 0
f = sum_rate_tra/sum_rate
guess f
Is
f = guess
No
Yes
C4

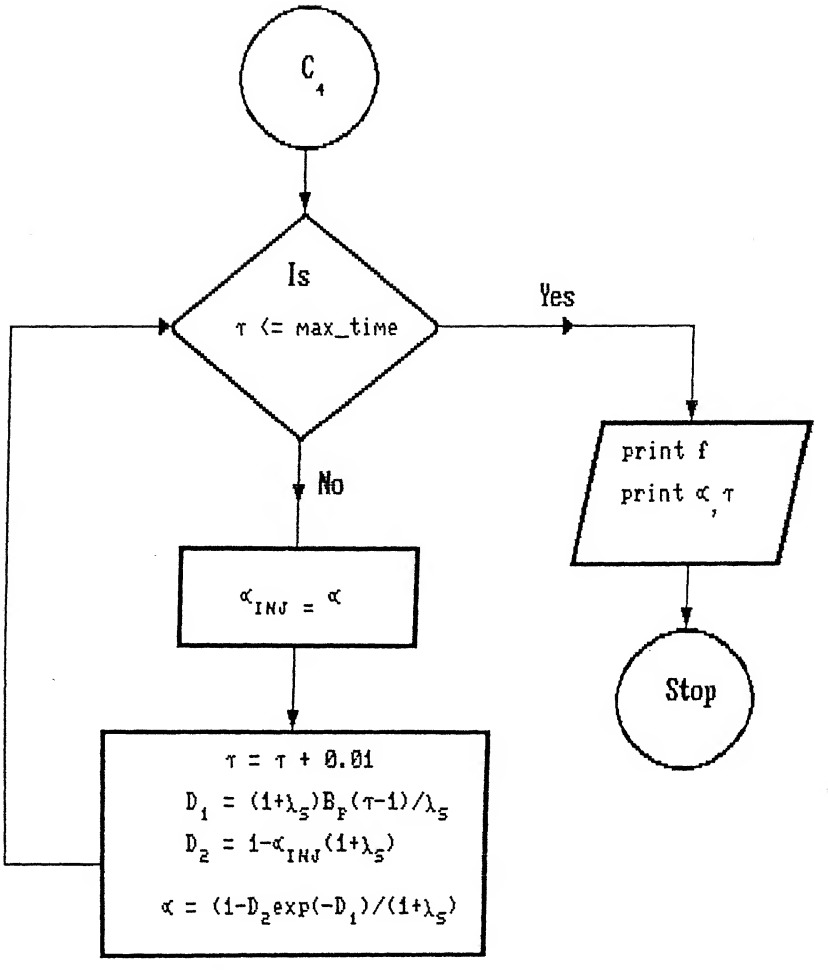
C4
Is
τ <= max_time
Yes
No
print f
print α, τ
Stop
α_INJ = α
τ = τ + 0.01
D1 = (1+λs)BF(τ-1)/λs
D2 = 1-α_INJ(1+λs)
α = (1-D2exp(-D1)/(1+λs)

FLOW CHART 2

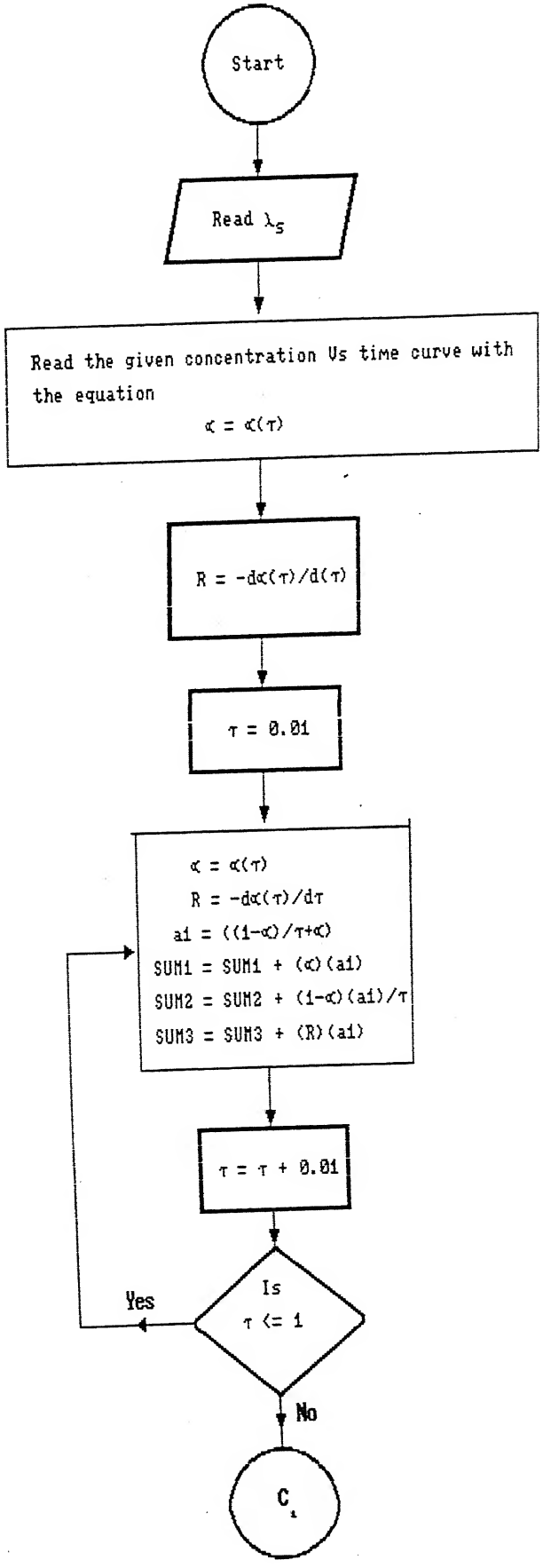
Start
Read λ_s
Read the given concentration Vs time curve with the equation
$\alpha = \alpha(\tau)$
$R = -d\alpha(\tau)/d(\tau)$
$\tau = 0.01$
$\alpha = \alpha(\tau)$
$R = -d\alpha(\tau)/d\tau$
ai = ((1-α)/τ+α)
SUM1 = SUM1 + (α)(ai)
SUM2 = SUM2 + (1-α)(ai)/τ
SUM3 = SUM3 + (R)(ai)
$\tau = \tau + 0.01$
Is
$\tau <= 1$
Yes
No
C_i

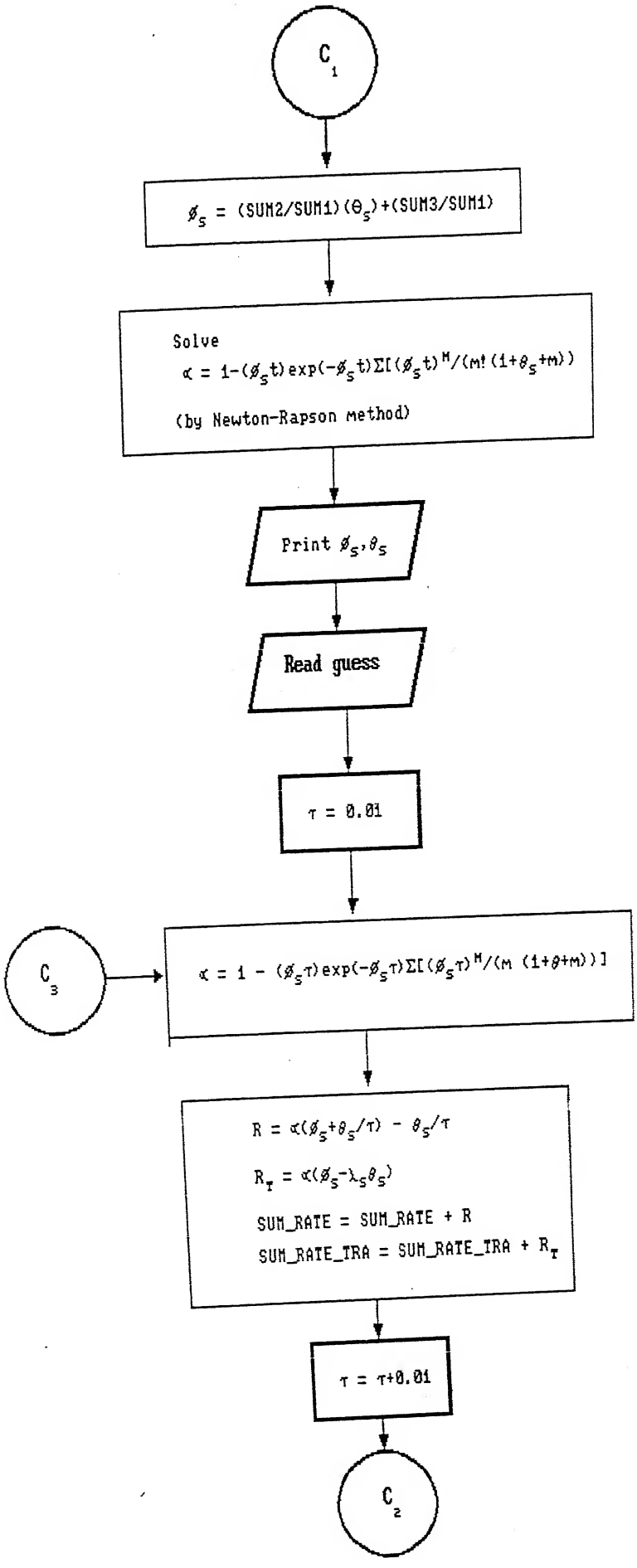
C1
ϕ_S = (SUM2/SUM1)(θ_S)+(SUM3/SUM1)
Solve
$\alpha = 1-(\phi_S t)\exp(-\phi_S t)\Sigma[(\phi_S t)^M/(m!(1+\theta_S+m))$
(by Newton-Rapson method)
Print ϕ_S,θ_S
Read guess
τ = 0.01
C3
$\alpha = 1 - (\phi_S \tau)\exp(-\phi_S \tau)\Sigma[(\phi_S \tau)^M/(m\ (1+\theta+m))]$
$R = \alpha(\phi_S+\theta_S/\tau) - \theta_S/\tau$
$R_T = \alpha(\phi_S-\lambda_S\theta_S)$
SUM_RATE = SUM_RATE + R
SUM_RATE_TRA = SUM_RATE_TRA + R_T
$\tau = \tau+0.01$
C2

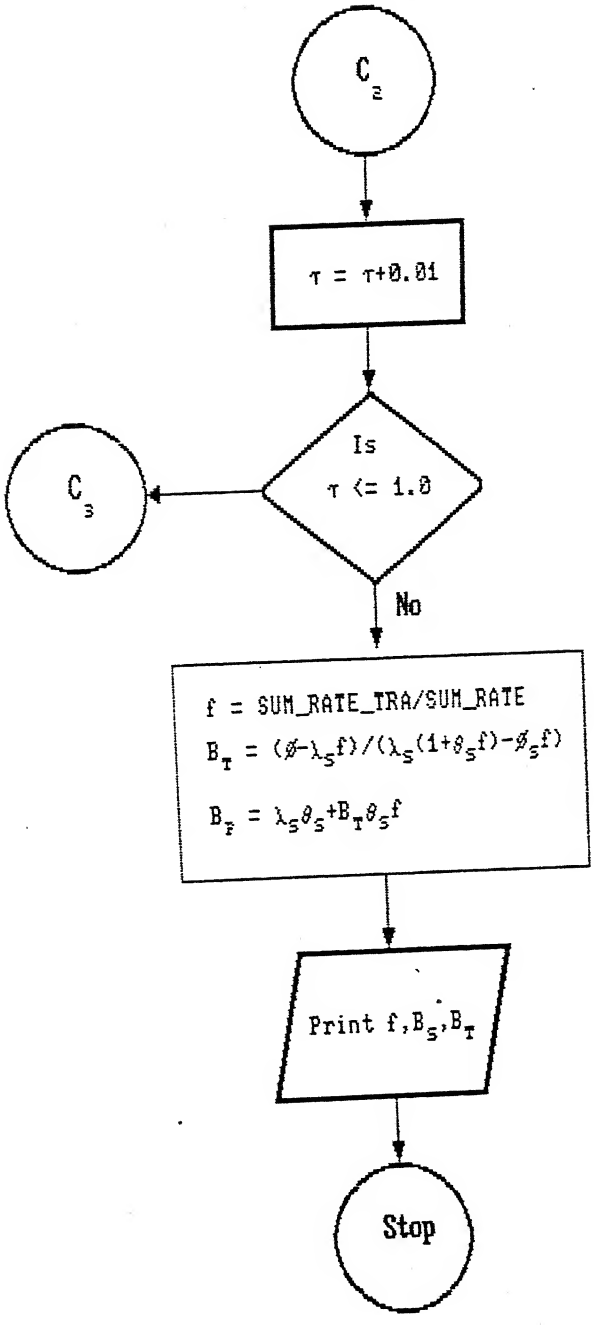
C2
τ = τ+0.01
Is
τ <= 1.0
C3
No
f = SUM_RATE_TRA/SUM_RATE
B_T = (∅-λ_S f)/(λ_S(1+θ_S f)-∅_S f)
B_F = λ_S θ_S+B_T θ_S f
Print f,B_S,B_T
Stop